STRUCTURAL AND FUNCTIONAL CHARACTERIZATION OF THE HELICOBACTER PYLORI FLAGELLAR MOTOR

by

KATHERINE HANEY GIBSON

(Under the Direction of Timothy R. Hoover)

ABSTRACT

Various bacterial species use flagella as a form of locomotion. Bacterial species exhibit a range of flagellar patterns including peritrichous arrangement (many flagella scattered around the cell body) to polar arrangement (flagella occur only at the cell pole), and ranging in number from one flagellum to many. *Helicobacter pylori,* a Gram-negative bacterium of the subphylum Epsilonproteobacteria, has a lophotrichous flagellation pattern with multiple flagella at a single cell pole. Many studies on the structure of the flagellum, along with regulation of localization and number of flagella per cell have been described in *Escherichia coli* and *Salmonella enterica* serovar Typhimurium. However, few studies exist on how a bacterium with a lophotrichous arrangement of flagella regulates the location and number of flagella. FlhF and FlhG are responsible for controlling localization and number of flagella, respectively, in various bacterial species. I generated and characterized Δ*flhF* and Δ*flhG* mutants in *H. pylori,* which revealed inherent differences in FlhF and FlhG of *H. pylori* compared to other bacteria. I additionally identified and deleted a gene directly downstream of *flhFG* that I designated as *flhH.* Characterization of a Δ*flhH* mutant in *H. pylori* showed FlhH had a role in motility that is still elusive. Whole genome

sequencing of suppressors of the Δ*flhF* and Δ*flhH* mutants that led to enhanced motility identified novel genes that may have roles in flagellar biosynthesis, structure, or function. Finally, ultrastructural studies of the *H. pylori* flagellar motor revealed interesting new insights into motor stator location and novel motor embellishments not observed in other species.

INDEX WORDS: *Helicobacter pylori,* flagella, motor, sheath

STRUCTURAL AND FUNCTIONAL CHARACTERIZATION OF THE HELICOBACTER PYLORI FLAGELLAR MOTOR

by

KATHERINE HANEY GIBSON

B.S., The University of South Carolina, 2015

A Dissertation Submitted to the Graduate Faculty of The University of Georgia in Partial Fulfillment of the Requirements for the Degree

DOCTOR OF PHILOSOPHY

ATHENS, GEORGIA

2020

STRUCTURAL AND FUNCTIONAL CHARACTERIZATION OF THE HELICOBACTER PYLORI FLAGELLAR MOTOR

by

KATHERINE HANEY GIBSON

Major Professor:	Timothy R. Hoover
Committee:	Diana M. Downs
	Robert J. Maier
	Vincent J. Starai
	Christine M. Szymanski

Electronic Version Approved:

Ron Walcott
Vice Provost for Graduate Education and Dean of the Graduate School
The University of Georgia
December 2020

DEDICATION

This dissertation is dedicated to those closest to me. Firstly to my parents, who have always supported me and never even thought to question the decisions I have made that have led me to this point. Their unwavering support both emotionally, and, at times, financially have made such a difference. They have always been just a phone call or a text away when I needed to talk or needed advice about how to be an independent adult, and I have never once had to buy a lightbulb, as my dad provides a constant supply. Secondly, to my grandparents, none of which are still here physically, but are with me in spirit and in my dreams. They were always so proud of me and bragged about me to all of their friends. It meant so much to me that they were so proud, even at some of my lowest moments. Thirdly, to my friends, both those I knew before graduate school and those I have made since. I cannot express how wonderful it was to have such a large support system through these years. There was always someone I could call, or text, or talk in person with, be it a time when I was sad, or angry, or felt like giving up. They have all helped me more than they will ever know. Finally, and most importantly, I dedicate this dissertation and all the work that went into it to my husband, Wade. Wade is the shining star in my life, my guiding light, my strength. He has faced all of my tears, all of my complaints, all of my joy throughout these five and a half years with a smile and gentle words. He believed in me even when I did not believe in myself. He kept me going when I felt like this journey was one that would never end. He always had the right words, the right actions, to bring me

back to myself, even in the darkest moments. These years have been the hardest of my life, but also some of the most rewarding. I owe it all to those that I love the most.

ACKNOWLEDGEMENTS

There are so many people who have set me on the path I am on today. I like to think it all started in high school in my AP biology class. My teacher, Angela Menz, now Mullins, was absolutely incredible. She had the biggest personality and encouraged my love for science. In my undergraduate studies, my academic advisor turned mentor, Dr. Charles Lovell, was the one who introduced me to microbiology and the one who encouraged me to apply for and attend graduate school. My advisor while in graduate school, Dr. Timothy Hoover, has been an endless well of scientific inquiry, always asking questions and getting me thinking. I would also like to thank Tim for putting up with my sarcasm, sass, and mood swings. I know I have not always been the easiest student to mentor, but I am grateful that Tim has always tried his best to understand how I am feeling and support me throughout my time here. I additionally cannot go without thanking the rest of my committee: Dr. Diana Downs, Dr. Robert Maier, Dr. Vincent Starai, and Dr. Christine Szymanski, who have always been there to offer science chat, words of advice, and reagents/ equipment when I needed them. I especially want to thank Vinny for always taking the time to check on me and my mental health through the last few years, it meant a lot knowing that there was someone on my committee that understood what I was going through. I would also like to thank Joshua Chu, who helped me to learn just about every technique I've done in graduate school. Finally, I have to thank the many people who have helped me with all of my microscopy work: Dr. John Shields and Mary Ard at the Georgia Electron microscopy facility, Dr. Jun Liu and

Shiwei Zhu who helped me to learn cryo-electron tomography, and Edward Sheppard and Nathan Glueck who helped me on numerous occasions to do fluorescence microscopy.

TABLE OF CONTENTS

Page

LIST OF TABLES

Page

LIST OF FIGURES

Page

CHAPTER 1

INTRODUCTION/ LITERATURE REVIEW

H. pylori epidemiology and pathogenesis

Helicobacter pylori is a Gram-negative pathogenic bacterium of the subphylum Epsilonproteobacteria that infects roughly fifty percent of the world's population. Infection with *H. pylori* is often lifelong, and most infected individuals are asymptomatic, although *H. pylori* infection can result in gastric ulcers, chronic gastritis, and, if untreated, gastric adenocarcinoma and gastric mucosa-associated lymphoid tissue (MALT) lymphoma [1]. Because of its association with gastric cancer, the World Health Organization has classified *H. pylori* as a group 1 carcinogen [1]. Socioeconomic status is a risk factor for *H. pylori* infection, with individuals in less developed areas and crowded living quarters more likely to be infected [1]. More developed nations, such as the United States, see a smaller percentage of colonized individuals, with roughly 1 in 3 people infected [1]. In addition to decreased prevalence in developed areas, prevalence in children is also falling worldwide, suggesting that *H. pylori* infection may die out in the future [2]. Decreasing prevalence is likely due to development, less overcrowding, access to clean water, and better hygiene practices [1, 3].

H. pylori infection is often successfully treated with antibiotics. Two common regimens are often used, one based on clarithromycin combined with amoxicillin and a proton-pump inhibitor (PPI), and another regimen consisting of bismuth, tetracycline, metronidazole and a PPI [1]. However, as with many pathogens currently, the issue of

antibiotic resistance is of growing concern. Prevalence of antibiotic resistance in *H. pylori* varies greatly between continents and individual countries, and can also vary between distinct geographic areas within countries; however, multidrug resistance remains low worldwide [4]. The greatest risk to antibiotic resistance is previous treatment for infection, although resistance to some drugs has been linked to their use in eradicating other infections [4].

Virulence and Colonization Factors

Like many pathogens, *H. pylori* has a number of virulence and colonization factors. Perhaps the most important virulence factors are vacuolating cytotoxin A (VacA) and the *cag* pathogenicity island.

VacA is a secreted toxin that binds to transmembrane proteins on the surface host cells such as receptor-like protein tyrosine phosphatases in order to be endocytosed, leading to the accumulation of acidic vacuoles in the cytoplasm of stomach epithelial cells [4-6]. VacA is initially produced as a protoxin that undergoes proteolytic cleavage yielding a smaller mature toxin protein [5]. VacA is secreted through an autotransporter type V pathway into the extracellular space, or it can remain attached to the bacterial cell surface [5]. Proteins that are transported via the type V autotransporter pathway typically share common domains: an N-terminal domain that contains a signal peptide responsible for secretion of the protein across the inner membrane; a passenger domain that has varied functions including adhesion, autoaggregation, invasion, and cytotoxicity, among others; and, finally a C-terminal β-domain that assists in translocating the passenger domain across the membrane [7]. While almost all *H. pylori* strains harbor *vacA,* not all *vacA* alleles have *in vitro* cytotoxin activity [8]. Mutation of *vacA* did not reduce inflammation in the mouse

stomach, but did lead to reduction in epithelial mucosal damage, implicating the cytotoxic product in mucosal injury [8].

cagA is a marker for the *cag* pathogenicity island which is present in approximately 60% of *H. pylori* strains [9]. Presence of the *cag* pathogenicity island in human infectious strains has been correlated with an increased chance of severe illness, with *cagA* being present in the majority (80-100%) of patients with duodenal ulcers and to a lesser extent (40-60%) in patients with only gastritis [8]. Also contained on the pathogenicity island are genes encoding a type IV secretion system responsible for injection of CagA into host cells where it can cause myriad effects, including, but not limited to, cytoskeletal rearrangements, loss of cell polarity, and signal transduction interference [4].

Another important virulence factor is lipopolysaccharide (LPS), a component of the outer membrane of Gram-negative bacteria that gives stability to the membrane. Though embedded in the outer membrane, LPS molecules can be released as bacteria die or divide [10]. LPS plays many roles including activation of the host immune system by providing binding sites for host antibodies, toxicity/ virulence of the pathogen, and prevention of uptake of bacteria by host phagocytes [10]. *H. pylori* LPS disrupts the gastric mucus coating and has low proinflammatory activity allowing for evasion of host defenses and long-term colonization by the bacterium [9]. The low immunological activity is due to the unique structure of *H. pylori* LPS, which differs significantly from that of other pathogenic bacteria [10]. Lipid A of *H. pylori* has an unusual fatty acid composition and phosphorylation pattern compared with other bacterial species [11, 12]. Specifically, lipid A of *H. pylori* has a backbone of a D-glucosamine disaccharide that is phosphorylated at position 1 but not at position 4 [13]. Conversely, *E. coli* lipid A has a D-hexosamine

disaccharide backbone that is phosphorylated at position 1 and 4 [13]. *H. pylori* also has unusually long 3-hydroxy fatty acids [13]. Both of these features lead to the low biological activity of *H. pylori* LPS.

Urease activity of *H. pylori* is required for colonization and virulence in gnotobiotic piglets [14], and is also toxic to human gastric epithelial cells [15] making it both a colonization and virulence factor. Generally, urease is thought to aid the bacterium in surviving the high acidity of the human stomach by converting urea into ammonia and carbamate. Carbamate then spontaneously decomposes into another ammonia molecule and carbonic acid. The net result of these reactions is a localized increase in pH around the *H. pylori* cell. *H. pylori* is neutrophilic, so urease activity is critical to its survival in the host. It has also been shown that increase in the pH of the area around the cell causing the gastric mucin (a large glycoprotein) to transition from a viscoelastic gel to a viscous solution that the cell can then swim through [16].

Motility of *H. pylori* is necessary for both initial colonization of the gastric mucosa, and persistence of the bacterium in the stomach. Aflagellated or motility deficient bacteria are unable to infect mouse [17] or piglet models [18]. This is due to flagella and subsequent motility being required for the organism to migrate through the gastric mucous layer to reach the gastric epithelium. In fact, *H. pylori* is better equipped to swim with high velocity in viscous media compared to other motile bacteria, likely due to their helical shape, exclusively polar flagella, and large flagellar motor [19, 20].

The *H. pylori* flagellum

Motility of *H. pylori* is accomplished through a cluster of two to six flagella at a single cell pole. Flagella from various bacterial species have three major structures that are

built sequentially- the basal body, hook, and filament (Fig. 1.1). The basal body serves to anchor the flagellum within the cell envelope and houses the flagellar motor components. Also included in the basal body are the MS-ring (FliF), the flagellar type 3 secretion system (fT3SS)/ export apparatus (FlhA, FlhB), and the cytoplasmic ring (C-ring, FliG, FliM, FliN, FliY). The MS-ring is one of the earliest flagellar component assembled; it is embedded in the bacterial inner membrane and surrounds the fT3SS at its core [19]. The fT3SS consists of a membrane component comprised of FlhA, FlhB, FliO, FliP, FliQ, and FliR, and a soluble component comprised of FliH, FliI, and FliJ which form an ATPase and chaperone that provides more efficient transport by shuttling export substrates to the basal body [21]. Specifically, FliI is an ATPase that facilitates transport of the protein substrates across the cell membrane; FliH regulates the ATPase activity of FliI; and FliJ is a chaperone that keeps the protein substrates in an unfolded state [21]. The fT3SS is similar to Type III secretion systems found in Gram-negative bacterial pathogens that serves to export effector molecules across the cell envelope. In the case of the fT3SS though, flagellar subunits instead of endotoxic effector molecules are exported across the cell membrane for assembly of the axial components (i.e., rod, hook and filament) of the flagellum [21]. The C-ring is situated on the cytoplasmic side of the MS-ring and functions as the switch complex, switching between rotating the flagellum clockwise to counterclockwise [19]. The C-rings of *H. pylori* and other Epsilonproteobacteria are unique in containing four C-ring proteins. In contrast to *E. coli,* which contains FliG, FliM, and FliN in its C-ring, *H. pylori* contains also contains FliY, which shares homology with FliN at its C terminal end [22].

The hook serves as a universal joint, and once it reaches a specified length, the fT3SS switches from hook-type substrates to filament-type substrates to continue assembling the nascent flagellum [21]. The hook transfers torque from the rod to the flagellar filament, a whip-like structure that rotates and powers movement. The hook is flexible, which allows torque to be transferred from the rod to the filament even when the axes of the rod and filament are perpendicular to each other.

The switch to filament substrates is mediated by the hook length control protein FliK and autocleavage of FlhB [23]. FlhB is a component of the export apparatus that is membrane bound. Once the assembly of the hook is assembled, FliK interacts with the C-terminal cytoplasmic domain of FlhB ($FlhB_C$) [24]. This induces autocleavage and conformational changes to FlhB and leads to the termination of hook growth [23]. FlhB processing may serve as a molecular clock that regulates the switch in substrate specificity [23] and is required for export of filament substrates and therefore complete flagellum assembly in *H. pylori* (Fig. 1.1) [25].

Many thousands of filament subunits assemble in a hollow tube to form the external filament of the flagellum. Unfolded subunits move through the tube and assemble at the tip of the growing flagellum where they fold into their tertiary structure and spontaneously assemble into the nascent flagellum [26, 27]. Evans *et al*. presented data to suggest filament growth was accomplished through a chain mechanism where filament subunits are linked head to tail in the filament channel [27]. As one subunit is captured and folds into place at the filament tip, a force is exerted at its free end, pulling the next subunit upward through the channel [27]. An alternate growth model, the injection-diffusion model was presented by Renault [28] to explain the mechanics of flagellum growth in *Salmonella*. The

"injection" part comprising the initial fast growth rate is due to the direct coupling of the proton motive force to secretion through the fT3SS [28]. As the filament elongates, there is a transition to diffusion of the filament subunits on which the growth rate depends [28]. Growth rate of the filament decreases with filament length in both *Salmonella* (peritrichous flagella) and *Vibrio alginolyticus* (single polar sheathed flagellum) [28, 29].

A study in *Pseudomonas fluorescens* identified mutants of *flaG* to have unusually long flagellar filaments [30]. These mutants produced similar swim halos to the wild-type in motility assays, and increased halo diameter when supplemented with rich media. Additionally *flaG* mutants were shown by Western blot to export more flagellin, although overall flagellin protein levels were unchanged relative to the wild-type [30]. Moreover, ORF3 in *Vibrio anguillarum*, which has homology to *flaG* from *Vibrio parahaemolyticus*, was shown to have slightly decreased motility along with abnormally long flagella [31]. Homologs of *flaG* are absent from the genome of *E. coli* and the function of FlaG is thus far undetermined, but these findings indicate FlaG plays a role in determining filament length. The mechanism by which FlaG controls filament length is unknown, but potential mechanisms include modulating fT3SS activity, inhibiting the rate at which flagellin subunits diffuse along the filament, or terminating incorporation of flagellin subunits at the end of the growing filament.

H. pylori flagellar gene regulation

The coordinated expression of well over 40 structural, accessory, and regulatory genes is required for building a complete flagellum [32-34]. In general, expression of bacterial flagellar genes is regulated by a transcriptional hierarchy, in which genes encoding proteins needed early in flagellum assembly must be expressed before genes

whose products are needed later in the assembly process can be expressed. The flagellar genes in *H. pylori* are arranged in upwards of 35 operons scattered throughout the genome instead of a central flagellation core operon(s) as found in *E. coli* and *Salmonella*. This scattering of flagellar genes throughout the genome is observed for most members of the subphylum Epsilonproteobacteria, the notable exception being *Arcobacter butzleri* and its close relatives, which clusters their flagellar genes into a few operons, reminiscent of flagellar gene organization in *E. coli* [35].

Flagellar genes are generally grouped into classes based on the regulatory proteins that are involved in coordinating the transcriptional hierarchy. In *Salmonella enterica* serovar Typhimurium (*S.* Typhimurium), the early (class I) flagellar genes consist of *flhC* and *flhD*, which encode a master regulator that initiates expression of the flagellar gene transcriptional hierarchy and is responsive to environmental and cell state cues [36].

In *V. cholerae*, class I flagellar genes consists of the master regulator encoded by *flrA*, the expression of which begins the regulatory cascade for flagellar gene expression. FlrA activates transcription of class II genes encoding the fT3SS, along with genes encoding other basal body components that are required early in flagellum assembly, such as the membrane and supra-membrane ring (MS-ring; FliF) protein [37]. Following completion of these structures, class III and class IV transcription is initiated, completing synthesis of the flagellum.

Unlike several bacterial species, there is no identified master regulator of flagellar gene expression in *H. pylori* or other closely related bacterial species. Instead, those genes needed early in the assembly process are under control of the housekeeping sigma factor (σ^{70}) and appear to be expressed constitutively [19]. Two alternative sigma factors, σ^{54} and

σ^{28}, control expression of the middle and late genes, respectively. Genes under control of σ^{70}, known as the early genes, include those encoding the MS-ring, the fT3SS/ export apparatus, and the C-ring. This regulon of early genes also contains the genes *flgS* and *flgR,* which encode the protein histidine kinase and response regulator, respectively, of a two-component system. After the completion of the basal body assembly, FlgS becomes activated via an unknown signal, stimulating its autokinase activity [19]. FlgS was shown to bind a peptide corresponding to the N-terminus of the export apparatus component FlhA *in vitro* [38]. However, the interaction of FlgS with the peptide failed to stimulate FlgS autokinase activity *in vitro* [38]. There are nine subunits of FlhA in the fT3SS, and binding of FlgS monomers to these subunits may facilitate dimerization of FlgS and the subsequent stimulation of its autokinase activity [38]. Once phosphorylated, FlgS transfers the phosphate to FlgR, and FlgR-phosphate then activates transcription of the flagellar genes in the middle of the transcriptional hierarchy by σ^{54}-RNA polymerase holoenzyme [39-41]. The σ^{54}-dependent flagellar genes encode the hook protein (FlgE), hook-length control protein (FliK), hook associated proteins (FlgL and FlgK), a minor flagellin (FlaB), as well as other proteins (Table 1.1).

In models such as *Salmonella,* the switch from exporting hook-type substrates to filament-type substrates results in export of FlgM, an anti-sigma factor of FliA (σ^{28}). FliA, once released from FlgM, is required for transcription of late flagellar genes, including those encoding the major flagellin (FliC in *Salmonella,* FlaA in *H. pylori*) [21, 42]. In contrast to the *Salmonella* paradigm, *H. pylori* FlgM lack the N-terminal domain that directs its secretion and is therefore, not secreted outside of the cell [43]. Rust and co-workers proposed a model in which FlgM is released from FliA via interactions with other

proteins, such as FlhA, which was found to interact with FlgM in a bacteria two-hybrid system assay [43].

The flagellar sheath

One unique feature of *H. pylori* flagella is the presence of a surrounding membranous sheath that is contiguous with the outer membrane [19] (Fig. 1.3). Sheaths have thus far been found almost exclusively in bacteria with polar flagella [44]. Each flagellum of *H. pylori* is encased in its own separate sheath terminating with a bulb-like structure at the distal end of the flagellum [44]. Very little is known about the function of the flagellar sheath or about how it is synthesized. Is has been suggested that the flagellar sheath helps to shield the flagella from being recognized by the host immune system, which recognizes and targets flagellin subunits [19]. Another possibility is that the sheath protects the flagella from stomach acid, which could cause the depolymerization of the flagellin subunits [44]. In *Vibrio fischeri,* the flagellar sheath has been proposed to release outer membrane vesicles that are required for proper development of the light organ in the Hawaiian bobtail squid, *Euprymna scolopes,* the symbiosis partner of *V. fischeri* [45, 46]. Finally, the flagellar sheath may protect against flagellotropic phages, which use flagellar filaments as host receptors for initial attachment before being translocated to the bacterial cell body, presumably through flagellar rotation [44].

It has been proposed that the sheath is assembled simultaneously with the flagellar filament as mutations in genes that produce shorter filaments also produce shorter sheaths [47]. Additionally, flagellar assembly intermediates observed by cryo-ET in *H. pylori* provide further evidence that the sheath grows simultaneously with the flagellar hook and filament [20]. In contrast, mutants of *V. cholerae* were generated that possessed flagellar

sheaths that appears to lack internal filaments [48]. These coreless sheaths appeared primarily at non-polar sites and had irregular diameters [48]. Thus, it appears that flagellar filament assembly and sheath biosynthesis may be able to be uncoupled in some bacteria, although this does not appear to be the case in *H. pylori.*

There is little information available on the fatty acid composition of the flagellar sheath for any bacterium. A study of *Bdellovibrio bacteriovorus* suggested that this organism is able to partition specific LPS molecules to the flagellar sheath compared to those contained in the outer membrane [49]. Studies of the flagellar sheath of *H. pylori* have shown no fatty acids to be uniquely associated with the sheath, although the fatty acid composition profile of the sheath differed from that of the cell membrane [50]. Further, sheaths of *H. pylori* were found to contain a significant amount of cardiolipin, a phospholipid with high intrinsic negative curvature (Chu, 2019, University of Georgia thesis). In *E. coli* cardiolipin has been shown to recruit ProP and MscS to the cell pole [51], and it is possible that cardiolipin may also recruit specific proteins to the sheath in *H. pylori.*

Localization of proteins to the flagellar sheath has thus far been relatively unexplored. One protein of note is the *H. pylori* adhesion A (HpaA), which was shown to be specifically localized to the flagellar sheath [52, 53]. However, other reports using the same technique of immunogold labelling reported that HpaA was only present in the cytoplasm and inner membrane, while absent from the outer membrane [54], while another study reported localization of HpaA to be in both the sheath and the outer membrane [55]. While there appears to be some variability in the results, this could be due to strain differences or differences in growing conditions [44].

Radin *et al*. identified a type V autotransporter similar to VacA, designated FaaA, to be localized to the flagellar sheath [7]. Mutation of *faaA* resulted in flagellar deficiencies including aflagellation and localization of flagella to non-polar sites, although there is some ambiguity in the interpretation of this latter result. *H. pylori faaA* cells were attenuated for colonization in a murine model [7], which might be attributed to the flagellation deficiencies. It is so far unclear what, if any, role FaaA plays in regards to the flagellar sheath function or biosynthesis.

The flagellar motor

Housed within the basal body are the motor proteins MotA and MotB, which generate torque, powering the flagellar motor. These proteins form stator components composed of a $MotA_4/MotB_2$ heterohexamer [56]. *H. pylori* has the largest flagellar motor to date, incorporating 18 stators into its motor (Fig. 1.3). In comparison, *E. coli* incorporates 11 stators into its flagellar motor, *V. fischeri* incorporates 13 stators, and *C. jejuni* contains 17 stators [57]. MotA has four transmembrane domains and is embedded in the inner membrane. MotA serves as a channel through the inner membrane across which protons are pumped to generate torque, which is then exerted onto the C-ring protein FliG, turning the flagellum [58]. MotB has a single transmembrane region at its N-terminus while the rest of the protein is periplasmic. MotB engages the peptidoglycan layer via interactions with the P-ring protein FlgI and through a predicted peptidoglycan binding domain, thus maintaining the structural integrity and stability of the stator complex [59, 60].

Interaction between MotA and FliG can be regulated in a number of ways. Power can be cut from the flagellum by molecular clutch proteins. EspE is a clutch protein in *B. subtilis* that binds to the rotor and disengages it from the stators, thus preventing rotation

[61]. Another method of control is accomplished by molecular brake proteins. *Rhodobacter sphaeroides* CheY (a chemotaxis protein) increases the resistance between the rotor and the stators, locking out rotation [62]. Finally, in the case of bacteria that vary the number of stators incorporated into their motors, increasing stators leads to increased power of the motor [63, 64].

In *E. coli,* stator components are not stably incorporated into the flagellar motor and thus cannot be observed in cryo-electron tomography (cryo-ET) images [57]. The assembly of stators into the *E. coli* motor is a highly dynamic process, with stators incorporated in the motor freely exchanging with a pool of additional components in the inner membrane [65]. The number of stators in the motor is dependent on the external load experienced by the flagellum, with increased load leading to more stators being added to the motor [63, 64]. In contrast, stator complexes in the flagellar motors of Epsilonproteobacteria, such as *C. jejuni* and *H. pylori,* are more stably incorporated and do not seem to be dependent on external load, as they can be visualized by cryo-ET [57].

Heterogeneity of bacterial flagellar motors

In addition to the stator components MotA and MotB, Epsilonproteobacteria also have additional motor embellishments when compared to the motors of *E. coli* or *S.* Typhimurium. These include additional ring structures around the rod. In Epsilonproteobacteria these structures have been shown to be formed by subunits of FlgP, FlgQ, PflA, and PflB [57] (Fig. 1.4).

FlgO and FlgP are also present in the genome of *V. cholerae* and are regulated by RpoN. Deletions in *flgO* and *flgP* resulted in decreased motility of *V. cholerae* strain O395, with the *flgP* mutant producing a larger decrease in motility than the *flgO* mutant [66].

These mutants produced fewer flagella than the wild-type, and they appeared truncated, although they still had a flagellar sheath [66]. Both FlgO and FlgP were found to be localized to the outer membrane in *V. cholerae*; however, neither was found to localize to a specific pole [66, 67]. FlgO was predicted to form a novel ring in the flagellar motor of *Vibrio alginolyticus* [68]. This ring, designated the O-ring, was localized to where the flagellum intersects the outer membrane and is associated with a 90^{o} bend in the outer membrane that forms the sheath surrounding the flagellar hook [68]. The O-ring has thus been proposed to function as a scaffold allowing remodeling of the outer membrane during sheath biosynthesis. *A. butzleri* is the only member of the Epsilonproteobacteria to possess an *flgO* homolog [57].

In *C. jejuni*, subunits of FlgP assemble in 17-fold symmetry into an Archimedean spiral around the P-ring to form the structure designated as the basal disk, which has been proposed to add structural support to the outer membrane as the motor rotates [57]. Interestingly, in *C. jejuni*, this disk appears cup shaped and presses against the outer membrane, causing a concave indentation in the membrane [69]. In *C. jejuni*, FlgQ and FlgP are required for formation of the basal disk [69]. Assembly of the basal disk structure is necessary for the formation of the periplasmic medial ring, formed of PflA (Fig. 1.5). Finally, PflB subunits assemble into the proximal disk (Fig. 1.4), which is associated with the inner membrane and has been shown to be essential for stator complex incorporation into the *C. jejuni* flagellar motor [69]. Deletion of *flgP*, *pflA*, or *pflB* in *C. jejuni* resulted in cells that were non-motile yet still made flagellar filaments [69]. The 17-fold symmetry observed in these disk structures produce a wider stator ring, allowing for the incorporation of more stator complexes than seen in the motors of *E. coli* or *Salmonella* [69]. Outer

membrane disks, such as that formed by FlgP, have been proposed to serve as stabilizers for flagellar sheaths and, additionally, when coupled with the disks formed by PflA and PflB, to support higher occupancy stator complex incorporation in higher torque motors [57].

H. pylori has the largest flagellar motor observed to date, boasting 18-fold symmetry of stator components and other periplasmic features (Fig. 1.3) [20]. *H. pylori* also has a C-ring with much larger diameter than that of *Salmonella*, similar to the large C-ring contained by *C. jejuni.* In addition to the disks formed by FlgP, PflA, and PflB, *H. pylori* appears to have a perpendicular medial ring (termed 'the cage'), similar to that observed in *Wollinella succinogenes;* however, the cage in *H. pylori* is larger than that in *W. succinogenes* [57] (Fig. 1.3). The cage spans from the inner membrane to the outer membrane, encompassing the entire periplasmic section of the flagellar motor [20]. Around the flagellar rod exists the basal disk, which is similar in location to the P-ring in *Salmonella*, and between the basal disk and the outer membrane/ flagellar sheath is a smaller disk of unknown composition or function [20]. Comparable to the disks formed by FlgP, PflA, and PflB, the periplasmic cage in *H. pylori* may facilitate incorporation of the 18 stator units into the motor to generate the high torque needed by the bacterium to swim in viscous medium, as well as protect the integrity of the outer membrane during high torque generation.

Regulation of flagellar localization and number in *H. pylori* and other bacteria

Motile bacteria present different flagellation patterns, including peritrichous arrangement (flagella arranged around the cell body) and polar flagellation. Polar flagellates can be monotrichous (single flagellum at single pole), ampitrichous (one

flagellum at each pole), or lophotrichous (tuft of flagella at a single pole). Of interest is how different species with different polar flagellar patterns regulate both the number of flagella per cell and the localization of those flagella to the cell pole. Two genes that have been shown to regulate these activities in many polar flagellated bacteria are *flhF* and *flhG.* Although these genes are generally restricted to polar flagellates, a notable exception the peritrichous bacterium *Bacillus subtilis.*

Understanding how bacteria target proteins to specific location is an important and fascinating area of study in microbiology. Bacterial proteins are targeted to specific cellular locations through various methods. One general method is known as diffusion and capture, whereby a protein travels in two dimensions within a membrane or three dimensions through the cytosol until it encounters and is captured by another protein or other macromolecule to which it binds [70]. An alternative method of protein localization is self-assembly, which does not depend on any other cellular cue, but proteins are instead "captured" by the self-assembly itself [70]. Another way for proteins to localize is through direct sensing of cell shape and curvature [51]. Specifically, the cell pole in rod-shaped cells has high negative curvature that can be sensed by proteins in order for their localization to the cell pole [51]. Further, proteins may localize to the cell pole by having affinity for polar features of the cell envelope that differ from those found at sidewall locations of the cell [51]. Although FlhF has been shown to be involved in the proper localization of flagella to the cell pole in several bacterial species [71-74], the mechanism by which FlhF facilitates the localization of flagella to the cell pole is unknown.

FlhF

FlhF is a signal recognition particle GTPase that has homology to FtsY and Ffh (Fig. 1.5). GTPases generally act as molecular switches and much more is known about the molecular mechanisms used to accomplish biological function and structure-function relationships of FtsY and Ffh than about FlhF. Signal recognition particles (SRPs) are used by cells to target proteins to membranes upon binding to a signal sequence on the N-terminus of targeted proteins as they exit the ribosome. Once transported to the membrane, interaction of the SRP with the SRP receptor (SR) allows the transfer of the ribosome nascent chain complex to the translocation machinery. In *E.coli,* the SRP is composed of Ffh and the 4.5S RNA, both of which are essential [75]. In bacteria, FtsY serves as the SRP receptor, which has GTPase activity and sequence and structural homology to the GTPase domain of Ffh [75]. FtsY has also been demonstrated to interact with the inner membrane, although weakly, perhaps through interaction with membrane phospholipids [76, 77]. Both Ffh and FtsY have three domains. The N and G domains of each protein exhibit structural homology to each other and contain the GTPase domain [75]. The G domains of these proteins contain a unique insertion box domain (IBD) giving them low affinity for nucleotides and offering protein stability in an empty conformation [78-80]. The amino terminal, methionine-rich M domain of Ffh contains conserved residues that are essential for binding to the SRP RNA along with a binding pocket for the signal sequence [75], while the A domain of FtsY is believed to directly interact with lipids in the membrane [81]. The GTPases of Ffh and FtsY may act as GTPase activating proteins (GAPs) for each other, becoming mutually simulated upon forming a heterodimeric complex together [82, 83], leading to the rapid exchange of GDP and GTP of these proteins [78]. No external GAP or

guanine nucleotide exchange factors (GEFs) have been identified for Ffh and FtsY. The dimer formed by Ffh and FtsY is nearly symmetrical, allowing for the coordination of their GTPase activities [84, 85]. The 4.5S RNA has been shown to enhance the rate of complex formation between Ffh and FtsY when GTP is bound to both proteins [86]. GTP hydrolysis by Ffh and FtsY results in dissociation of the complex. Hydrolysis of GTP by both proteins is also stimulated by the 4.5S RNA [86].

FlhF also contains the conserved NG domains of Ffh and FtsY (Fig. 1.5), and is also involved in protein trafficking, most specifically in targeting the flagellar MS-ring protein (FliF) to the cell pole in polar flagellated bacteria [87]. FlhF also contains an N-terminal B domain that may be involved in the targeting of FliF to the cell pole [87]. Upon binding GTP, FlhF forms a homodimer, which is the protein's active form [88]. In contrast to the Ffh/FtsY heterodimer, homodimerization of FlhF does not result in reciprocal GTPase activation, resulting in a more stable, GTP bound homodimer [88]. To this end, Bange *et al*. found that YlxH (FlhG) of *B. subtilis* was able to bind to the GTP-bound homodimer form of FlhF, and further showed that the ATP-bound form of FlhG stimulates the GTPase activity of FlhF [89]. Figure 1.6 demonstrates the dynamic interactions of FlhF and FlhG. Briefly, upon binding their respective nucleotides, FlhF and FlhG dimerize and transition to the 'ON' state. The dimerization of FlhG results in a conformational change that exposes the membrane targeting sequence (MTS) that interacts with the inner membrane [90]. 'ON' FlhG can then interact with 'ON' FlhF, stimulating its GTPase activity. Upon nucleotide hydrolysis, FlhF and FlhG break into their apo- forms and enter the 'OFF' state.

Deletions of FlhF in *V. cholerae* result in a majority of cells lacking flagella. Of those cells that were able to assemble flagella, flagella were no longer restricted to the cell pole. Both aflagellation and mislocalization of flagella led to significant motility defects. Overexpression of FlhF in *V. cholerae* also severely reduced motility [87]. FlhF was found exclusively in the insoluble fraction of cell fractionation experiments, even in the absence of flagellar genes, and was shown to associate tightly with the inner membrane [87]. Polar localization of *V. cholerae* FlhF tagged with green fluorescent protein (GFP) was shown to occur even in the absence of flagellar genes, and *V. cholerae* FlhF-GFP fusion expressed in *E. coli*, which does not possess an *flhF* homolog, similarly localized to the cell pole [87]. Taken together, these findings suggest polar localization of FlhF is intrinsic to the protein [87]. Studies with *Pseudomonas aeruginosa* and *Vibrio alginolyticus* showed FlhF to target to the old cell pole containing the flagellum [74, 91]. However, it is unknown how *flhF* discriminates between the poles in a newly divided daughter cell that has not yet assembled a flagellum. Polar targeting of FlhF is mediated by the N-domain, as the B- and G- domains are non-essential for proper localization [87]. FlhF was further shown to impact the localization of the MS-ring protein FliF. In the absence of other flagellar genes and FlhF, FliF tagged with GFP exhibited a diffuse signal throughout cell membrane. Upon addition of FlhF, the FliF-GFP fusion formed distinct loci at a single cell pole. This localization of FliF was abolished when the B- or G-domains of FlhF were absent [87]. The recruitment of FliF to the cell pole likely promotes flagellar biosynthesis at the proper location.

FlhF plays a role in flagellar gene expression in *V. cholerae.* Examination of *lacZ* reporter genes fused to various flagellar gene promotors revealed decreased expression of class III (genes encoding the basal body, hook, and major flagellin) and class IV (genes

encoding the minor flagellin and motor components) flagellar genes in an *flhF* mutant, indicating positive regulation of these classes of flagellar genes by FlhF [37]. The role of FlhF in regulating expression of class III and IV flagellar genes in *V. cholerae* is likely an indirect effect, resulting from the failure of the basal body to assemble and subsequent formation of a cellular cue that is sensed by the transcriptional regulatory machinery controlling expression of the class III and IV flagellar genes.

Similarly, deletion of *flhF* in *Campylobacter jejuni* results in aflagellated cells that are defective for motility [71]. FlhF was reported to be necessary for expression of the σ^{54}-dependent flagellar genes in *C. jejuni* [92], and the same research group reported later that the requirement of FlhF for expression of the σ^{54}-dependent flagellar genes appears to be mediated through a pathway that is separate from the FlgSR two-component system [71]. It is not clear from the data presented by Balaban and co-workers that the decrease in σ^{54}-dependent gene expression in the *flhF* mutant did not result from the interruption in basal body assembly, which would disrupt signaling to the FlgSR two-component system [71]. The role of FlhF in flagellar gene regulation in *C. jejuni* was further blurred by a recent paper from Li and co-workers who reported that FlhF binds to the promoter regions of some flagellar genes [93]. The validity of this report is questionable though, as high amounts of purified FlhF were used in the electrophoretic mobility shift assays, no competitor DNA was included in the assays, and the fraction of DNA probe that was shifted was low.

Mutation of conserved residues in the G2 region of the GTPase domain, D321A and R324A, of *C. jejuni flhF* produced an intermediate motility phenotype and had no effect on expression of σ^{54}-dependent genes [71]. These residues are part of a conserved

DXXR motif within the G2 region that is predicted to be involved in GTP hydrolysis in other GTPases [94]. Although expression of flagellar genes was unperturbed, mutation of these residues impacted proper flagellum biosynthesis producing cells with no flagella, cells with two or more flagella at a single pole, cells with flagella localized to non-polar sites, or flagella that were significantly shorter than those produced by the wild-type [71]. This is in contrast to a Δ*flhF* mutant, which rarely produced any flagella, suggesting that the GTPase domain of FlhF is dispensable for producing a flagellum, but that full length protein is needed for proper flagellation [95].

FlhG

FlhG is a member of the ParA superfamily of ATPases and shares significant structural homology with MinD [90] (Fig. 1.7). *E. coli* MinD has a core ATPase domain and a C-terminal membrane targeting sequence (MTS). The MTS houses an amphipathic helix that can interact with the inner membrane upon binding of ATP by MinD. Schuhmacher reported that FlhG from *Geobacillus thermodenitrificans* was able to bind the membranes of large unilamellar vesicles exclusively in the presence of ATP in a homodimeric form [90]. When bound to ADP or with no bound nucleotide, FlhG from *G. thermodenitrificans* is monomeric and unable to bind lipids. *H. pylori* FlhG is predicted to have a C-terminal amphipathic helix, which may similarly function as the MTS. *H. pylori* FlhG additionally shares homology with the ATPase domain of MinD, including the conserved lysine and aspartate residues that are involved in ATP binding and hydrolysis, respectively [96] (Fig. 1.7). In contrast to MinD, *H. pylori* FlhG has an N-terminal extension with a conserved glutamine residue that has been shown in some bacterial species to be involved in stimulating FlhF activity [89, 96]. Substitution of this glutamine in for

alanine (Q4A) in *C. jejuni* resulted in a lower proportion of cells having a wild type flagellation pattern, with many cells presenting as hyperflagellated [96]. Further, this mutant was unable to stimulate the GTPase activity of FlhF *in vitro*, suggesting this residue is necessary for proper interaction between FlhG and FlhF [96].

In *B. subtilis*, a peritrichous flagellate, deletion of *flhG* results in tufts of flagella at individual sites along the cell and aggregation of basal bodies, although these flagellar biosynthesis effects did not reduce motility of the bacteria [97]. FlhG from *B. subtilis* was found to interact with C-ring proteins FliM and FliY in a nucleotide independent manner [90]. Localization studies of FlhG in *B. subtilis* revealed that FlhG mainly localized to the membrane and demonstrated dynamic, highly mobile behavior [90].

Deletion of *flhG* in *V. cholerae* results in hyperflagellation, or more than a single flagellum at one cell pole [37]. This resulted in decreased motility, both due to the inability of *V. cholerae* to coordinate the movement of multiple flagella, and also the aggregation of cells due to entanglement of the multiple flagella [37]. Perhaps most interesting is that this phenotype was unstable. When incubated for longer than one day, regardless of medium type, *flhG* mutant cells became increasingly motile and reduced their flagellar number to one or two [37]. All cells showed this effect and thus it was likely due to adaptive behavior rather than individual cells accumulating suppressor mutations [37]. Additionally, one day old *flhG* cells (presenting the multiflagellate phenotype) showed an upregulation of *flrA*, the flagellar master regulator in *V. cholerae*, along with upregulation of all other classes of flagellar genes, suggesting that *flhG* negatively regulates the transcription of *flrA* [37]. If this is the case, the absence of *flhG* would result in increased transcription of the flagellar master regulator, and thus to up-regulation of all other flagellar genes, perhaps leading to

an increased number of flagella per cell as there are more available subunits for incorporation into flagella. Furthermore, FlhG stimulates the GTPase activity of FlhF, thereby converting FlhF into an inactive form with regard to stimulating flagellum assembly at the cell pole. Therefore, loss of FlhG would be expected to result in hyperactive FlhF that would initiate flagellum assembly at a higher frequency than normal.

Mutations of *flhG* in *C. jejuni* also result in hyperflagellation, and, in addition, an increase in minicell production [95]. *C. jejuni* does not have a Min system to prevent asymmetric cell division and appears to use FlhG to fill this capacity. The Min system has been most studied in *E. coli* and consists of the proteins MinC, MinD, and MinE. MinD localizes to the cell pole via membrane interactions and recruits MinC. MinC prevents polymerization of the FtsZ ring from forming at the pole, thereby preventing asymmetric cell division [98]. MinE is then recruited to the pole and stimulates the ATP hydrolysis activity of MinD, releasing it from the membrane. MinD then freely diffuses to the other cell pole generating a dynamic oscillation of these proteins [98].

Interestingly, when *H. pylori flhG* was used to complement an *flhG* deletion in *C. jejuni*, normal flagellation patterns were restored along with a decrease in the minicell population [95]. *H. pylori* encodes both *flhG* and a Min system and it is not well understood how these systems may interact together. It is possible that *flhG* and *minD* are at least partially redundant in *H. pylori.* Also of interest in *H. pylori* is how its already "hyperflagellated" state may be impacted by the loss of FlhG.

Research summary

This work sought to characterize the flagellar motor of *H. pylori*, both in terms of unknown structural components of the motor and how *H. pylori* regulates the placement and number of flagella it constructs. Information is available on these processes for other bacteria including other Epsilonproteobacteria. However, it is still unknown how bacteria with a lophotrichous arrangement of flagella regulate the number and location of their flagella.

In chapter 2, I describe my research on mutational analysis of *flhF* and *flhG* in *H. pylori* Deletions of *flhF* and *flhG* in *H. pylori* were constructed and their phenotypes characterized. Loss of FlhF resulted in significant motility defects as a result of either aflagellated cells or cells with mislocalized flagella, which was a phenotype that was similar to that reported for *flhF* mutation *C. jejuni* [95]. Loss of FlhG in *H. pylori* did not result in any motility defects, however the distribution of flagellar number per cell was affected, with a higher proportion of cells that lacked flagella or had a single flagellum and a small percentage of the population that had >8 flagella. Suppressors of the Δ*flhF* mutant were isolated following an enrichment for motile variants that was done through repeated passage of the mutant in a soft agar medium. Single nucleotide polymorphisms (SNPs) were identified by whole genome sequencing (WGS) of three independent motile variants. All three motile variants had SNPs in *faaA*, two of the variants had an additional SNP in HPG27_170 (encodes a hypothetical protein), and one of the variants had a missense mutation in *fliF* that resulted in the conversion of Asn-225 to Asp. Cells of the motile variant with the *fliF* missense mutation produced significantly more flagella than the Δ*flhF* parental strain, suggesting that in the absence of FlhF the $FliF^{N225D}$ variant can initiate

assembly of the MS-ring more efficiently than the wild-type FliF. The other two motile variants contained the same frameshift mutation in *faaA*, and although the number of flagella per cell for these motile variants was not significantly different from that of the Δ*flhF* parental strain, the proportion of flagella that correctly localized to the cell pole was significantly higher in these motile variants. We hypothesize that in the absence of FlhF, FaaA interferes with flagellum assembly at the cell pole. Since FaaA is an autotransporter that is inserted in the outer membrane, our model suggests assemblies of flagellum components associated with the inner and outer membranes occur somewhat independently of each other, which is a major deviation from the current model in which the flagellar basal body is assembled in a stepwise fashion from the inner membrane to the outer membrane.

In chapter 3, I describe my research on a novel gene located immediately downstream of *flhFG* and conserved in members of the subphylum Epsilonproteobacteria. Deletion of the novel gene resulted in a motility defect in soft agar and decreased numbers of flagella per cell, and so we designated it as *flhH*. Three independent motile variants of the Δ*flhH* mutant were isolated following repeated passage of the mutant on soft agar medium. Interestingly, all of the motile variants produced abnormally long flagella. Whole genome sequencing identified frameshift mutations in *faaA* and *flaG* in all three motile variants. Each of the motile variants also possessed a third unique SNP. These SNPs were a missense mutation in HPG27_543 (*fliY*-2), which changed Thr-29 to Ala; a frameshift mutation in HPG27_1372; and a frameshift mutation in HPG27_261, which encodes a member of the TrkA_C protein family (pfam02080; regulator of K+ conductance). The function of FliY-2 is unknown but it shares homology with the C-ring protein FliY. The

function of HPG27_1372 (HP1451 in *H. pylori* 26695) is not known, but a crystal structure was reported for a fragment of HP1451 bound to the N-terminal domain of HP0525, which is an essential component of the Cag Type IV secretion system and acts as an inner membrane associated ATPase [99]. We predict that the SNP in *flaG* is responsible for the long flagella given that disrupting *flaG* homologs in other species results in a long flagellum phenotype [30, 31].

Preliminary data suggested that disrupting both *faaA* and *flaG* were required to rescue motility in the Δ*flhH* mutant, as mutation of *flaG* alone was not able to fully rescue motility. We predict that FlhH has a role in stabilizing the stator components in the flagellar motor. The longer flagellar filaments produced by mutations in *flaG* would add external load onto the motor and may assist in stabilizing the stator components, as external load increases stator incorporation into the flagellar motor of *E. coli* [63, 64]. As indicated above, we hypothesize that FaaA interferes with flagellum biosynthesis at the cell pole in the absence of FlhF by impeding the assembly of flagellar components associated with the outer membrane. We postulate that in addition to having a role in recruitment of stator complexes to the motor, FlhH is need to stabilize or recruit one or more of the embellishments in the *H. pylori* flagellar motor, and in the absence of these embellishments FaaA interferes with flagellum assembly. Examination of the flagellar motor of the Δ*flhH* motor by cryo-ET should help us to test our hypotheses as we predict that the stator units, as well as one or more motor embellishment, will not be visible in the cryo-ET images of the motor of the Δ*flhH* mutant.

In chapter 4, I describe my work on a unique ‘cage-like’ structure with 18-fold symmetry situated at the periphery of the *H. pylori* flagellar motor. In a comparative

bioinformatic analysis of genomes of *Helicobacter* species that possess a sheath (FS^+) compared with *Helicobacter* species that have sheath-less flagella (FS^-), we identified several genes that were conserved in FS^+ species but were absent in FS^- species, four of which encoded a predicted efflux system. Deletion of these genes in *H. pylori* B128 resulted in motility deficiencies and reduction in the number of flagella per cell, and we designated the genes as *faeABCD* (flagellum-associated efflux system genes ABCD). Examination of the flagellar motors of Δ*faeA* and Δ*faeCD* mutants by cryo-ET revealed that some embellishments of the flagellar motor, including the cage, were missing in the efflux system mutants. We hypothesize that the FaeABCD efflux system constitutes part of the cage surrounding the *H. pylori* flagellar motor cage. The validity of our hypothesis can be tested with a variety of experimental approaches, including immunogold-labeling or fluorescence microscopy with one of the components of the FaeABCD efflux system tagged with green fluorescent protein to see if the FaeABCD efflux system is localized to the flagellar pole.

Finally, I discuss my work to identify the MotA/MotB stator complexes in the cryo-ET images of the *H. pylori* flagellar motor in chapter 5. In the original report on the cryo-ET images of the *H. pylori* motor, Qin and co-workers could not unambiguously identify the location of the stator relative to the cage and other motor embellishments [20]. I constructed a *motAB* deletion in *H. pylori* B128, and cryo-ET studies of the flagellar motor of the mutant showed that the stators are closely associated with the motor cage.

My studies have yielded interesting and unexpected findings on how *H. pylori* controls its flagellation pattern, as well as important new findings on the structure and function of the *H. pylori* flagellar motor. Results from my studies have led to new

hypotheses on the assembly and operation of the *H. pylori* flagellum, and has opened exciting and novel avenues for future studies. Findings from my work highlight the structural and functional diversity among bacterial flagellar motors, as well as point to the necessity of expanding structure-function studies of the flagellar motor beyond the *E. coli/Salmonella* archetypes if we are to extend our understanding of the evolution of the flagellar motor.

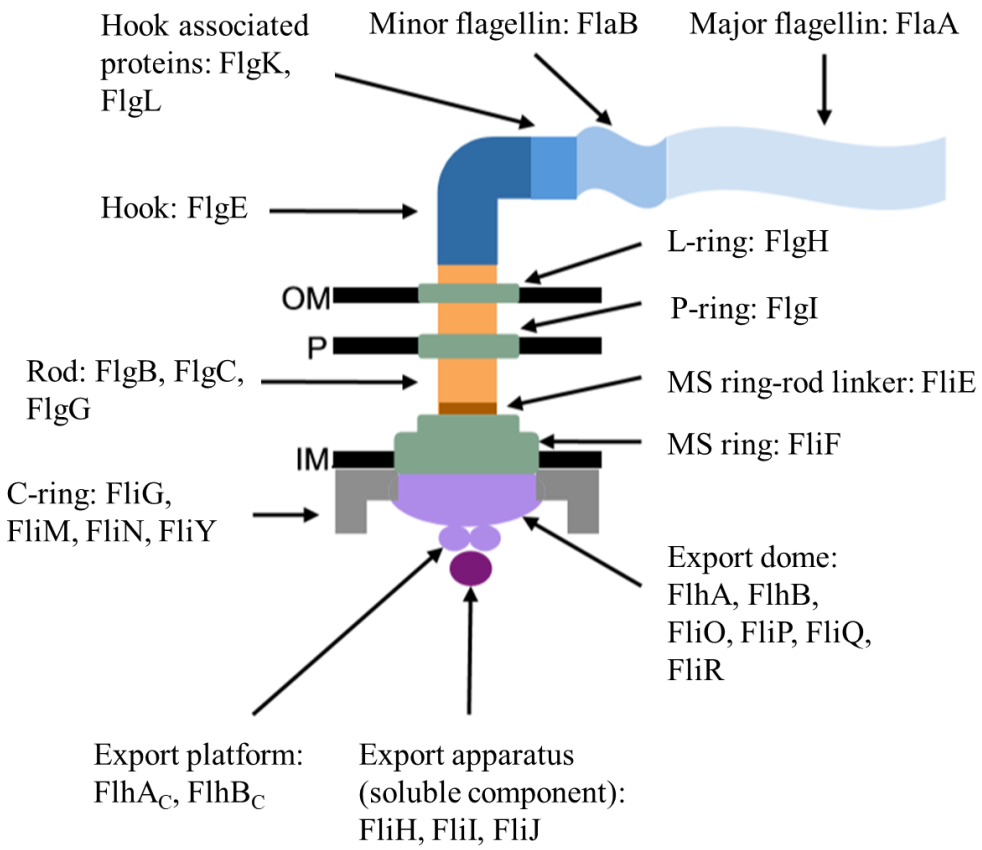

Figure 1.1. Basic structure of *H. pylori* flagellum. Proteins assembling specific structures are indicated.

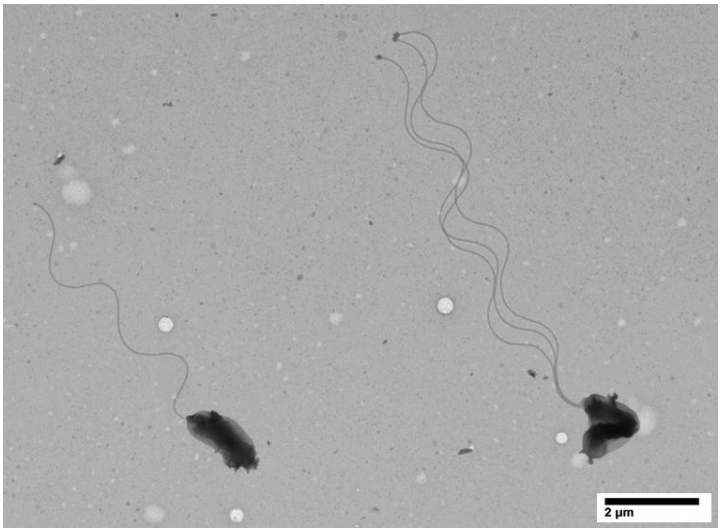

Figure 1.2. Image of *H. pylori* cells with abnormally long flagella. Cells were visualized on a JEOL 1011 TEM operated at 80 kV at the Georgia Electron Microscopy facility. Direct magnification of 1500X.

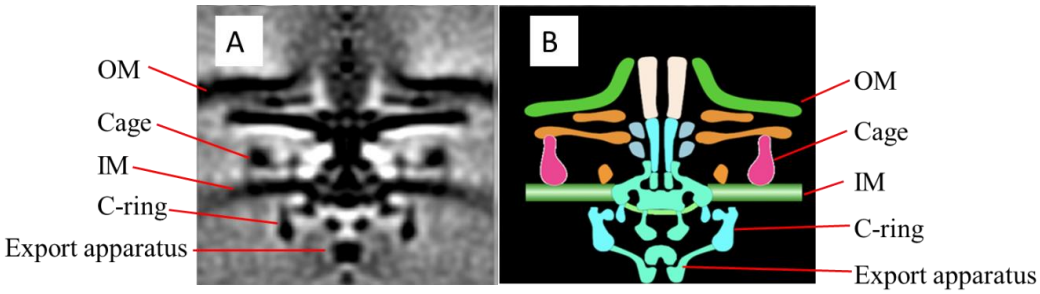

Figure 1.3. (**A**) Cryo-electron tomography reconstruction of *H. pylori* flagellar motor. Outer membrane (OM), cage, inner membrane (IM), C-ring, and export apparatus are identified. (**B**) Cartoon model of *H. pylori* flagellar motor.

.

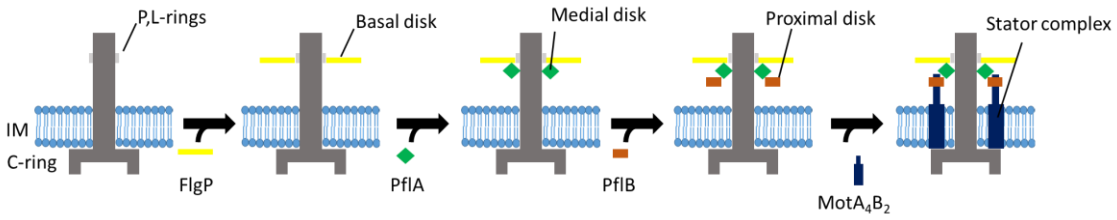

Figure 1.4. Proposed motor assembly pathway in *C. jejuni* that shows the additional ring structures formed by FlgP, PflA, and PflB. Based on information from Beeby, *et.* al., 2016 [69].

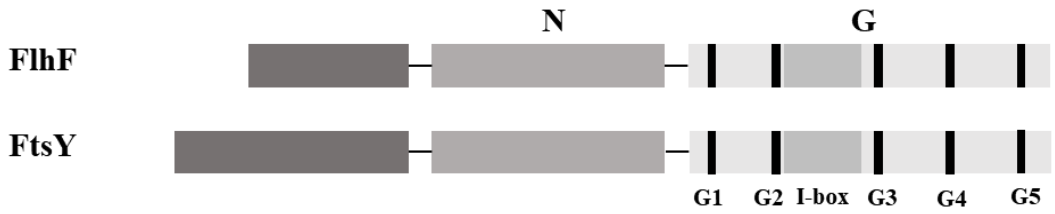

Figure 1.5. Structural comparison of SRP GTPases FlhF and FtsY. Conserved N and G domains are indicated, along with the conserved I-box and nucleotide binding elements (G1-G5).

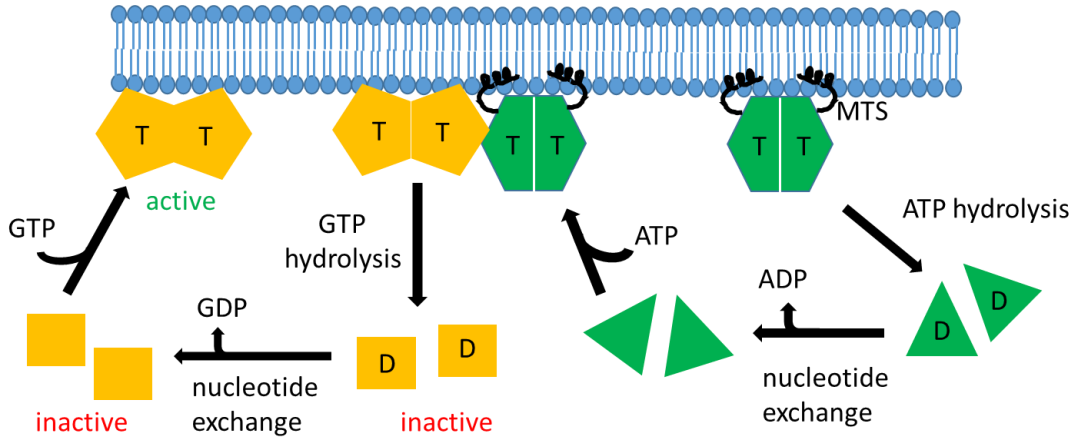

Figure 1.6. Interactions between FlhF and FlhG. Upon binding of GTP, FlhF (yellow) forms a homodimer becoming active and transitioning to the active 'ON' state. Upon binding of ATP, FlhG (green) forms a homodimer entering the active 'ON' state. Formation of the FlhG homodimer results in a conformational change exposing the membrane targeting sequence (MTS), which then interacts with the membrane. The N-terminus of FlhG homodimer interacts with FlhF, stimulating GTP hydrolysis of 'ON' FlhF. After hydrolysis of GTP, GDP bound FlhF dissociates into monomers entering the inactive 'OFF' state. ATP hydrolysis of FlhG results in dissociation into monomers of ADP bound FlhG which can no longer interact with the membrane.

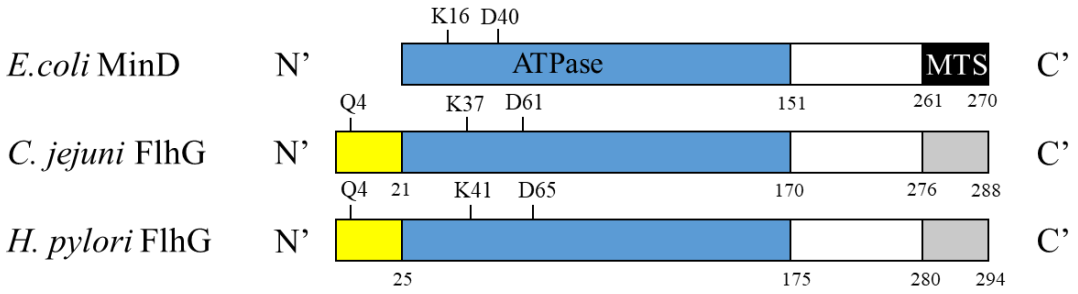

Figure 1.7. Structural comparisons between *E. coli* MinD, *C. jejuni* FlhG and *H. pylori* FlhG. Blue box indicates the homologous ATPase domains. *E. coli* membrane targeting sequence (MTS) is indicated by the black box. Putative MTS for *C. jejuni* FlhG and *H. pylori* FlhG is indicated by grey boxes. N-terminal extension is indicated by yellow boxes. Conserved residues responsible for ATP binding (K16, K37, K41), ATP hydrolysis (D40, D61, D65), and FlhF stimulation (Q4) are indicated.

Table 1.1. *Helicobacter pylori* flagellar, flagellar-associated and flagellar regulatory genes.

[a]locus number	gene name	[b]sigmulon	predicted or known function
flagellum and flagellum-associated components			
HP0351	*fliF*	RpoD	MS-ring protein
HP0352	*fliG*	RpoD	rotor protein; C-ring component
HP1031	*fliM*	RpoD	C-ring component
HP1032	*fliY*	RpoD	C-ring component
HP0584	*fliN*	RpoD	C-ring component
HP0173	*fliR*	RpoD	flagellar export apparatus protein
HP0353	*fliH*	RpoD	flagellar export apparatus protein; regulator of FliI
HP0583	*fliO*	RpoD	flagellar export apparatus protein
HPG27_642	*fliP*	RpoD	flagellar export apparatus protein
HP0770	*flhB*	RpoD	flagellar export apparatus protein
HP1041	*flhA*	RpoD	flagellar export apparatus protein
HP1419	*fliQ*	RpoD	flagellar export apparatus protein
HP1420	*fliI*	RpoD	flagellar export apparatus protein; ATPase
HP1557	*fliE*	RpoD/RpoN	MS-ring/rod junction protein
HP1558	*flgC*	RpoD/RpoN	proximal rod protein
HP1559	*flgB*	RpoD/RpoN	proximal rod protein
HP1233	*flgJ* (predicted)	RpoN	muramidase/rod cap protein
HP1092		RpoD	distal rod protein
HP1585	*flgG*	RpoD	distal rod protein
HP0246	*flgI*	RpoD	P-ring protein
HP0325	*flgH*	RpoD	L-ring protein
HP0907	*flgD*	RpoN	hook cap protein
HP0870	*flgE*	RpoN	hook protein
HP0908	*flgE2*	RpoN	potential second hook protein
HP0295	*flgL*	RpoN	hook-associated protein 3
HP1121	*flgK*	RpoN	hook-associated protein 1
HP0752	*fliD*	FliA	filament cap protein
HP0115	*flaB*	RpoN	minor flagellin
HP0601	*flaA*	FliA	major flagellin
HP0815	*motA*	RpoD	stator protein of flagellar motor
HP0816	*motB*	RpoD	stator protein of flagellar motor
HP0702	*flgQ*	RpoD	predicted basal disk protein
HPG27_795	*flgP*	RpoD	predicted basal disk protein
HP1274	*pflA*	RpoD	medial disk protein
HP1479	*pflB*	RpoD	proximal disk protein

HP0809	*fliL*	RpoD	inner membrane protein associated with stator
flagellar protein chaperones			
HP0256	*fliJ* (predicted)	RpoD	flagellar export apparatus protein; co-chaperone
HP0753	*fliS*	FliA	flagellin chaperone
HP1076		RpoN	predicted co-chaperone with FliS
HP1154	*fliW*	RpoN	predicted chaperone
HP1477	*flgA*	RpoD	periplasmic chaperone involved in P-ring assembly
flagellin modification proteins			
HP0178	*pseI*	RpoD	pseudaminic acid biosynthesis
HP0326	*pseF* (*neuA*)	RpoD	pseudaminic acid biosynthesis
HP0327	*pseH*	RpoD	pseudaminic acid biosynthesis
HP0366	*pseC*	RpoN	pseudaminic acid biosynthesis
HP0840	*pseB*	RpoD	pseudaminic acid biosynthesis
regulatory proteins			
HP0244	*flgS*	RpoD	histidine kinase; transcription of σ^{54}-dependent genes
HP0703	*flgR*	RpoD	response regulator for σ^{54}-dependent genes
HP0714	*rpoN*	RpoD	sigma factor, σ^{54}
HP0958	*flgZ*	RpoD	prevents rapid turnover of σ^{54}
HP1032	*fliA*	RpoD	sigma factor, σ^{28}
HP1122	*flgM*	RpoD	anti- σ^{28} factor
HP1035	*flhF*	RpoD	GTPase required for localization of flagella to cell pole
HP1034	*flhG*	RpoD	ATPase that regulates GTPase activity of FlhF
HP0751	*flaG*	FliA	role in control of filament length
HP0906	*fliK*	RpoN	hook-length control protein

[a]Locus numbers are given for *H. pylori* 26695 unless the annotated gene is reported as two separate open reading frames, in which case, the locus number for *H. pylori* G27 is indicated.

[b]Indicates sigma factor (σ^{80} (RpoD); σ^{54} (RpoN); or σ^{28} (FliA)) required for transcription of the gene.

References

1. Crowe, S.E., *Helicobacter pylori Infection.* N Engl J Med, 2019. **380**(12): p. 1158-1165.

2. Burucoa, C. and A. Axon, *Epidemiology of Helicobacter pylori infection.* Helicobacter, 2017. **22 Suppl 1**.

3. Salih, B.A., *Helicobacter pylori infection in developing countries: the burden for how long?* Saudi J Gastroenterol, 2009. **15**(3): p. 201-7.

4. Testerman, T.L. and J. Morris, *Beyond the stomach: an updated view of Helicobacter pylori pathogenesis, diagnosis, and treatment.* World J Gastroenterol, 2014. **20**(36): p. 12781-808.

5. Cover, T.L., S.A. Halter, and M.J. Blaser, *Characterization of HeLa cell vacuoles induced by Helicobacter pylori broth culture supernatant.* Hum Pathol, 1992. **23**(9): p. 1004-10.

6. de Bernard, M., et al., *The multiple cellular activities of the VacA cytotoxin of Helicobacter pylori.* Int J Med Microbiol, 2004. **293**(7-8): p. 589-97.

7. Radin, J.N., et al., *Flagellar localization of a Helicobacter pylori autotransporter protein.* mBio, 2013. **4**(2): p. e00613-12.

8. Blaser, M.J., *Role of vacA and the cagA locus of Helicobacter pylori in human disease.* Aliment Pharmacol Ther, 1996. **10 Suppl 1**: p. 73-7.

9. Dunn, B.E., H. Cohen, and M.J. Blaser, *Helicobacter pylori.* Clin Microbiol Rev, 1997. **10**(4): p. 720-41.

10. Moran, A.P., *The role of lipopolysaccharide in Helicobacter pylori pathogenesis.* Aliment Pharmacol Ther, 1996. **10 Suppl 1**: p. 39-50.

11. Moran, A.P., I.M. Helander, and T.U. Kosunen, *Compositional analysis of Helicobacter pylori rough-form lipopolysaccharides.* J Bacteriol, 1992. **174**(4): p. 1370-7.

12. Geis, G., et al., *Unusual fatty acid substitution in lipids and lipopolysaccharides of Helicobacter pylori.* J Clin Microbiol, 1990. **28**(5): p. 930-2.

13. Muotiala, A., et al., *Low biological activity of Helicobacter pylori lipopolysaccharide.* Infect Immun, 1992. **60**(4): p. 1714-6.

14. Eaton, K.A., et al., *Essential role of urease in pathogenesis of gastritis induced by Helicobacter pylori in gnotobiotic piglets.* Infect Immun, 1991. **59**(7): p. 2470-5.

15. Smoot, D.T., et al., *Helicobacter pylori urease activity is toxic to human gastric epithelial cells.* Infect Immun, 1990. **58**(6): p. 1992-4.

16. Celli, J.P., et al., *Helicobacter pylori moves through mucus by reducing mucin viscoelasticity.* Proc Natl Acad Sci U S A, 2009. **106**(34): p. 14321-6.

17. Ottemann, K.M. and A.C. Lowenthal, *Helicobacter pylori uses motility for initial colonization and to attain robust infection.* Infect Immun, 2002. **70**(4): p. 1984-90.

18. Eaton, K.A., D.R. Morgan, and S. Krakowka, *Motility as a factor in the colonisation of gnotobiotic piglets by Helicobacter pylori.* J Med Microbiol, 1992. **37**(2): p. 123-7.

19. Lertsethtakarn, P., K.M. Ottemann, and D.R. Hendrixson, *Motility and chemotaxis in Campylobacter and Helicobacter.* Annu Rev Microbiol, 2011. **65**: p. 389-410.

20. Qin, Z., et al., *Imaging the motility and chemotaxis machineries in Helicobacter pylori by cryo-electron tomography.* J Bacteriol, 2017. **199**(3): p. e00695-16.

21. Chevance, F.F. and K.T. Hughes, *Coordinating assembly of a bacterial macromolecular machine.* Nat Rev Microbiol, 2008. **6**(6): p. 455-65.

22. Lowenthal, A.C., et al., *Functional analysis of the Helicobacter pylori flagellar switch proteins.* J Bacteriol, 2009. **191**(23): p. 7147-56.

23. Ferris, H.U., et al., *FlhB regulates ordered export of flagellar components via autocleavage mechanism.* J Biol Chem, 2005. **280**(50): p. 41236-42.

24. Fraser, G.M., et al., *Substrate specificity of type III flagellar protein export in Salmonella is controlled by subdomain interactions in FlhB.* Mol Microbiol, 2003. **48**(4): p. 1043-57.

25. Smith, T.G., L. Pereira, and T.R. Hoover, *Helicobacter pylori FlhB processing-deficient variants affect flagellar assembly but not flagellar gene expression.* Microbiology (Reading), 2009. **155**(Pt 4): p. 1170-1180.

26. Iino, T., *Polarity of flagellar growth in salmonella.* J Gen Microbiol, 1969. **56**(2): p. 227-39.

27. Evans, L.D., et al., *A chain mechanism for flagellum growth.* Nature, 2013. **504**(7479): p. 287-90.

28. Renault, T.T., et al., *Bacterial flagella grow through an injection-diffusion mechanism.* Elife, 2017. **6**.

29. Chen, M., et al., *Length-dependent flagellar growth of Vibrio alginolyticus revealed by real time fluorescent imaging.* Elife, 2017. **6**.

30. Capdevila, S., et al., *Analysis of Pseudomonas fluorescens F113 genes implicated in flagellar filament synthesis and their role in competitive root colonization.* Microbiology, 2004. **150**(Pt 11): p. 3889-3897.

31. McGee, K., P. Horstedt, and D.L. Milton, *Identification and characterization of additional flagellin genes from Vibrio anguillarum.* J Bacteriol, 1996. **178**(17): p. 5188-98.

32. Rajagopala, S.V., et al., *The protein network of bacterial motility.* Mol Syst Biol, 2007. **3**: p. 128.

33. Muller, V., et al., *Characterization of the fliE genes of Escherichia coli and Salmonella typhimurium and identification of the FliE protein as a component of the flagellar hook-basal body complex.* J Bacteriol, 1992. **174**(7): p. 2298-304.

34. Niehus, E., et al., *Genome-wide analysis of transcriptional hierarchy and feedback regulation in the flagellar system of Helicobacter pylori.* Mol Microbiol, 2004. **52**(4): p. 947-61.

35. Miller, W.G., et al., *The complete genome sequence and analysis of the epsilonproteobacterium Arcobacter butzleri.* PLoS One, 2007. **2**(12): p. e1358.

36. Chilcott, G.S. and K.T. Hughes, *Coupling of flagellar gene expression to flagellar assembly in Salmonella enterica serovar typhimurium and Escherichia coli.* Microbiol Mol Biol Rev, 2000. **64**(4): p. 694-708.

37. Correa, N.E., F. Peng, and K.E. Klose, *Roles of the regulatory proteins FlhF and FlhG in the Vibrio cholerae flagellar transcription hierarchy.* J Bacteriol, 2005. **187**(18): p. 6324-32.

38. Tsang, J., et al., *Helicobacter pylori FlhA Binds the Sensor Kinase and Flagellar Gene Regulatory Protein FlgS with High Affinity.* J Bacteriol, 2015. **197**(11): p. 1886-92.

39. Beier, D. and R. Frank, *Molecular characterization of two-component systems of Helicobacter pylori.* J Bacteriol, 2000. **182**(8): p. 2068-76.

40. Brahmachary, P., et al., *Helicobacter pylori FlgR is an enhancer-independent activator of sigma54-RNA polymerase holoenzyme.* J Bacteriol, 2004. **186**(14): p. 4535-42.

41. Spohn, G. and V. Scarlato, *Motility of Helicobacter pylori is coordinately regulated by the transcriptional activator FlgR, an NtrC homolog.* J Bacteriol, 1999. **181**(2): p. 593-9.

42. Geis, G., et al., *Ultrastructure and chemical analysis of Campylobacter pylori flagella.* J Clin Microbiol, 1989. **27**(3): p. 436-41.

43. Rust, M., et al., *The Helicobacter pylori anti-sigma factor FlgM is predominantly cytoplasmic and cooperates with the flagellar basal body protein FlhA.* J Bacteriol, 2009. **191**(15): p. 4824-34.

44. Chu, J., J. Liu, and T.R. Hoover, *Phylogenetic Distribution, Ultrastructure, and Function of Bacterial Flagellar Sheaths.* Biomolecules, 2020. **10**(3).

45. Aschtgen, M.S., et al., *Rotation of Vibrio fischeri Flagella Produces Outer Membrane Vesicles That Induce Host Development.* J Bacteriol, 2016. **198**(16): p. 2156-65.

46. Brennan, C.A., et al., *A model symbiosis reveals a role for sheathed-flagellum rotation in the release of immunogenic lipopolysaccharide.* Elife, 2014. **3**: p. e01579.

47. Josenhans, C., A. Labigne, and S. Suerbaum, *Comparative ultrastructural and functional studies of Helicobacter pylori and Helicobacter mustelae flagellin mutants: both flagellin subunits, FlaA and FlaB, are necessary for full motility in Helicobacter species.* J Bacteriol, 1995. **177**(11): p. 3010-20.

48. Richardson, K., et al., *Transposon-induced non-motile mutants of Vibrio cholerae.* J Gen Microbiol, 1990. **136**(4): p. 717-25.

49. Thomashow, L.S. and S.C. Rittenberg, *Isolation and composition of sheathed flagella from Bdellovibrio bacteriovorus 109J.* J Bacteriol, 1985. **163**(3): p. 1047-54.

50. Geis, G., et al., *Ultrastructure and biochemical studies of the flagellar sheath of Helicobacter pylori.* J Med Microbiol, 1993. **38**(5): p. 371-7.

51. Laloux, G. and C. Jacobs-Wagner, *How do bacteria localize proteins to the cell pole?* J Cell Sci, 2014. **127**(Pt 1): p. 11-9.

52. Luke, C.J. and C.W. Penn, *Identification of a 29 kDa flagellar sheath protein in Helicobacter pylori using a murine monoclonal antibody.* Microbiology (Reading), 1995. **141 (Pt 3)**: p. 597-604.

53. Jones, A.C., et al., *A flagellar sheath protein of Helicobacter pylori is identical to HpaA, a putative N-acetylneuraminyllactose-binding hemagglutinin, but is not an adhesin for AGS cells.* J Bacteriol, 1997. **179**(17): p. 5643-7.

54. O'Toole, P.W., et al., *The putative neuraminyllactose-binding hemagglutinin HpaA of Helicobacter pylori CCUG 17874 is a lipoprotein.* J Bacteriol, 1995. **177**(21): p. 6049-57.

55. Lundstrom, A.M., et al., *HpaA shows variable surface localization but the gene expression is similar in different Helicobacter pylori strains.* Microb Pathog, 2001. **31**(5): p. 243-53.

56. Kojima, S. and D.F. Blair, *Solubilization and purification of the MotA/MotB complex of Escherichia coli.* Biochemistry, 2004. **43**(1): p. 26-34.

57. Chaban, B., I. Coleman, and M. Beeby, *Evolution of higher torque in Campylobacter-type bacterial flagellar motors.* Sci Rep, 2018. **8**(1): p. 97.

58. Zhou, J., S.A. Lloyd, and D.F. Blair, *Electrostatic interactions between rotor and stator in the bacterial flagellar motor.* Proc Natl Acad Sci U S A, 1998. **95**(11): p. 6436-41.

59. Hizukuri, Y., et al., *The peptidoglycan-binding (PGB) domain of the Escherichia coli pal protein can also function as the PGB domain in E. coli flagellar motor protein MotB.* J Biochem, 2009. **146**(2): p. 219-29.

60. Hizukuri, Y., S. Kojima, and M. Homma, *Disulphide cross-linking between the stator and the bearing components in the bacterial flagellar motor.* J Biochem, 2010. **148**(3): p. 309-18.

61. Blair, K.M., et al., *A molecular clutch disables flagella in the Bacillus subtilis biofilm.* Science, 2008. **320**(5883): p. 1636-8.

62. Pilizota, T., et al., *A molecular brake, not a clutch, stops the Rhodobacter sphaeroides flagellar motor.* Proc Natl Acad Sci U S A, 2009. **106**(28): p. 11582-7.

63. Lele, P.P., B.G. Hosu, and H.C. Berg, *Dynamics of mechanosensing in the bacterial flagellar motor.* Proc Natl Acad Sci U S A, 2013. **110**(29): p. 11839-44.

64. Tipping, M.J., et al., *Load-dependent assembly of the bacterial flagellar motor.* mBio, 2013. **4**(4).

65. Leake, M.C., et al., *Stoichiometry and turnover in single, functioning membrane protein complexes.* Nature, 2006. **443**(7109): p. 355-8.

66. Martinez, R.M., et al., *Characterization of two outer membrane proteins, FlgO and FlgP, that influence vibrio cholerae motility.* J Bacteriol, 2009. **191**(18): p. 5669-79.

67. Morris, D.C., et al., *Lipidation of an FlrC-dependent protein is required for enhanced intestinal colonization by Vibrio cholerae.* J Bacteriol, 2008. **190**(1): p. 231-9.

68. Zhu, S., et al., *Molecular architecture of the sheathed polar flagellum in Vibrio alginolyticus.* Proc Natl Acad Sci U S A, 2017. **114**(41): p. 10966-10971.

69. Beeby, M., et al., *Diverse high-torque bacterial flagellar motors assemble wider stator rings using a conserved protein scaffold.* Proc Natl Acad Sci U S A, 2016. **113**(13): p. E1917-26.

70. Rudner, D.Z. and R. Losick, *Protein subcellular localization in bacteria.* Cold Spring Harb Perspect Biol, 2010. **2**(4): p. a000307.

71. Balaban, M., S.N. Joslin, and D.R. Hendrixson, *FlhF and its GTPase activity are required for distinct processes in flagellar gene regulation and biosynthesis in Campylobacter jejuni.* J Bacteriol, 2009. **191**(21): p. 6602-11.

72. Schniederberend, M., et al., *The GTPase activity of FlhF is dispensable for flagellar localization, but not motility, in Pseudomonas aeruginosa.* J Bacteriol, 2013. **195**(5): p. 1051-60.

73. Pandza, S., et al., *The G-protein FlhF has a role in polar flagellar placement and general stress response induction in Pseudomonas putida.* Mol Microbiol, 2000. **36**(2): p. 414-23.

74. Kusumoto, A., et al., *Collaboration of FlhF and FlhG to regulate polar-flagella number and localization in Vibrio alginolyticus.* Microbiology, 2008. **154**(Pt 5): p. 1390-1399.

75. Doudna, J.A. and R.T. Batey, *Structural insights into the signal recognition particle.* Annu Rev Biochem, 2004. **73**: p. 539-57.

76. de Leeuw, E., et al., *Membrane association of FtsY, the E. coli SRP receptor.* FEBS Lett, 1997. **416**(3): p. 225-9.

77. de Leeuw, E., et al., *Anionic phospholipids are involved in membrane association of FtsY and stimulate its GTPase activity.* EMBO J, 2000. **19**(4): p. 531-41.

78. Lu, Y., et al., *Evidence for a novel GTPase priming step in the SRP protein targeting pathway.* EMBO J, 2001. **20**(23): p. 6724-34.

79. Freymann, D.M., et al., *Structure of the conserved GTPase domain of the signal recognition particle.* Nature, 1997. **385**(6614): p. 361-4.

80. Halic, M. and R. Beckmann, *The signal recognition particle and its interactions during protein targeting.* Curr Opin Struct Biol, 2005. **15**(1): p. 116-25.

81. Zelazny, A., et al., *The NG domain of the prokaryotic signal recognition particle receptor, FtsY, is fully functional when fused to an unrelated integral membrane polypeptide.* Proc Natl Acad Sci U S A, 1997. **94**(12): p. 6025-9.

82. Miller, J.D., et al., *GTP binding and hydrolysis by the signal recognition particle during initiation of protein translocation.* Nature, 1993. **366**(6453): p. 351-4.

83. Powers, T. and P. Walter, *Reciprocal stimulation of GTP hydrolysis by two directly interacting GTPases.* Science, 1995. **269**(5229): p. 1422-4.

84. Focia, P.J., et al., *Heterodimeric GTPase core of the SRP targeting complex.* Science, 2004. **303**(5656): p. 373-7.

85. Egea, P.F., et al., *Substrate twinning activates the signal recognition particle and its receptor.* Nature, 2004. **427**(6971): p. 215-21.

86. Peluso, P., et al., *Role of SRP RNA in the GTPase cycles of Ffh and FtsY.* Biochemistry, 2001. **40**(50): p. 15224-33.

87. Green, J.C., et al., *Recruitment of the earliest component of the bacterial flagellum to the old cell division pole by a membrane-associated signal recognition particle family GTP-binding protein.* J Mol Biol, 2009. **391**(4): p. 679-90.

88. Bange, G., et al., *The crystal structure of the third signal-recognition particle GTPase FlhF reveals a homodimer with bound GTP.* Proc Natl Acad Sci U S A, 2007. **104**(34): p. 13621-5.

89. Bange, G., et al., *Structural basis for the molecular evolution of SRP-GTPase activation by protein.* Nat Struct Mol Biol, 2011. **18**(12): p. 1376-80.

90. Schuhmacher, J.S., et al., *MinD-like ATPase FlhG effects location and number of bacterial flagella during C-ring assembly.* Proc Natl Acad Sci U S A, 2015. **112**(10): p. 3092-7.

91. Murray, T.S. and B.I. Kazmierczak, *FlhF is required for swimming and swarming in Pseudomonas aeruginosa.* J Bacteriol, 2006. **188**(19): p. 6995-7004.

92. Hendrixson, D.R. and V.J. DiRita, *Transcription of sigma54-dependent but not sigma28-dependent flagellar genes in Campylobacter jejuni is associated with*

formation of the flagellar secretory apparatus. Mol Microbiol, 2003. **50**(2): p. 687-702.

93. Li, X., et al., *Investigating the Role of FlhF Identifies Novel Interactions With Genes Involved in Flagellar Synthesis in Campylobacter jejuni.* Front Microbiol, 2020. **11**: p. 460.

94. Leipe, D.D., et al., *Classification and evolution of P-loop GTPases and related ATPases.* J Mol Biol, 2002. **317**(1): p. 41-72.

95. Balaban, M. and D.R. Hendrixson, *Polar flagellar biosynthesis and a regulator of flagellar number influence spatial parameters of cell division in Campylobacter jejuni.* PLoS Pathog, 2011. **7**(12): p. e1002420.

96. Gulbronson, C.J., et al., *FlhG employs diverse intrinsic domains and influences FlhF GTPase activity to numerically regulate polar flagellar biogenesis in Campylobacter jejuni.* Mol Microbiol, 2016. **99**(2): p. 291-306.

97. Guttenplan, S.B., S. Shaw, and D.B. Kearns, *The cell biology of peritrichous flagella in Bacillus subtilis.* Mol Microbiol, 2013. **87**(1): p. 211-29.

98. Rowlett, V.W. and W. Margolin, *The bacterial Min system.* Curr Biol, 2013. **23**(13): p. R553-6.

99. Hare, S., et al., *Identification, structure and mode of action of a new regulator of the Helicobacter pylori HP0525 ATPase.* EMBO J, 2007. **26**(23): p. 4926-34.

CHAPTER 2

THE FLAGELLATION PATTERN IN *HELICOBACTER PYLORI* IS INFLUENCED BY DIVERSE GENETIC DETERMINANTS

Katherine H. Gibson, Vincent J. Starai and Timothy R. Hoover. To be submitted to The Journal of Bacteriology.

ABSTRACT

In many polar flagellated bacteria, the localization and number of flagella are controlled by FlhF and FlhG, respectively. Most studies on FlhF and FlhG have been done in bacterial species that possess a single polar flagellum. *Helicobacter pylori*, a member of the subphylum Epsilonproteobacteria, has a lophotrichous arrangement of sheathed flagella. Deletion of *flhG* in *H. pylori* G27 altered the flagellation pattern from a normal distribution where most cells had ~4 flagella to a more even distribution in which a greater proportion of cells lacked flagella or possessed a single flagellum and a few cells were hyperflagellated (≥ 8 flagella per cell). As reported for *flhF* mutants in other polar flagellated bacteria, the *H. pylori* G27 Δ*flhF* mutant produced fewer flagella per cell, many of which localized to nonpolar sites. Three independent motile variants of the Δ*flhF* mutant were isolated. The number of flagella per cell for two of the motile variants was similar to that of the Δ*flhF* parent, but a higher proportion of flagella localized correctly to the cell pole in the variants. The third motile variant produced more flagella than the Δ*flhF* parent, but the proportion of flagella that localized to the cell pole did not differ significantly from that of the parental strain. Whole genome sequencing of the motile variants revealed all three had a frameshift mutation in *faaA*, which encodes an autotransporter that localizes to the flagellar sheath. We predict that in the absence of FlhF, FaaA inhibits flagellum assembly at the cell pole. The motile variant with an increased number of flagella had a missense mutation in *fliF* (encodes the MS-ring protein) that changed Asn-255 to aspartate. FlhF is thought to facilitate MS-ring assembly and we postulate the $FliF^{N255D}$ variant is enhanced in its ability to form the MS-ring in the absence of FlhF.

INTRODUCTION

The bacterial flagellum is a complex nanomachine that is organized into three basic structures referred to as the basal body, hook and filament [1-3]. The basal body, which anchors the flagellum in the cell envelope, includes a rotary motor and a flagellar protein export apparatus that transports axial components of the flagellum (e.g., rod, hook and filament subunits) across the cell membrane. The motor consists of the MS-ring (base for the motor), C-ring (switch complex that forms the rotor together with the MS-ring and also regulates motor rotation), rod (motor driveshaft), P- and L-rings (bushing for the motor), and stator (torque generator) [1-3]. The stator consists of four subunits of MotA and two subunits of MotB [4]. MotB has a transmembrane region and a C-terminal periplasmic region that anchors the stator to the peptidoglycan layer through interactions with the P-ring protein FlgI and the peptidoglycan layer [5, 6]. MotA has four transmembrane domains and with MotB forms a proton channel in the inner membrane that converts proton flow across the inner membrane into rotation of the motor through interactions of the stator with the rotor protein FliG [7, 8]. Torque is transmitted from the rod, through the hook and to the filament, which functions as a propeller. In addition to these core structures, the *H. pylori* flagellar motor has several additional features, including a basal disk, medial disk, proximal disk, outer disk, outer ring and cage-like structure that surrounds the motor [9].

The human gastric pathogen *Helicobacter pylori* uses a cluster of polar sheathed flagella for motility, which is required for colonization in animal models for infection [10, 11]. FlhF and FlhG control the flagellation patterns in several bacterial species with polar flagella, as well as in *Bacillus subtilis*, which has a peritrichous arrangement of flagella [12]. Genetic, biochemical and structural studies of FlhF and FlhG have provided valuable information on

how these proteins control flagellation patterns, but the mechanisms by which these proteins affect the proper location and number of flagella remain obscure. Moreover, most studies on FlhF or FlhG have been with bacteria that have a single polar flagellum, and little is known about the function of these proteins in bacteria with a lophotrichous arrangement of flagella.

FlhF belongs to the GTP-binding signal recognition particle family, which includes Ffh and FtsY, proteins required for targeting various secretory and membrane proteins to the cell membrane [13]. FlhF is a GTPase that cycles between a GTP-bound form, which facilitates flagellum assembly at the cell pole, and an inactive GDP-bound or apo-form [12]. In various polar-flagellated bacteria, deleting *flhF* reduces the proportion of flagellated cells and results in the localization of flagella to nonpolar sites [14-17]. Green and co-workers reported *Vibrio cholerae* FlhF localizes to the cell pole where it mediates assembly of a FliF-green fluorescent protein fusion (FliF is the MS-ring protein) into distinct fluorescent foci [15]. In *Campylobacter jejuni*, FlhF variants with reduced GTPase activity support flagellum biosynthesis, but many of the cells expressing the FlhF variants display aberrant flagellar phenotypes, including lack of flagella, multiple flagella at one cell pole, flagella at nonpolar sites, and significantly shorter flagella [14].

FlhG belongs to the MinD/ParA ATPase family whose members act in cell-division site determination and plasmid/chromosome partitioning [18]. Deleting *flhG* in bacteria that normally have a single polar flagellum typically results in hyperflagellation [19-23]. The N-terminal region of *B. subtilis* FlhG interacts with FlhF to stimulate the GTPase activity of FlhF, and a conserved glutamine residue in this region is required for the stimulation [24]. Substituting the conserved glutamine with alanine in *C. jejuni* FlhG (Q4) results in

hyperflagellation [25], which suggests *C. jejuni* FlhG controls flagella number by modulating the GTPase activity of FlhF. Upon binding ATP, *Geobacillus thermodenitrificans* FlhG forms a dimer and an amphipathic helix at the C-terminus known as the membrane targeting sequence (MTS) is exposed, which allows FlhG to interact with the inner membrane [26]. It is the ATP-bound form of FlhG that stimulates the GTPase activity of FlhF, converting it to its inactive GDP-bound form [12]. After hydrolyzing ATP, FlhG undergoes a conformation change that converts the protein to a monomer and buries the MTS in the protein [12, 26].

In addition to modulating flagella number, *C. jejuni* FlhG helps to prevent cell division near the cell pole [19]. In many bacteria, the Min system inhibits assembly of the cell division apparatus at the cell poles [27], but *C. jejuni* lacks the Min system. Components of the Min system include MinD; MinC, which inhibits FtsZ polymerization into the Z-ring; and MinE, which is a topological specificity factor that restricts MinCD complexes to the cell poles [28-33]. In *C. jejuni*, FlhG appears to function with components of the flagellar motor and switch complex to inhibit division at the cell poles [19].

To investigate the roles of *flhF* and *flhG* in controlling the flagellation pattern in *H. pylori*, we deleted the genes in *H. pylori* G27 and examined the motility and flagellation phenotypes of the resulting mutants. Deletion of *flhG* had little effect on motility, although a greater proportion of the mutant cells lacked flagella or possessed a single flagellum. Similar to what has been reported for *flhF* mutants in other bacteria [14-17], deleting *flhF* in *H. pylori* G27 resulted in a reduction in the number of flagella, as well as the improper placement of flagella at nonpolar sites. Three independent motile variants of the Δ*flhF* mutant were isolated and characterized. For two of the motile variants, the number of

flagella per cell was similar to that of the Δ*flhF* parental strain, but the motile variants had a significantly higher proportion of flagella that localized correctly to the cell pole. The third motile variant produced more flagella than the Δ*flhF* parental strain, but the proportion of polar flagella in this strain did not differ significantly from that of the parental strain. Mutations responsible for suppressing the motility defect were identified by re-sequencing the genomes of the motile variants. A missense mutation in *fliF* that altered Asn-255 to aspartate was identified in the motile variant that produced more flagella than the Δ*flhF* parental strain, suggesting the $FliF^{N255D}$ variant is enhanced in its ability to form the MS-ring in the absence of FlhF. A frameshift mutation in *faaA*, which encodes an autotransporter that localizes to the flagellar sheath [34], appeared to increase the proportion of flagella that localized correctly to the cell pole. We hypothesize that in the absence of FlhF, FaaA inhibits flagellum biosynthesis at the cell pole by interfering with assembly of motor components located in the periplasmic space or outer membrane.

RESULTS

Characterization of *flhF* and *flhG* deletion mutants in *H. pylori* G27. Previous studies reported that disrupting *flhG* (*ylxH*) in *H. pylori* 11A or *flhF* in *H. pylori* strains N6 and 88-3887 (motile isolate of 26695) resulted in loss of flagellum biosynthesis [35, 36]. Since *flhF* and *flhG* were disrupted by insertion of antibiotic resistance cassettes in these studies, the apparent requirement of *flhF* and *flhG* in flagellum biosynthesis may have been due to polar effects on the downstream flagellar genes *fliAMY*. To address this issue, we constructed unmarked deletions of *flhF* and *flhG* in *H. pylori* G27 and characterized the phenotypes of the resulting mutants.

Motility of the Δ*flhG* mutant in soft agar medium was unaffected, while motility of the Δ*flhF* mutant was impaired significantly (Fig. 2.1). To determine if the flagellation patterns of the Δ*flhG* and Δ*flhF* mutants were altered, cells of the mutants were examined by transmission electron microscopy (TEM). A histogram of the number of flagella per cell for wild type *H. pylori* G27 appeared symmetrical and unimodal, consistent with a normal distribution for the data (Fig. 2.2). Four flagella per cell was both the mode and mean for the wild-type sample and greater than 68% of the wild-type cells (82%) were within one standard deviation of the mean, providing further evidence for a normal distribution of the data. The histogram for the flagella counts of the Δ*flhG* mutant appeared to be bimodal with peaks at five (n=19) and two (n=18) flagella per cell (Fig. 2.2). In contrast to the hyperflagellated phenotype observed for deletion of *flhG* in bacteria that normally have a single polar flagellum [19-23], only a small fraction of the *H. pylori* Δ*flhG* mutant cells were hyperflagellated (>7 flagella per cell), although some cells had as many as twelve flagella. Compared to wild type, there were a greater number of cells with either no flagella or a single flagellum in the Δ*flhG* mutant population (18% versus 1%; Fig. 2.2). Taken together, these data indicate FlhG is not required for flagellar biosynthesis in *H. pylori*, but does play a role in controlling flagella number so that most cells in the population have approximately the same number of flagella.

As observed in other bacterial species [14, 21, 37], deletion of *flhF* in *H. pylori* G27 resulted in both a significant reduction of the number of flagella per cell (Fig. 2.2) and the incorrect placement of flagella at nonpolar sites (Fig. 2.3). Approximately 30% of the Δ*flhF* mutant cells lacked flagella, and ~45% of the cells had a single flagellum (Fig. 2.3). FlhF facilitates assembly of the MS-ring in *V. cholerae* [15], which likely accounts for the

reduced number of flagella for the *H. pylori* Δ*flhF* mutant. The flagellum assembly defect in the *H. pylori* Δ*flhF* mutant may also be exasperated by decreased expression of flagellar genes since transcriptional activation of the σ^{54}-dependent flagellar genes is responsive to a flagellum assembly checkpoint associated with the flagellar protein export apparatus [35, 38-41]. About 37% of the flagella of the Δ*flhF* mutant localized correctly to the cell pole, while the remaining flagella were located near the cell pole (subpolar; ~25% of the flagella) or on the side of the cell (lateral; ~37%) (Fig. 2.4).

Isolation and characterization of motile variants of the *H. pylori* Δ*flhF* mutant. To gain a better understanding of the mechanism by which FlhF controls the flagellation pattern of *H. pylori*, as well as find other genes that have possible roles in affecting flagellation in *H. pylori*, we sought to isolate and identify suppressors that rescued motility in the *H. pylori* Δ*flhF* mutant. The Δ*flhF* mutant was passaged six times successively in soft agar medium, with cells from the edge of the swim halo used to inoculate the subsequent passage. After the final passage, clonal isolates from three independent enrichments were examined for their motility in soft agar medium. The isolates had motilities in the soft agar medium that were significantly improved compared to the Δ*flhF* parental strain (Fig. 2.4), and were designated as Δ*flhF* motile variants 1 through 3 (MV1, MV2, and MV3). Motility of MV3 did not differ significantly from that of wild type, while the motilities of MV1 and MV2 were slightly less than that of wild type (Fig. 2.4).

Cells of the motile variants were examined by TEM to determine if their flagellation patterns differed from that of the Δ*flhF* parental strain. For MV1 and MV2, the number of flagella per cell did not differ significantly from that of the parental Δ*flhF* strain (Fig. 2.5). In contrast, the degree to which the MV3 cells were flagellated differed significantly from

that of the parental strain, having a lower proportion of non-flagellated cells and a higher proportion of cells that possessed >2 flagella per cell (Fig. 2.5). MV1 and MV2 localized a significantly higher proportion of flagella correctly to the cell pole compared to the parental strain, with 70 to 80% of the flagella positioned at the cell pole versus 37% for the Δ*flhF* parental strain (Table 2.1). There appeared to be an increase in the proportion of flagella that localized to the cell pole in MV3 (53%), but the difference compared to the Δ*flhF* parental strain was not significant (*p*-value = 0.29). Interestingly, a few of the cells for MV2 and MV3 had a single flagellum at each cell pole or amphitrichous arrangement of flagella, which was a phenotype that was not observed in wild type or Δ*flhF* parental strain.

Identification of mutations in the Δ*flhF* motile variants responsible for rescuing motility. Genome sequencing of the motile variants identified single nucleotide polymorphisms (SNPs) in their genomic DNA. All three motile variants had a frameshift mutation in *faaA* (HPG27_570), which encodes an autotransporter that localizes to the flagellar sheath [34]. The coding sequence of *faaA* is over 9.5 kbp in length and encodes a predicted protein that is 3,192 amino acid residues in length. MV1 and MV2 contained the same mutation in *faaA*, a deletion of a T residue within a seven-nucleotide repeat located at nucleotide position 5,041 of the *faaA* coding region. In the case of MV2, this was the only SNP identified, suggesting the frameshift mutation in *faaA* was responsible for the increase in the proportion of polar flagella in both MV2 and MV1. MV3 had a deletion of a G residue within a stretch of eight G residues near nucleotide position 7,921 of the *faaA* coding region.

MV1 and MV3 also contained SNPs in HPG27_170, but different alleles. HPG27_170 encodes a protein of unknown function, although a crystal structure for the corresponding protein in *H. pylori* 26695 (HP0184) has been reported that includes the ligands 1,2-ethanediol and 2-deoxyguanosine-5'-triphosphate (https://www.rcsb.org/structure/2atz). MV1 contained a frameshift mutation in HPG27_170, resulting in a truncation of the protein, while MV3 contained a missense mutation that changes Ala-43 to Val, which is located near a guanosine nucleotide binding pocket involving Tyr-35, Asn-36, Lys-37 and Phe-38.

MV3 contained an additional SNP in *fliF* (encodes the MS-ring protein) that resulted in a change of Asn-255 to Asp. A high-resolution structure of the MS-ring from *Salmonella enterica* serovar Typhimurium obtained by cryo-electron microscopy was recently reported [42]. Analysis of the *H. pylori* G27 FliF sequence using the Phyre2 program [43] revealed Asn-255 was in a region (residues 127 to 424) predicted to have significant structural homology (100% confidence; 37% amino acid identity) with the *S. enterica* serovar Typhimurium (*S.* Typhimurium) FliF protein.

FlhF and FlhG localize to the cell pole only transiently in *H. pylori*. FlhF and FlhG are reported to localize at the cell pole in various bacteria [15, 19, 44-47], and we wished to determine if FlhF and FlhG similarly localized to the cell pole in *H. pylori*. To examine the localization of FlhF and FlhG in *H. pylori*, we fused either cyan fluorescent protein (CFP) or yellow fluorescent protein (YFP), respectively, to the flagellar proteins and expressed the fusion proteins from the native loci of the flagellar genes. Motility of the strain expressing the FlhG-YFP fluorescent fusion did not differ from that of the wild type (40.3 ± 3.8 mm versus 42.7 ± 2.5 mm after 5 days, *p*-value = 0.42). The strain expressing the

FlhF-CFP fluorescent fusion was slightly more motile than the wild type (55.3 ± 1.3 mm versus 51.4 ± 2.1 mm, *p*-value = 0.003). Since the C-terminal fluorescent fusions did not interfere with motility, we inferred that the fusions do not interfere with the activity of FlhF or FlhG. Distinct fluorescent foci were not observed for the *H. pylori* cells expressing the FlhF-CFP fusion protein, but rather the fluorescence appeared as diffuse signal throughout the cell body (Fig. 2.6A). The FlhG-YFP fusion signal was generally diffuse as well, although distinct foci were observed at the cell pole in a small proportion of cells (Fig. 2.6B). Based on localization studies of FlhF and FlhG in other bacteria, we assume that FlhF and FlhG must reside at the flagellated cell pole during the earliest stages of flagellum assembly. Our data suggest the FlhF-CFP and FlhG-YFP fusion proteins exist predominantly in their GDP-/ADP- or apo-forms under the growth conditions used to prepare the cells for fluorescence microscopy.

FlhG does not substitute for MinD in cell division in *H. pylori*. Rather than use the Min system to prevent cell division near the cell pole, *C. jejuni* employs FlhG, working in conjunction with components of the flagellar motor and switch complex, to inhibit division at the cell poles [19]. *H. pylori flhG* complements the *C. jejuni flhG* mutation [19], indicating *H. pylori* FlhG can interact with the cell division machinery in *C. jejuni* to prevent cytokinesis at the cell pole and suggesting it may also be able to do so in *H. pylori*. To address this hypothesis, we deleted *minD* in the wild-type and Δ*flhG* mutant of *H. pylori* G27 and examined the phenotypes of the resulting mutants by light microscopy. Cells of the Δ*flhG* and Δ*minD* mutants were indistinguishable from the wild-type cells in terms of motility (Fig. 2.7). In contrast, the Δ*flhG*/Δ*minD* double mutant was significantly less motile than the wild-type (Fig. 2.7). Similar to a report by Nishida and co-workers on the

phenotype of a Δ*minD* mutant in *H. pylori* HPK5 [48], we observed the *H. pylori* G27 Δ*minD* mutant produced a significantly higher proportion of filamentous cells than wild type (Fig. 2.8). Cell length profiles for the wild type and Δ*flhG* mutant did not differ significantly from each other (Fig. 2.8). Deleting *flhG* in the Δ*minD* mutant did not alter the cell length profiles (Fig. 2.8), indicating loss of *flhG* in the Δ*minD* mutant does not exacerbate the cell division defect in the Δ*minD* mutant and suggesting further that FlhG does not substitute for MinD in cell division in *H. pylori.* However, the motility results are intriguing as only the Δ*flhG*/Δ*minD* double mutant was motility deficient. We do not know if the motility defect in the Δ*flhG*/Δ*minD* mutant is due to an impairment in flagellar biosynthesis, flagellum function or chemotaxis.

DISCUSSION

The molecular mechanisms used by bacteria to control their flagellation patterns is a fascinating but poorly understood area. Although recent studies on FlhF and FlhG from various bacterial species have provided valuable insights into structure-function relationships in these proteins [12, 14, 15, 19, 25, 26], elucidating the mechanisms by which FlhF and FlhG control the location and number of flagella has remained elusive. In addition, most studies on the roles of FlhF and FlhG in governing flagellation patterns have focused on bacteria that have a single polar flagellum and there are few reports on the roles for these proteins in bacteria that have other flagellar arrangements. In examining the roles of FlhF and FlhG in regulating the flagellation pattern in *H. pylori*, we found the phenotypes of *H. pylori flhF* and *flhG* mutants to be both similar and different from those reported for bacteria that have a single polar flagellum.

In contrast to the hyperflagellation and reduced motility phenotypes observed for *flhG* mutants in other bacteria [19-23], deletion of *flhG* in *H. pylori* did not result in hyperflagellation, save for a few cells in the population, nor did it influence motility. Wild-type *H. pylori* G27 cells displayed a normal distribution for the number of flagella per cell that was lost in the Δ*flhG* mutant (Fig. 2.2), indicating that FlhG plays a role in controlling flagella number in *H. pylori* so that all of the cells in the population have about the same number of flagella. Compared to wild type, a higher proportion of the *H. pylori* Δ*flhG* mutant cells were either aflagellated or had a single flagellum. The increased number of under-flagellated cells for the Δ*flhG* mutant may be due to unregulated FlhF activity that results in cells initiating assembly of more nascent flagella than can be completed with the levels of flagellar protein subunits synthesized. Insufficient levels of flagellar protein subunits might also explain the low number of hyperflagellated cells observed for the Δ*flhG* mutant. Alternatively, the increased proportion of under-flagellated cells for the Δ*flhG* mutant may have resulted from a defect in formation of the C-ring since FlhG from *B. subtilis* and *Shewanella putrefaciens* were reported to facilitate assembly of the C-ring *in vitro* [26], and the C-ring has a role in protein secretion by the flagellar protein export apparatus [49, 50].

The phenotype of the *H. pylori* Δ*flhF* mutant was similar to that reported for other bacterial species [14, 21, 37], namely, reduced motility, a high proportion of aflagellated cells, and a substantial number of flagella located at non-polar sites (Figs. 2.1-2.3). The proportion of flagella that localized to the cell pole in the *H. pylori* Δ*flhF* mutant was about 37% (Fig. 2.3; Table 2.1). For a rod-shaped bacterium with dimensions similar to the typical *H. pylori* cell, we estimated the area of the flagellated cell pole represents less than

10% of the total surface area. In addition to the polar flagella in the Δ*flhF* mutant, ~36% of the flagella in the mutant were positioned near the cell pole (Fig. 2.3; Table 2.1). These findings indicate flagella in the Δ*flhF* mutant are not distributed randomly around the cell periphery but tend to position at or near the cell pole in the absence of FlhF, suggesting other factors contribute to targeting flagella to the cell pole.

One factor that may contribute to polar localization of flagella is a landmark protein that recruits FliF or other flagellar proteins to the cell pole [51]. In *Caulobacter crescentus*, the landmark protein TipN is required for the correct placement of the flagellum at the cell pole rather than FlhF [52]. TipN, an integral membrane protein that localizes to the new pole in both daughter cells following cell division, recruits TipF, which in turn recruits PflI, both of which are required for correct flagellum placement [53, 54]. HubP is a landmark protein that works in concert with FlhG to control the number of flagella in *Vibrio* species. In *Vibrio alginolyticus*, HubP is thought to recruit FlhG to the cell pole where it inhibits the activity of FlhF to prevent hyperflagellation [55]. Both TipN and HubP are restricted phylogenetically and homologs of these proteins are not found in *H. pylori*.

Alternatively, FliF or other flagellar proteins may be recruited to the cell pole by lipid species, such as cardiolipin, that accumulate at the cell pole. The cardiolipin molecule has a small hydrophilic head and large hydrophobic tail consisting of four acyl side chains, and the cone-shaped structure of cardiolipin contributes to its accumulation in regions of the membrane with negative curvature, such as the cell pole or septum [56, 57]. In *E. coli*, localization of some proteins to the cell, including the osmosensory transporter ProP and the cardiolipin synthase ClsA, is dependent on cardiolipin [58, 59].

In *Vibrio* species and *Shewanella oneidensis*, FlhF-GFP fusion proteins form very distinct fluorescent foci at the cell pole [15, 45-47]. In contrast, we did not observe distinct fluorescent foci in *H. pylori* cells expressing the FlhF-CFP fusion protein, instead we observed a diffuse fluorescence signal throughout the cell body (Fig. 2.6A). The absence of polarization of the FlhF-CFP fusion protein in *H. pylori* may reflect the slower growth rate of the bacterium compared to *Vibrio* species. Compared to *Vibrio* species, initiation of flagellum assembly in *H. pylori* may proceed at a slower rate that is commensurate with the slower growth rate of *H. pylori*. Reduced rates in flagellum assembly initiation might be achieved if the *H. pylori* FlhG was more active than its counterpart in *Vibrio* species in stimulating GTP hydrolysis by FlhF. It would be interesting to test this hypothesis by examining the localization of the FlhF-CFP fusion protein in a *H. pylori* Δ*flhG* mutant or using an FlhF variant that is deficient in GTP hydrolysis.

Mutations in motile variants of the *H. pylori* Δ*flhF* mutant apparently rescued motility by increasing either the number of flagella or the proportion of polar flagella. The FliF^{N255D} variant expressed in MV3 apparently allowed *H. pylori* to synthesize more flagella in the absence of FlhF than wild-type FliF (Fig. 2.5). FliF forms the MS-ring, which is one of the earliest flagellar structures to assemble [60]. Together with the C-ring protein FliG, the MS-ring forms the rotor of the flagellar motor, as well as houses the flagellar protein export apparatus. FliF contains three ring-building motifs (RBMs) that are present in ring-forming proteins of other protein secretion systems [61]. RBM3 is formed by two stretches of sequence denoted as RBM3a and RBM3b, which are separated by a stretch of β-strands that form a structure referred to as the β-collar and forms the drive-shaft housing [42]. Ala-251 of *S.* Typhimurium FliF is located in an α-helix within RBM3a

and corresponds to Asn-255 of *H. pylori* FliF. In the *S.* Typhimurium MS-ring, RMB3 forms a ring with 33-fold symmetry and Ala-251 is located at the interface between RBM3s of adjacent FliF monomers [42]. The predicted location of Asn-255 in *H. pylori* MS-ring suggests the aspartate substitution at this position renders the complex more stable, which may account for the increased number of flagella in the Δ*flhF* mutant.

On the other hand, FliF monomers from other bacteria oligomerize on their own and the total surface area of the FliF monomer that is buried in the *S.* Typhimurium FliF ring is extensive, totaling 36% of the available monomer surface [42]. Thus, it is difficult to envision how a conservative change of Asn-255 to aspartate in *H. pylori* FlhF would enhance auto-assembly of the MS-ring. Alternatively, it is possible MS-ring assembly in *H. pylori* is inhibited by a protein that binds FliF to prevent its oligomerization, and the aspartate substitution at Asn-255 reduces the affinity of this other protein for FliF. If this hypothesis is correct, then FlhF may stimulate MS-ring assembly by promoting dissociation of the inhibitory protein from FliF. Isolation of additional suppressor mutations that rescue motility of the *H. pylori* Δ*flhF* mutant by increasing flagella number may lead to the identification of a potential inhibitor of FliF oligomerization.

A frameshift mutation in *faaA* apparently improved motility in the *H. pylori* Δ*flhF* mutant by increasing the proportion of flagella that localized correctly to the cell pole (Table 2.1). All three of the motile variants had frameshift mutations in *faaA*, with MV1 and MV2 having the same mutation, but the *faaA* allele in MV3 did not result in a significant increase in the proportion of polar flagella (Table 2.1). The frameshift mutation in the *faaA* allele from MV3 resulted from a deletion in a homopolymeric run of eight G residues and we postulate that low-level expression of FaaA occurs from the *faaA* due to

translational frameshifting, which accounted for the failure of the *faaA* allele to increase significantly the proportion of flagella that localized to the cell pole. Alternatively, the frameshift mutation in the *faaA* allele from MV3 is nearly 2,900 bp downstream of the frameshift in *faaA* from MV1 and MV2. Thus, MV3 has the potential of expressing a significantly longer truncated FaaA protein than MV1 and MV2, which may have accounted for the differences between the motile variants in the proportion of flagella that localized to the cell pole.

FaaA is a Type V secretion system transporter, also referred to as an autotransporter, that localizes to the flagellar sheath of *H. pylori* [34]. Autotransporters consist of two distinct regions, a β-barrel domain that usually occurs at the C-terminal end of the protein and resides in the outer membrane, and a passenger domain that is secreted across the outer membrane through the β-barrel domain [62]. Although the function of FaaA is unknown, passengers of autotransporters function as adhesins, toxins or enzymes. Our finding that a frameshift mutation in *faaA* increased the proportion of flagella that localized correctly to the cell pole in the Δ*flhF* mutant was enigmatic as disrupting *faaA* in *H. pylori* strains J99, X47 and 60190 resulted in decreased numbers of flagella and localization of some flagella to non-polar sites [34].

Our data suggest that in the absence of FlhF, FaaA interferes with assembly of flagella at the cell pole, which suggests a possible role for FaaA in coupling flagellum assembly with the biosynthesis of the flagellar sheath. How FaaA might accomplish this though is unclear. Deletion analysis of *faaA* would be valuable for determining if the β-barrel domain and/or passenger of FaaA are required for the inhibition of polar localization of flagella. In addition, further characterization, localization studies of FaaA and ultrastructural studies

of the flagellar motors in the Δ*flhF* and *faaA* suppressor strains will likely provide valuable insight into how FaaA influences polar localization of flagella.

MATERIALS AND METHODS

Bacterial strains and growth conditions. *E. coli* DH5α, which was used for cloning and plasmid construction, was grown in LB liquid or agar medium supplemented with ampicillin (100 μg/ml) or kanamycin (30 μg/ml) when appropriate. *H. pylori* strains were grown microaerobically under an atmosphere consisting of 10% CO_2, 4% O_2 and 86% N_2 at 37°C on tryptic soy agar (TSA) supplemented with 5% horse serum. Liquid cultures of *H. pylori* were grown in Brain Heart Infusion broth (BHI) supplemented with 5% heat-inactivated horse serum with shaking in serum bottles under an atmosphere consisting of 5% CO_2, 10% H_2, 10% O_2 and 75% N_2. *H. pylori* growth medium was supplemented with kanamycin (30 μg/ml) or sucrose (2.5%) where appropriate.

Strain construction. All primers used for PCR in the construction of *H. pylori* mutants are listed in Supplemental Table S2.1. Genomic DNA from *H. pylori* G27 was purified using the Wizard genomic DNA purification kit (Promega) and used as the PCR template to construct the deletion mutants. Primers 58 and 59 were used to amplify a 607 base pair region corresponding to the sequence directly upstream of *flhF*. Primers 60 and 61 were used to amplify a 617 base pair region corresponding to the sequence directly downstream of *flhF*. The resulting amplicons were joined by PCR SOEing and was incubated with *Taq* polymerase (Promega) at 72^o C for 1 h to add 3'-A overhangs, which facilitated cloning of the amplicon into the pGEM-T Easy vector (Promega) to generate plasmid pKHG27.

Plasmid pJC038 carries a cassette bearing a kanamycin-resistance gene (kan^R) and *Bacillus subtilis sacB* under control of the *H. pylori ureA* promoter [63]. The kan^R-*sacB* cassette from pJC038 was introduced into unique NheI and XhoI sites in plasmid pKHG27 to generate suicide plasmid pKHG30. The suicide plasmid was introduced by natural transformation into *H. pylori* G27 to replace *flhF* with the kan^R-*sacB* cassette through homologous recombination and were screened by plating on TSA supplemented with horse serum and kanamycin. Presence of the kan^R-*sacB* cassette (KG41) was verified by PCR. The kan^R-*sacB* cassette was removed by transforming plasmid pKHG27 into a kanamycin-resistant isolate and using a sucrose-based counter-selection to select for the desired recombinant [64]. The genotype of the resulting *H. pylori* G27 Δ*flhF* mutant (KG43) was confirmed by PCR.

A similar method was used to generate an unmarked deletion of *flhG*. Primers 143 and 144 were used to amplify a 611 base pair region corresponding to the upstream sequence of *flhG*. Primers 145 and 146 were used to amplify 720 base pairs corresponding to the downstream sequence of *flhG*. The resulting amplicons were joined by PCR SOEing. The resulting amplicon was incubated with *Taq* polymerase (Promega) at 72^o C for 1 h to add 3'-A overhangs, which facilitated cloning of the amplicon into the pGEM-T Easy vector (Promega) to generate plasmid pKHG31. Plasmid pKHG31 was cut at unique XhoI and NheI restriction sites and ligated with the *kan-sacB* cassette to generate plasmid pKHG33 which was introduced into *H. pylori* G27 generating KG46. Plasmid pKHG31 introduced into KG46 and screened on TSA supplemented with sucrose as described above. The genotype of the resulting *H. pylori* G27 Δ*flhG* mutant (KG47) was confirmed by PCR.

Primers 115 and 116 were used to amplify a 528 base pair region corresponding to the upstream sequence of *minD*. Primers 117 and 118 were used to amplify 523 base pairs corresponding to the downstream sequence of *minD*. The resulting amplicons were joined by PCR SOEing. The resulting amplicon was cloned into the pGEM-T Easy vector (Promega) to generate plasmid pKHG60. Plasmid pKHG60 was cut at unique XhoI and NheI restriction sites and ligated with the *kan-sacB* cassette to generate plasmid pKHG61which was introduced into *H. pylori* G27 and KG47 to replace *minD* with the kan^R-*sacB* cassette. Plasmid pKHG60 was introduced into kanamycin-resistant isolates to replace the kan^R-*sacB* cassette with the unmarked *minD* deletion as described above. The genotypes of the resulting *H. pylori* G27 Δ*minD* mutant (KG59) and G27 Δ*flhG* Δ*minD* (KG57) were confirmed by PCR.

PCR primers 58 and 69 amplified *flhF* and an upstream flanking region totaling 1,959 bp and omitting the *flhF* stop codon. Primers 70 and 71 were used to amplify CFP and added a flexible linker to the N-terminus of CFP (Gly-Ser-Ala-Gly-Ser-Gly). Primers 72 and 61 amplified a 585 bp downstream sequence of *flhF*. PCR SOEing was used to join the all three fragments, and the resulting amplicon was cloned into pGEM-T Easy to generate the suicide plasmid pKHG32. Plasmid pKHG32 was introduced KG41. Transformants where the *kan-sacB* cassette was replaced with the *flhF-cfp* allele were isolated by plating onto TSA supplemented with horse serum and sucrose as described above. The presence of *flhF-cfp* was confirmed by PCR generating strain KG56.

PCR primers 62 and 100 amplified *flhG* and an upstream flanking region totaling 1,379 bp and omitting the *flhG* stop codon. Primers 75 and 101 were used to amplify YFP and added a flexible linker to the N-terminus of YFP (Gly-Ser-Ala-Gly-Ser-Gly). Primers

102 and 103 amplified a 540 bp downstream sequence of *flhG*. PCR SOEing was used to join the all three fragments, and the resulting amplicon was cloned into pGEM-T Easy to generate the suicide plasmid pKHG62. Plasmid pKHG62 was introduced to KG46 to replace the kan^R-*sacB* cassette with the *flhG-yfp* allele, and plated onto TSA supplemented with horse serum and sucrose as described above. The presence of *flhG-yfp* was confirmed by PCR generating strain KG55.

Motility assay. Motility was assessed using a soft agar medium consisting of Mueller-Hinton broth, 10% heat-inactivated horse serum, 20 mM 2-(N-morpholino)ethanesulfonic acid (MES; pH 6.0), 5 μM $FeSO_4$ and 0.4% Noble agar. The soft agar medium was stab-inoculated with *H. pylori* cells grown for 5 days on TSA supplemented with horse serum. The inoculated plates were incubated for 7 days at 37° C in an atmospheric condition consisting of 10% CO_2, 4% O_2 and 86% N_2, after which the diameters of the swim halos emanating from the point of inoculation were measured. At least six replicates were done for each strain, mean values for the diameters of the swim halos were calculated, and the two-sample *t* test was used to determine statistical significance.

Isolation of motile variants of Δ*flhF* mutants. Motile variants of the *H. pylori* Δ*flhF* mutants were isolated by inoculating the mutant strains in soft agar medium and allowing the cells to migrate from the point of inoculation as described for the motility assay. Cells were picked from the edge of the swim halos, inoculated into soft agar medium, and allowed to migrate from the point of inoculation. The process was repeated five more times, at which point, cells from the edge of the swim halo were streaked onto TSA supplemented with 10% horse serum to obtain single colonies. Motilities of the cells from

the isolated colonies in soft agar medium were examined to verify that they were more motile than the parental Δ*flhF* strain.

Transmission electron microscopy. *H. pylori* cultures were grown to late-log phase (A_{600} = ~1.0) in BHI supplemented with 10% heat-inactivated horse serum. Cells from the cultures were collected by centrifugation, fixed with formaldehyde and glutaraldehyde, and stained with uranyl acetate as described [63]. Cells were visualized using a JEOL JEM 1011 transmission electron microscope operated at 80 kV. Flagella counts were determined for at least 100 cells for each strain. Mann-Whitney U test was employed to determine whether differences in number of flagella per cell or location of flagella for the various *H. pylori* strains were significant.

Light microscopy and cell length measurement. We examined cells by light microscopy (100X objective under oil immersion) and directly measured cells using Fiji software [65]. These length measurements were then sorted into 10 size groups and classified as minicells, normal cells, or elongated cells based on their length.

Fluorescence microscopy. *H. pylori* was grown on TSA supplemented with horse serum for 4 days. Cells were collected by centrifugation, resuspended in 1X phosphate buffered saline, then applied to a microscope slide and allowed to dry before heat fixation. One drop of ProLong Gold Antifade reagent (Thermo) was added to slides and allowed to cure overnight before sealing with a coverslip. FlhG-YFP was visualized on an Eclipse Ni fluorescence microscope (Nikon) using a YFP filter cube. Images were captured with a digital charge-coupled-device camera (Photometrics CoolSNAP MYO) and analyzed using NIS-Elements AR software version 4.20 (Nikon). FlhF-CFP was visualized on a DM IRB inverted microscope (Leica Microsystems) using a CFP filter cube and images captured

with a digital charge-coupled-device camera (Hamamatsu Photonics K.K.). Images were analyzed using Openlab version 5.5.0 (PerkinElmer).

DNA sequencing and analysis. Genomic libraries, prepared with the Illumina iTruSeq adaptor kit from 500 ng of gDNA from various *H. pylori* strains, were sequenced at the University of Georgia Genomics Facility by Illumina sequencing. Quality of the reads were assessed with FastQC and trimmed using Trimmomatic [66, 67]. Reads for *H. pylori* gDNA sequences were mapped using Bowtie2 with the published NCBI genome for *H. pylori* G27 (Accession no.: NC_011333.1) and visualized in Geneious. The gDNA sequence of the *H. pylori* Δ*flhF* mutant was aligned with that of *H. pylori* G27, which served as the backbone for aligning the gDNA sequences of the motile variants. SNPs were identified in the genome sequences of the motile variants using Geneious.

AUTHOR CONTRIBUTIONS

TRH and KHG designed experiments and wrote the manuscript. KHG performed all experiments. VJS oversaw the fluorescence microscopy experiments.

ACKNOWLEDGEMENTS

We thank Winsen Wijaya and Nathan Glueck for their technical assistance and Julien Bergeron for helpful discussions on FliF. This work was supported by NIH grants AI140444 and AI146907 to T.R.H.

Table 2.1. Distribution of flagella to various cell surface sites in the *H. pylori* G27 Δ*flhF* mutant and motile variants of the mutant.

	Percentage of flagella at cell surface site (number of flagella counted in parentheses)				
strain	**polar**	**subpolar**	**lateral**	**amphitrichous**	***p*-value[a]**
Δ*flhF* parent	37 (41)	36 (40)	27 (30)	0 (0)	
MV1	80 (53)	12 (8)	8 (5)	0 (0)	<0.00001
MV2	71 (40)	13 (7)	14 (8)	2 (1)	0.00043
MV3	53 (27)	11 (6)	30 (16)	4 (2)	0.29

[a]Statistical significance determine using Mann-Whitney U test.

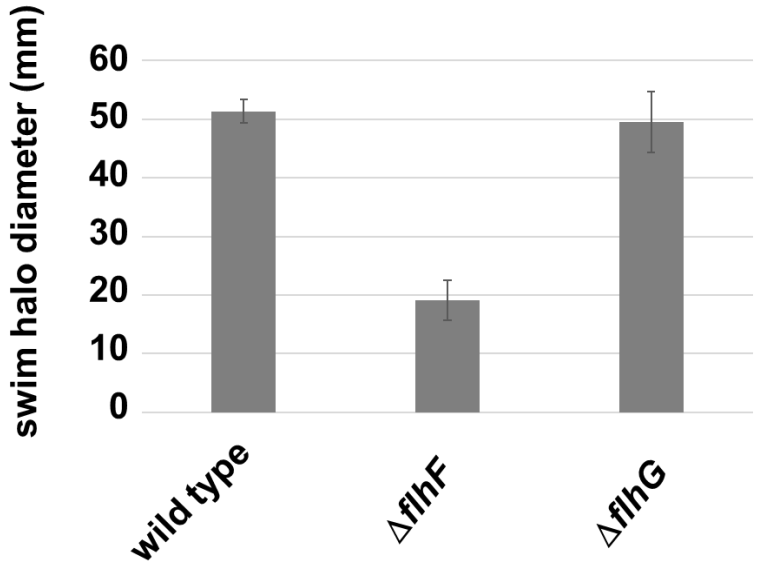

Figure 2.1. Motility phenotypes of the *H. pylori* G27 Δ*flhF* and Δ*flhG* mutants. Motility of the *H. pylori* G27 Δ*flhF* mutant in soft agar medium was reduced significantly compared to the wild type (*p*-value <0.00001). In contrast, motility of the *H. pylori* G27 Δ*flhG* mutant in soft agar medium was unimpaired. Gray bars indicate mean values for the swim halo diameter (n = 8 for wild type; n = 9 for the Δ*flhF* and Δ*flhG* mutants). Error bars indicate one standard deviation. Statistical analysis of the data was done using a two-sample *t* test.

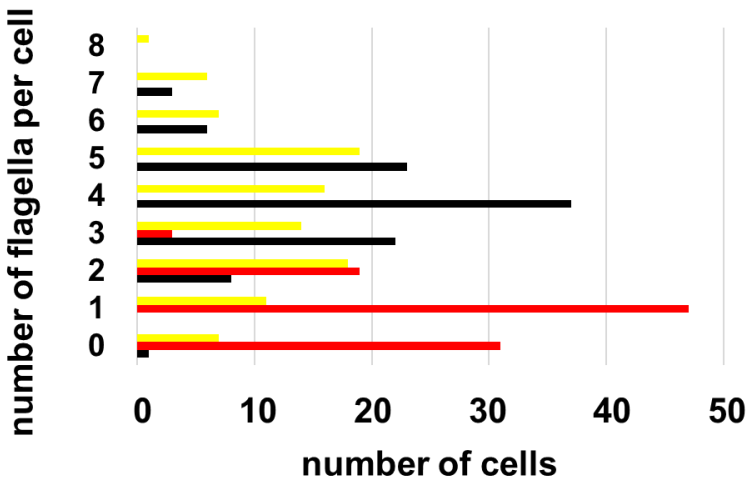

Figure 2.2. Flagella counts for the *H. pylori* G27 wild type, Δ*flhF* and Δ*flhG* mutant strains. Flagella were counted for 100 cells of each strain. Data for wild type are shown with black bars, data for Δ*flhF* mutant are presented with red bars, and data for Δ*flhG* mutant are indicated with yellow bars. One of the Δ*flhG* mutant cells that was counted had 12 flagella, which is not shown in the histogram. The mode, mean and standard deviation for the samples were: (wild type) 4, 4.0 and 1.2, respectively, (Δ*flhF* mutant) 1, 0.94 and 0.79, respectively, and (Δ*flhG* mutant) 5, 3.5 and 2.1, respectively. Distribution of the number of flagella per cell for both the Δ*flhF* (*p*-value <0.00001) and Δ*flhG* mutant (*p*-value = 0.035) differed from that of wild type. Statistical significance was determined using a Mann-Whitney U test.

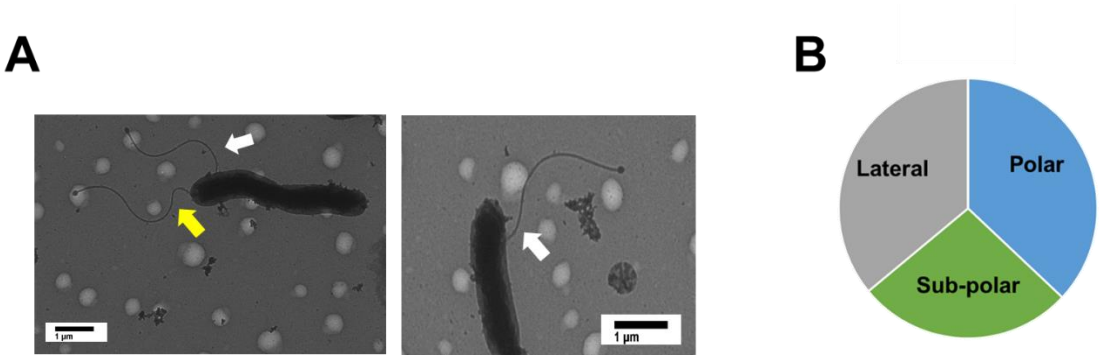

Figure 2.3. Flagella of *H. pylori* G27 Δ*flhF* mutant frequently localize improperly to nonpolar sites. (**A**) Transmission electron micrograph of Δ*flhF* mutant cells showing flagella located at nonpolar sites. White arrows indicate lateral flagella, and yellow arrow indicates a polar flagellum. Magnification 2000x. (**B**) Pie chart showing the distribution of flagella to polar, sub-polar or lateral sites for the Δ*flhF* mutant (n=100 cells).

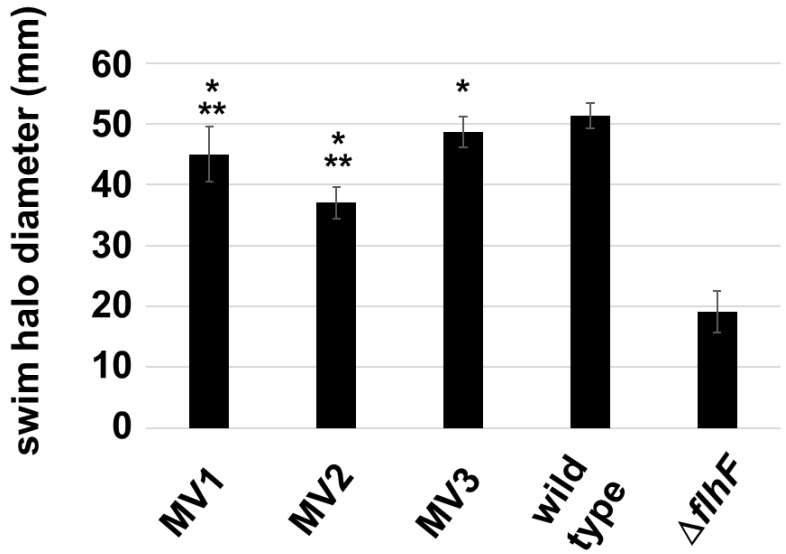

Figure 2.4. Motility phenotypes of the motile variants of the *H. pylori* G27 Δ*flhF* mutant. Motilities of the motile variants of the *H. pylori* G27 Δ*flhF* mutant in soft agar medium were significantly greater than that of the Δ*flhF* parental strain (indicated by *; *p*-value <0.00001). Motilities of MV1 and MV2 were significantly reduced compared to wild type (indicated by **; *p*-values = 0.008769 and <0.00001, respectively), whereas the motility of MV3 did not differ significantly from that of wild type (*p*-value = 0.099). Bars show mean values for the swim halo diameter (n = 3 for MV1, MV2 and MV3; n = 8 for wild type; n = 9 for the Δ*flhF* mutant). Error bars indicate one standard deviation. Statistical analysis of the data was done using a two-sample *t* test.

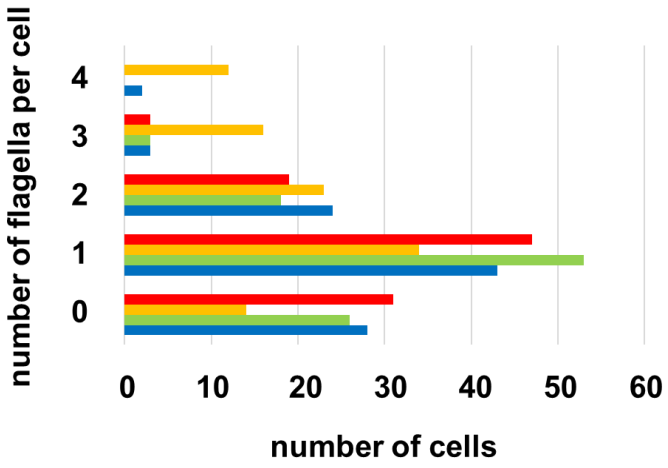

Figure 2.5. Flagella counts for the *H. pylori* G27 Δ*flhF* and motile variants of the Δ*flhF* mutant. Flagella were counted for 100 cells of each strain. Data for Δ*flhF* mutant are presented with red bars, data for MV1 are presented with blue bars, data for MV2 are presented with green bars, and data for MV3 are presented with orange bars. Distribution of the number of flagella per cell for MV3 differed from that of the Δ*flhF* parental strain (*p*-value <0.00001), while the distribution of the number of flagella per cell for MV1 and MV2 did not differ from that of the Δ*flhF* parental strain (*p*-values = 0.36 and 0.70, respectively). Mean values for the number of flagella per cell were 1.1, 0.98, 1.8 and 0.94 for MV1, MV2, MV3 and the Δ*flhF* parental strain, respectively. Statistical significance was determined using a Mann-Whitney U test.

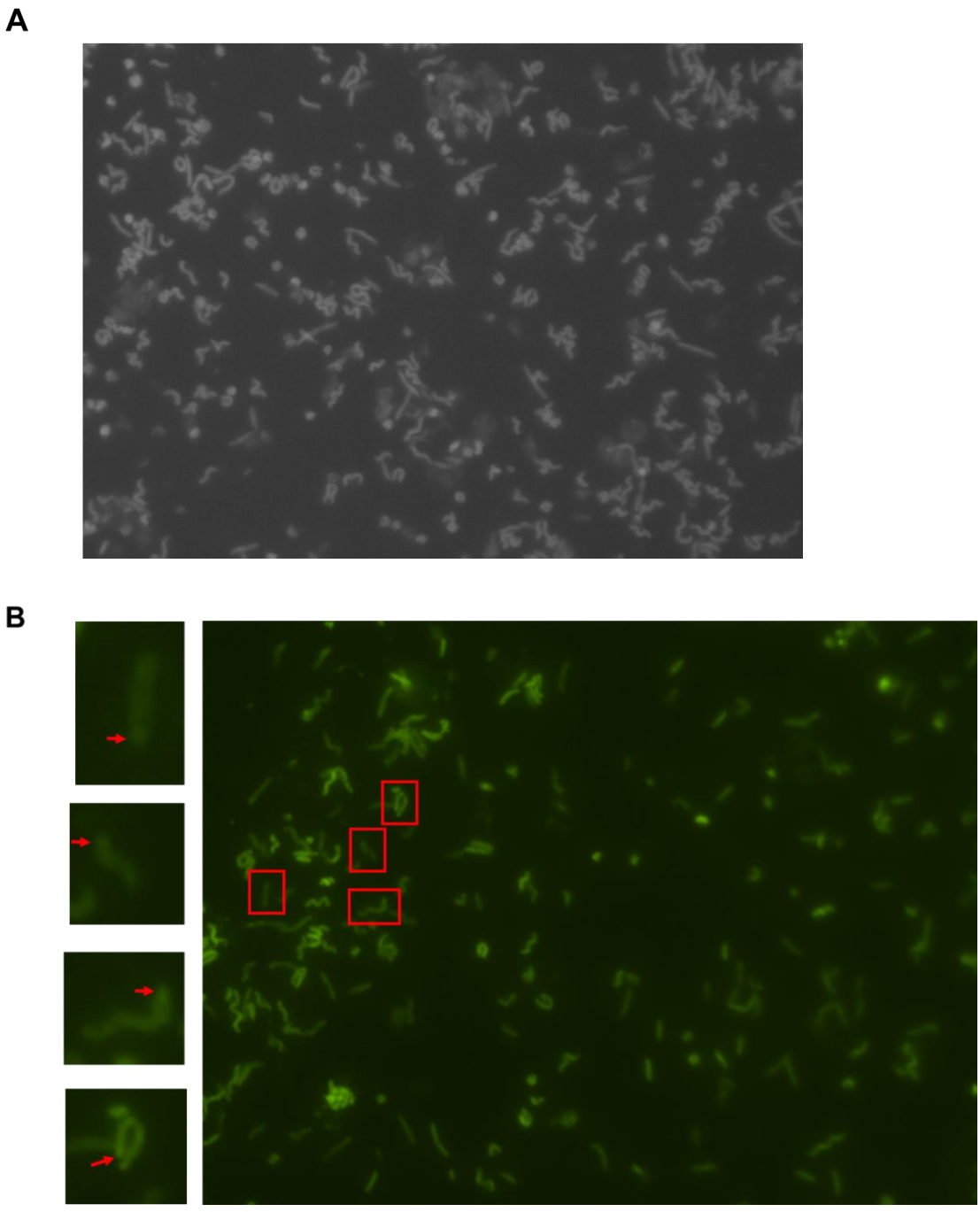

Figure 2.6. Fluorescence microscopy of FlhF-CFP and FlhG-YFP. Cells were applied to glass microscope slides and heat fixed, then stored in the dark until viewing. Slides were viewed under immersion oil using the 100X objective. **A.** FlhF-CFP cells exhibited diffuse fluorescent signal throughout the cell body. **B.** FlhG-YFP generally exhibited diffuse

fluorescent signal, but formed distinct foci at the cell pole in a small percentage of cells. Cells were viewed under 100X objective with immersion oil. Specific cells (red boxes) enlarged to show foci detail.

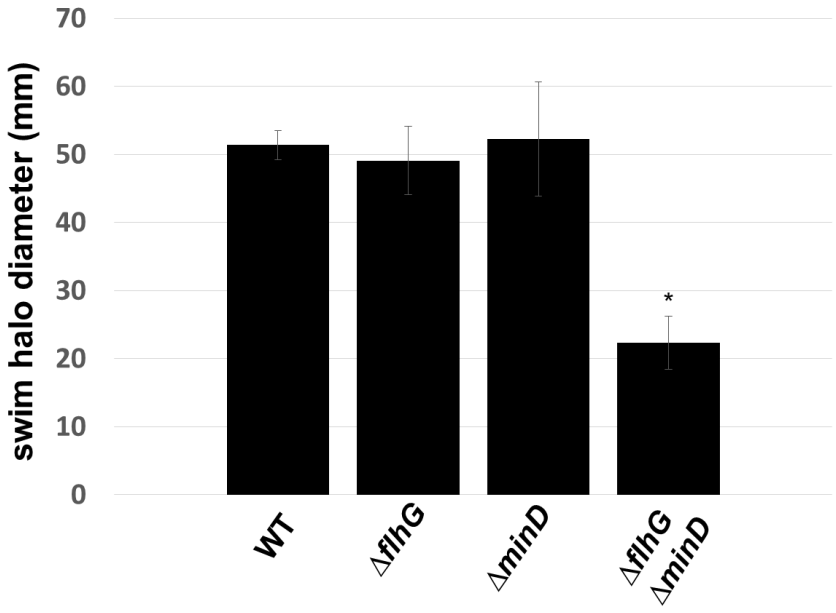

Figure 2.7. Motility of G27 wild type, Δ*flhG,* Δ*minD,* and Δ*flhG*/Δ*minD.* Motility of G27 Δ*flhG* and Δ*minD* mutants was uninhibited, while motility of the Δ*flhG*/Δ*minD* (*p <0.00001) mutant was significantly impaired. Gray bars indicate mean values for the swim halo diameter (n = 8 for wild type; n = 9 for the Δ*flhG* and Δ*flhG*/Δ*minD* mutants, n = 7 for Δ*minD* mutant). Error bars indicate one standard deviation. Statistical analysis of the data was done using a two-sample *t* test.

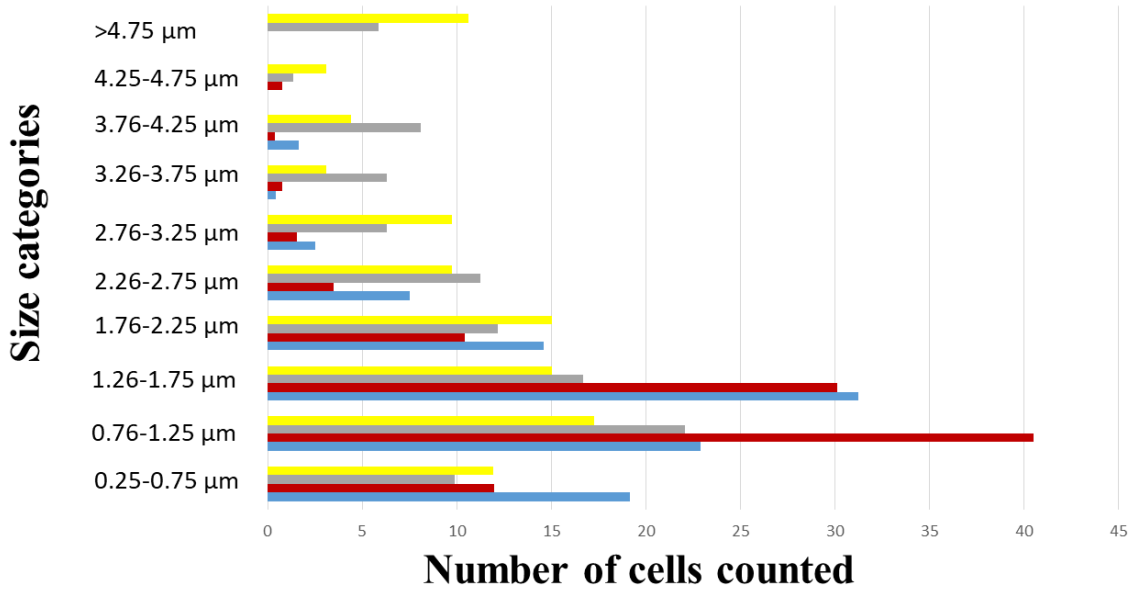

Figure 2.8. Cell length determination for G27 wild type, Δ*flhG*, Δ*minD*, and Δ*flhG*/Δ*minD*. Cell sizes were measured from light microscopy captured images using Fiji. Cells were then grouped into size classes. Wild type, blue bars; Δ*flhG*, dark red bars; Δ*minD*, grey bars; Δ*flhG*/Δ*minD*, yellow bars. The Δ*flhG* mutant did not have a significantly different length profile from the wild type. The Δ*minD* and Δ*flhG*/Δ*minD* mutants had a significantly different length profile compared to the wild type (p <0.0001) and from the Δ*flhG* mutant (p <0.00001), having more elongated cells than either the wild type or the Δ*flhG* mutant. The length profiles of the Δ*minD* and Δ*flhG*/Δ*minD* mutants did not differ. Significant was determined using a Mann-Whitney U test.

Table S2.1. List of primers used in this study.

Primer number	Name	Sequence
58	flhF US F	5’ AGG GCA TGG TGT TTT CTG
59	flhF US R + XhoI overhang	5’ GAA TTC GAT TAT CCT CGA GAG GTA TAG AAT TTC ACC ACT CC
60	flhF DS F + NheI overhang	5’ GAT AATCGA ATT CGC TAG CGC TTT AGT AAC CCT AAT AAG GAA C
61	flhF DS R	5’ TGT TAG CGA TAA GAA ACA ATT CAT
69	flhF R + linker + CFP overhang	5’ CCC GCT CCC AGC GCT CCC TGC TTG TTC CTT ATT AGG GTT AC
70	CFP F + linker + flhF overhang	5’ GGG AGC GCCT GGG AGC GGG ATG GTG AGC AAG GGC G
71	CFP F + flhF overhang	5’ CGG CTC GCT TGA TTG TCT ACT TGT ACA GCT CGT CCA TG
72	flhF DS F + CFP overhang	5’ CAT GGA CGA GCT GTA CAA GTA GAC AAT CAA GCG AGC CG
143	flhG US F	5’ ATC ACT TTA GAC AAT TAT CGC ATT GGG
144	flhG US R + XhoI + linker + NheI	5’ CTC GAG GAT CGA ATC GCT AGC TCC CTT ACC GCT TGT GAT AGC
145	flhG DS F + NheI + linker + XhoI	5’ GCT AGC GAT TCG ATC CTC GAG TTG AAA CGC TAT GTG AGG GAG
146	flhG DS R	5’ TGG CTA ATT TAA TCA ATT CTT CAG TGC
62	flhGH US F	5’ ACT TTA GAC AAT TAT CGC ATT GGG G
100	flhG R + YFP linker	5’ CCC GCT CCC AGC GCT CCC CCC CAA ATA ATT CAA AAG CCT TTT AAA AAA
75	YFP F + linker	5’ GGG AGC GCT GGG AGC GGG ATG GTG AGC AAG GGC GA
101	YFP R + flhG overhang	5’ TGG ATA AAA TTT TGC ACT TTC ATC AGC TTA CTT GTA CAG CTC GTC CA
102	flhG DS F + YFP overhang	5’ TGG ACG AGC TGT ACA AGT AAG CTG ATG AAA GTG CAA AAT TTT ATC CA
103	flhG DS R	5’ TGG CTA ATT TAA TCA ATT CTT CAG TGC

115	minD US F	5’ GAG CAA GCG GTT TTG TGC
116	minD US R + XhoI	5’ GCT AGC ATA ATC GAA TTC CTC GAG CTT TTT ACC GCT CTC AGC CAA
117	minD DS F + NheI	5’ CTC GAG GAA TTC GAT TAT GCT AGC CGC ATC ACC AGA CGG ATT
118	minD DS R	5’ AGC TAG AGT GAT CGT GTG TTG

Table S2.2. Plasmids and *H. pylori* strains used in this study.

Plasmid name	**Description**	**Reference**
pKHG27	pGEM-T Easy *flhF* flanking sequences	This study
pKHG30	pGEM-T Easy *flhF::*kan^R-*sacB*	This study
pKHG31	pGEM-T Easy *flhG* flanking sequences	This study
pKHG33	pGEM-T Easy *flhG::*kan^R-*sacB*	This study
pKHG32	pGEM-T Easy *flhF-cfp*	This study
pKHG60	pGEM-T Easy *minD* flanking sequences	This study
pKHG61	pGEM-T Easy *minD::*kan^R-*sacB*	This study
pKHG62	pGEM-T Easy *flhG-yfp*	This study
pJC038	pGEM-T Easy with kan^R-*sacB* cassette	[68]
***H. pylori* strain**	**Relevant Genotype**	
G27	Wild type	
KG41	*H. pylori* G27 *flhF::*kan^R-*sacB*	This study
KG43	*H. pylori* G27 Δ*flhF*	This study
KG46	*H. pylori* G27 *flhG::*kan^R-*sacB*	This study
KG47	*H. pylori* G27 Δ*flhG*	This study
KG55	*H. pylori* G27 *flhG-yfp*	This study
KG56	*H. pylori* G27 *flhF-cfp*	This study
KG57	*H. pylori* G27 Δ*flhG* Δ*minD*	This study
KG59	*H. pylori* G27 Δ*minD*	This study

REFERENCES

1. Berg, H.C., *The rotary motor of bacterial flagella.* Annu Rev Biochem, 2003. **72**: p. 19-54.

2. Chevance, F.F. and K.T. Hughes, *Coordinating assembly of a bacterial macromolecular machine.* Nat Rev Microbiol, 2008. **6**(6): p. 455-65.

3. Macnab, R.M., *How bacteria assemble flagella.* Annu Rev Microbiol, 2003. **57**: p. 77-100.

4. Kojima, S. and D.F. Blair, *Solubilization and purification of the MotA/MotB complex of Escherichia coli.* Biochemistry, 2004. **43**(1): p. 26-34.

5. Hizukuri, Y., S. Kojima, and M. Homma, *Disulphide cross-linking between the stator and the bearing components in the bacterial flagellar motor.* J Biochem, 2010. **148**(3): p. 309-18.

6. Hizukuri, Y., et al., *The peptidoglycan-binding (PGB) domain of the Escherichia coli pal protein can also function as the PGB domain in E. coli flagellar motor protein MotB.* J Biochem, 2009. **146**(2): p. 219-29.

7. Blair, D.F. and H.C. Berg, *The MotA protein of E. coli is a proton-conducting component of the flagellar motor.* Cell, 1990. **60**(3): p. 439-49.

8. Stolz, B. and H.C. Berg, *Evidence for interactions between MotA and MotB, torque-generating elements of the flagellar motor of Escherichia coli.* J Bacteriol, 1991. **173**(21): p. 7033-7.

9. Qin, Z., et al., *Imaging the motility and chemotaxis machineries in Helicobacter pylori by cryo-electron tomography.* J Bacteriol, 2017. **199**(3): p. e00695-16.

10. Eaton, K.A., D.R. Morgan, and S. Krakowka, *Motility as a factor in the colonisation of gnotobiotic piglets by Helicobacter pylori.* J. Med. Microbiol., 1992. **37**: p. 123-127.

11. Ottemann, K.M. and A.C. Lowenthal, *Helicobacter pylori uses motility for initial colonization and to attain robust infection.* Infect Immun, 2002. **70**(4): p. 1984-90.

12. Schuhmacher, J.S., K.M. Thormann, and G. Bange, *How bacteria maintain location and number of flagella?* FEMS Microbiol Rev, 2015. **39**(6): p. 812-22.

13. Halic, M. and R. Beckmann, *The signal recognition particle and its interactions during protein targeting.* Curr Opin Struct Biol, 2005. **15**(1): p. 116-25.

14. Balaban, M., S.N. Joslin, and D.R. Hendrixson, *FlhF and its GTPase activity are required for distinct processes in flagellar gene regulation and biosynthesis in Campylobacter jejuni.* J Bacteriol, 2009. **191**(21): p. 6602-11.

15. Green, J.C., et al., *Recruitment of the earliest component of the bacterial flagellum to the old cell division pole by a membrane-associated signal recognition particle family GTP-binding protein.* J Mol Biol, 2009. **391**(4): p. 679-90.

16. Murray, T.S. and B.I. Kazmierczak, *FlhF is required for swimming and swarming in Pseudomonas aeruginosa.* J Bacteriol, 2006. **188**(19): p. 6995-7004.

17. Pandza, S., et al., *The G-protein FlhF has a role in polar flagellar placement and general stress response induction in Pseudomonas putida.* Mol Microbiol, 2000. **36**(2): p. 414-23.

18. Lutkenhaus, J., *The ParA/MinD family puts things in their place.* Trends Microbiol, 2012. **20**(9): p. 411-8.

19. Balaban, M. and D.R. Hendrixson, *Polar flagellar biosynthesis and a regulator of flagellar number influence spatial parameters of cell division in Campylobacter jejuni.* PLoS Pathog, 2011. **7**(12): p. e1002420.

20. Campos-Garcia, J., et al., *The Pseudomonas aeruginosa motR gene involved in regulation of bacterial motility.* FEMS Microbiol Lett, 2000. **184**(1): p. 57-62.

21. Correa, N.E., F. Peng, and K.E. Klose, *Roles of the regulatory proteins FlhF and FlhG in the Vibrio cholerae flagellar transcription hierarchy.* J Bacteriol, 2005. **187**(18): p. 6324-32.

22. Dasgupta, N., S.K. Arora, and R. Ramphal, *fleN, a gene that regulates flagellar number in Pseudomonas aeruginosa.* J Bacteriol, 2000. **182**(2): p. 357-64.

23. Kusumoto, A., et al., *Regulation of polar flagellar number by the flhF and flhG genes in Vibrio alginolyticus.* J Biochem, 2006. **139**(1): p. 113-21.

24. Bange, G., et al., *Structural basis for the molecular evolution of SRP-GTPase activation by protein.* Nat Struct Mol Biol, 2011. **18**(12): p. 1376-80.

25. Gulbronson, C.J., et al., *FlhG employs diverse intrinsic domains and influences FlhF GTPase activity to numerically regulate polar flagellar biogenesis in Campylobacter jejuni.* Mol Microbiol, 2016. **99**(2): p. 291-306.

26. Schuhmacher, J.S., et al., *MinD-like ATPase FlhG effects location and number of bacterial flagella during C-ring assembly.* Proc Natl Acad Sci U S A, 2015. **112**(10): p. 3092-7.

27. Barak, I. and A.J. Wilkinson, *Division site recognition in Escherichia coli and Bacillus subtilis.* FEMS Microbiol Rev, 2007. **31**(3): p. 311-26.

28. de Boer, P.A., R.E. Crossley, and L.I. Rothfield, *Roles of MinC and MinD in the site-specific septation block mediated by the MinCDE system of Escherichia coli.* J Bacteriol, 1992. **174**(1): p. 63-70.

29. Fu, X., et al., *The MinE ring required for proper placement of the division site is a mobile structure that changes its cellular location during the Escherichia coli division cycle.* Proc Natl Acad Sci U S A, 2001. **98**(3): p. 980-5.

30. Hu, Z. and J. Lutkenhaus, *Topological regulation of cell division in E. coli. spatiotemporal oscillation of MinD requires stimulation of its ATPase by MinE and phospholipid.* Mol Cell, 2001. **7**(6): p. 1337-43.

31. Hu, Z., et al., *The MinC component of the division site selection system in Escherichia coli interacts with FtsZ to prevent polymerization.* Proc Natl Acad Sci U S A, 1999. **96**(26): p. 14819-24.

32. Marston, A.L. and J. Errington, *Selection of the midcell division site in Bacillus subtilis through MinD-dependent polar localization and activation of MinC.* Mol Microbiol, 1999. **33**(1): p. 84-96.

33. Raskin, D.M. and P.A. de Boer, *MinDE-dependent pole-to-pole oscillation of division inhibitor MinC in Escherichia coli.* J Bacteriol, 1999. **181**(20): p. 6419-24.

34. Radin, J.N., et al., *Flagellar localization of a Helicobacter pylori autotransporter protein.* mBio, 2013. **4**(2): p. e00613-12.

35. Niehus, E., et al., *Genome-wide analysis of transcriptional hierarchy and feedback regulation in the flagellar system of Helicobacter pylori.* Mol Microbiol, 2004. **52**(4): p. 947-61.

36. van Amsterdam, K. and A. van der Ende, *Helicobacter pylori HP1034 (ylxH) is required for motility.* Helicobacter, 2004. **9**(5): p. 387-95.

37. Kusumoto, A., et al., *Collaboration of FlhF and FlhG to regulate polar-flagella number and localization in Vibrio alginolyticus.* Microbiology, 2008. **154**(Pt 5): p. 1390-9.

38. Boll, J.M. and D.R. Hendrixson, *A regulatory checkpoint during flagellar biogenesis in Campylobacter jejuni initiates signal transduction to activate transcription of flagellar genes.* MBio, 2013. **4**(5): p. e00432-13.

39. Tsang, J., et al., *Helicobacter pylori FlhA Binds the Sensor Kinase and Flagellar Gene Regulatory Protein FlgS with High Affinity.* J Bacteriol, 2015. **197**(11): p. 1886-92.

40. Tsang, J. and T.R. Hoover, *Requirement of the flagellar protein export apparatus component FliO for optimal expression of flagellar genes in Helicobacter pylori.* J Bacteriol, 2014. **196**(15): p. 2709-17.

41. Tsang, J., et al., *Insertion mutations in Helicobacter pylori flhA reveal strain differences in RpoN-dependent gene expression.* Microbiology, 2013. **159**(Pt 1): p. 58-67.

42. Johnson, S., et al., *Symmetry mismatch in the MS-ring of the bacterial flagellar rotor explains the structural coordination of secretion and rotation.* Nature Microbiology, 2020. **5**(7): p. 966-+.

43. Kelley, L.A., et al., *The Phyre2 web portal for protein modeling, prediction and analysis.* Nature Protocols, 2015. **10**(6): p. 845-858.

44. Takekawa, N., et al., *HubP, a Polar Landmark Protein, Regulates Flagellar Number by Assisting in the Proper Polar Localization of FlhG in Vibrio alginolyticus.* J Bacteriol, 2016. **198**(22): p. 3091-3098.

45. Gao, T., et al., *Investigation into FlhFG reveals distinct features of FlhF in regulating flagellum polarity in Shewanella oneidensis.* Mol Microbiol, 2015. **98**(3): p. 571-85.

46. Kusumoto, A., et al., *Collaboration of FlhF and FlhG to regulate polar-flagella number and localization in Vibrio alginolyticus.* Microbiology, 2008. **154**(Pt 5): p. 1390-1399.

47. Kondo, S., et al., *Biochemical analysis of GTPase FlhF which controls the number and position of flagellar formation in marine Vibrio.* Sci Rep, 2018. **8**(1): p. 12115.

48. Nishida, Y., et al., *Intrinsic characteristics of Min proteins on the cell division of Helicobacter pylori.* FEMS Microbiol Lett, 2016. **363**(6).

49. Irikura, V.M., et al., *Salmonella typhimurium fliG and fliN mutations causing defects in assembly, rotation, and switching of the flagellar motor.* J Bacteriol, 1993. **175**(3): p. 802-10.

50. Paul, K., et al., *Energy source of flagellar type III secretion.* Nature, 2008. **451**(7177): p. 489-92.

51. Treuner-Lange, A. and L. Sogaard-Andersen, *Regulation of cell polarity in bacteria.* J Cell Biol, 2014. **206**: p. 7-17.

52. Lam, H., W.B. Schofield, and C. Jacobs-Wagner, *A landmark protein essential for establishing and perpetuating the polarity of a bacterial cell.* Cell, 2006. **124**(5): p. 1011-23.

53. Davis, N.J., et al., *De- and repolarization mechanism of flagellar morphogenesis during a bacterial cell cycle.* Genes Dev, 2013. **27**(18): p. 2049-62.

54. Obuchowski, P.L. and C. Jacobs-Wagner, *PflI, a protein involved in flagellar positioning in Caulobacter crescentus.* J Bacteriol, 2008. **190**(5): p. 1718-29.

55. Takekawa, N., et al., *HubP, a polar landmark protein, regulates flagellar number by assisting in the proper polar localization of FlhG in Vibrio alginolyticus.* J Bacteriol, 2016. **198**: p. 3091-3098.

56. Kawai, F., et al., *Cardiolipin domains in Bacillus subtilis Marburg membranes.* J Bacteriol, 2004. **186**(5): p. 1475-83.

57. Mileykovskaya, E. and W. Dowhan, *Visualization of phospholipid domains in Escherichia coli by using the cardiolipin-specific fluorescent dye 10-N-nonyl acridine orange.* J Bacteriol, 2000. **182**(4): p. 1172-5.

58. Romantsov, T., et al., *Cardiolipin synthase A colocalizes with cardiolipin and osmosensing transporter ProP at the poles of Escherichia coli cells.* Mol Microbiol, 2018. **107**(5): p. 623-638.

59. Romantsov, T., et al., *Cardiolipin promotes polar localization of osmosensory transporter ProP in Escherichia coli.* Mol Microbiol, 2007. **64**(6): p. 1455-65.

60. Jones, C.J. and R.M. Macnab, *Flagellar Assembly in Salmonella-Typhimurium - Analysis with Temperature-Sensitive Mutants.* Journal of Bacteriology, 1990. **172**(3): p. 1327-1339.

61. Bergeron, J.R., *Structural modeling of the flagellum MS ring protein FliF reveals similarities to the type III secretion system and sporulation complex.* Peerj, 2016. **4**.

62. Meuskens, I., et al., *Type V Secretion Systems: An Overview of Passenger Domain Functions.* Front Microbiol, 2019. **10**: p. 1163.

63. Chu, J.K., et al., *Loss of a cardiolipin synthase in Helicobacter pylori G27 blocks flagellum assembly.* J Bacteriol, 2019. **201**(21): p. e00372-19.

64. Copass, M., G. Grandi, and R. Rappuoli, *Introduction of unmarked mutations in the Helicobacter pylori vacA gene with a sucrose sensitivity marker.* Infect Immun, 1997. **65**(5): p. 1949-52.

65. Schindelin, J., et al., *Fiji: an open-source platform for biological-image analysis.* Nat Methods, 2012. **9**(7): p. 676-82.

66. Andrews, S., *FastQC: A quality control tool for high throughput sequence data.* 2014.

67. Bolger, A.M., M. Lohse, and B. Usadel, *Trimmomatic: a flexible trimmer for Illumina sequence data.* Bioinformatics, 2014. **30**(15): p. 2114-20.

68. Chu, J.K., et al., *Loss of a Cardiolipin Synthase in Helicobacter pylori G27 Blocks Flagellum Assembly.* J Bacteriol, 2019. **201**(21).

CHAPTER 3

A CONSERVED PROTEIN IN THE EPSILONPROTEOBACTERIA INFLUENCES FLAGELLUM FUNCTION IN *HELICOBACTER PYLORI*

Katherine H. Gibson, Vincent Starai and Timothy R. Hoover. To be submitted to the Journal of Bacteriology.

ABSTRACT

Members of the subphylum Epsilonproteobacteria have a conserved gene downstream of the flagellar genes *flhFG*. Deleting the gene in *Helicobacter pylori* G27 resulted in reduction in motility and the number of flagella per cell, and so we designated the gene *flhH*. Spontaneous mutations in the Δ*flhH* mutant that rescued motility were isolated and single nucleotide polymorphisms (SNPs) in motile variants were identified by whole genome sequencing. All three motile variants had a frameshift mutation in *faaA*, which encodes an autotransporter that localizes to the flagellar sheath, as well as mutations in *flaG*-2 that resulted in expression of truncated FlaG-2 proteins. The motile variants had flagella that were substantially longer than the wild-type flagellum, which was apparently due to the mutations in *flaG*-2. Deleting *flaG*-2 failed to rescue motility in the Δ*flhH* mutant, suggesting that simply producing longer flagella is not sufficient for restoring motility. Alternatively, a truncated FlaG-2 variant may be needed for generating the longer flagella and rescuing motility in the Δ*flhH* mutant. We hypothesize FlhH plays a role in stabilizing the flagellar motor and the combination of longer flagella resulting from disrupting *flaG*-2 and inactivation of *faaA* mitigates the destabilization of the motor and allows the motor to operate efficiently.

INTRODUCTION

Flagellum-mediated motility is a trait that occurs in diverse bacterial species. The bacterial flagellum is organized into three basic parts, which are the basal body, hook and filament [1-3]. The basal body contains a rotary motor that is powered by ion-motive forces to generate torque needed for motility [4]. Torque from the motor is transmitted from the rod (motor driveshaft) to the filament through the hook, which propels the swimming cell.

The flagellar motor of Gram-negative bacteria consists of various ring structures, a rotor and associated membrane-bound stator complexes [1-3]. The flagellar rings include the MS-ring, which forms the baseplate for the motor; the C-ring, which contains the rotor protein FliG that engages the stator and a switch complex that regulates motor rotation; and the P- and L-rings, which form a bushing for the motor. The stator consists of four subunits of MotA and two subunits of MotB [5]. MotB has a transmembrane region and a C-terminal periplasmic region that stabilizes the stator to the peptidoglycan layer through interactions with the P-ring protein FlgI and the peptidoglycan layer [6, 7]. MotA has four transmembrane domains that forms a proton channel with MotB in the inner membrane, which converts ion flow across the inner membrane into rotation of the flagellar motor [8, 9]. The number of stators in the motor varies among bacterial species, with as few as 11 stators in the motors of *Escherichia coli* and *Salmonella enterica* serovar Typhimurium (*S.* Typhimurium) and up to 18 stators in the *Helicobacter pylori* motor [10-12]. Stator units are not permanently fixed at the motor, but rather engage and disengage with the motor from a pool of unbound stators in the membrane [13, 14]. In *E. coli*, the number of stators engaged within the motor varies according to the load, ranging from one or two under very low loads to an estimated 6-11 stators at high loads [15].

The human gastric pathogen *H. pylori*, a member of the subphylum Epsilonproteobacteria, uses a cluster of polar sheathed flagella for motility, which is required for colonization in animal models for infection [16, 17]. In many polar-flagellated bacteria, the localization and number of flagella are controlled by FlhF and FlhG, respectively [18]. *H. pylori* has homologs of FlhF and FlhG, although roles for these proteins in controlling the flagellation pattern of the bacterium have not been reported.

FlhF belongs to the GTP-binding signal recognition particle family that includes Ffh and FtsY, proteins that target various secretory and membrane proteins to the cell membrane [19]. FlhF is a GTPase and cycles between a GTP-bound form that facilitates flagellum assembly at the cell pole and an inactive GDP-bound or apo-form [18]. In various polar-flagellated bacteria, disrupting *flhF* results in a substantial reduction in the proportion of flagellated cells, as well as the improper localization of flagella to nonpolar sites [20-23]. Green and co-workers reported *Vibrio cholerae* FlhF localizes to the cell pole where it mediates assembly of a green fluorescent protein-tagged MS-ring protein (FliF-GFP) into distinct fluorescent foci [21].

FlhG, which is a member of the MinD/ParA ATPase family, controls the number of flagella in bacteria that have a single polar flagellum as deletion of the gene results in hyperflagellation [24-28]. A conserved glutamine residue in the N-terminal region of *B. subtilis* FlhG stimulates the GTPase activity of FlhF [29]. Substituting this conserved glutamine with an alanine in *C. jejuni* FlhG results in hyperflagellation [30], which suggests FlhG controls flagella number by modulating the GTPase activity of FlhF. Upon binding ATP, *Geobacillus thermodenitrificans* FlhG forms a dimer and exposes an amphipathic helix at the C-terminus, known as the membrane targeting sequence, which allows the

protein to interact with the inner membrane [31]. The ATP-bound form of FlhG stimulates the GTPase activity of FlhF, converting it to its inactive GDP-bound form [18]. After hydrolyzing ATP, FlhG undergoes a conformation change that converts the protein to a monomer and buries the membrane targeting sequence in the protein [18, 31].

Genomes of *H. pylori* and other Epsilonproteobacteria contain a conserved gene located immediately downstream of *flhFG* (Fig. 3.1). To determine if this conserved gene has a role in flagellum biosynthesis or function, we deleted it and found the resulting mutant was impaired in its motility and had fewer flagella per cell. Given the apparent role of the gene in flagellum biosynthesis and function, we designated it as *flhH*. Three independent motile variants of the Δ*flhH* mutant were isolated by enriching for cells with increased motility. The motile variants produced flagellar filaments that were longer than the wild-type filament. Whole genome sequencing indicated the motile variants had a frameshift mutation in *flaG*-2 (locus tag HPG27_708), which was apparently responsible for the long filament phenotype since disrupting *flaG*-2 homologs in *Pseudomonas fluorescens* and *Vibrio anguillarum* similarly results in flagella with unusually long filaments [32, 33]. In addition to the mutation in *flaG*-2, all three of the motile variants had a frameshift mutation in *faaA*, which encodes an autotransporter that localizes to the flagellar sheath [34]. Disrupting *flaG*-2 in a naïve Δ*flhH* mutant background did not rescue motility, suggesting that both mutations are required to rescue motility. We hypothesize that under conditions where the load on the motor is low, FlhH recruits or stabilizes MotA/MotB stator complexes to the motor. In the absence of FlhH, the *H. pylori* motor functions inefficiently low load conditions, but the longer filaments of the *flaG*-2 mutant mitigate the absence of FlhH by increasing the load on the motor. Loss of FlhH also appears to result in a reduction in the

number of flagella per cell. The reduction in the number of flagella may be due to a deficiency in flagellum assembly or may result from decreased stability of the flagellum and subsequent disassembly of flagella, which is mitigated by disrupting *faaA*.

RESULTS

A gene linked to *flhFG* in members of the subphylum Epsilonproteobacteria is required for motility in *H. pylori*. The original annotation of *H. pylori* 26695 [35] indicates a hypothetical gene downstream of *flhG* that is oriented in the opposition direction, although the annotation was subsequently shown to be incorrect and the gene was shown to be in the same orientation as *flhG* and given the locus tag HP1033b (Fig. 3.1) [36]. In *H. pylori* G27, HPG27_395 is the HP1033b homolog, and homologs of the gene are found immediately downstream of *flhG* in genomes of other members of the subphylum Epsilonproteobacteria (Fig. S3.1; Table S3.1). HPG27_395 encodes a predicted membrane protein 104 amino acids in length with two transmembrane helices near the N-terminus. HPG27_395 homologs in other Epsilonproteobacteria encode predicted proteins of similar size and membrane topology.

The synteny of HPG27_395 and its homologs with *flhFG* suggested a role for the gene in flagellar biosynthesis or function. To examine this hypothesis, we deleted HPG27_395 in *H. pylori* G27 and found the resulting mutant to be impaired in its motility in soft agar medium (Fig. 3.2). In addition, flagellar biosynthesis or stability was inhibited in the mutant as about half of the mutant cells either lacked flagella or possessed a single flagellum (Fig. 3.3). Given the apparent role of HPG27_395 in flagellum biosynthesis or stability in *H. pylori* G27, we designated the gene as *flhH*.

The linkage of *flhH* with *flhFG* suggested FlhH functions with FlhG or FlhF. Deletion of *flhG* in *H. pylori* G27 does not impact motility of the bacterium in soft agar medium, but does reduce the number of flagella per cell and results in a higher proportion of aflagellated cells (K. Gibson, manuscript in preparation) (Fig. 3.2, 3.3). To determine if an epistatic relationship existed between *flhG* and *flhH*, we deleted both genes and compared the phenotype of the resulting mutant with the phenotypes of the Δ*flhG* and Δ*flhH* mutants. The Δ*flhGH* mutant was slightly more motile than the Δ*flhH* mutant, but not as motile as the Δ*flhG* mutant (Fig. 3.2). The Δ*flhGH* mutant also possessed more flagella per cell than the Δ*flhH* mutant, but fewer flagella per cell than the Δ*flhG* mutant (Fig. 3.3). Taken together, these data indicate a lack of epistasis between *flhG* and *flhH*, suggesting FlhH does not exert its effect on flagellum biosynthesis and motility by modulating the activity of FlhG.

Deletion of *flhF* in *H. pylori* G27 inhibits motility of the bacterium, reduces the number of flagella per cell, increases the proportion of aflagellated cells, and results in the localization of flagella to non-polar sites (K. Gibson, Chapter 2). Flagella in the Δ*flhH* mutant localized correctly to the cell pole, indicating FlhF does not require FlhH to prevent assembly of flagella at non-polar sites. Cells of the Δ*flhF* mutant possessed slightly fewer flagella per cell than cells of the Δ*flhH* mutant (Fig. 3.3). Despite being less flagellated and having a significant proportion of the flagella improperly localized to non-polar sites, the Δ*flhF* mutant was more motile than the Δ*flhH* mutant in soft agar medium, which suggested a defect in flagellum function in the Δ*flhH* mutant.

Isolation of mutations that suppressed the motility defect in the *H. pylori* Δ*flhH* mutant. To identify mutations that by-pass the requirement of FlhH for robust motility, we enriched for variants of the Δ*flhH* mutant that had enhanced motilities in soft agar medium.

Three independent motile variants were isolated (designated MV1 through MV3) that had near wild-type motility in soft agar medium (Fig. 3.4A). Interestingly, all three of the motile variants possessed flagella that were substantially longer than normal (Fig. 3.4B). Measurements of flagellum length revealed that most of the flagella of MV1 and MV3 were significantly longer than the wild type, and were on average ~2.5 longer than the wild type flagella (Table 3.1). Although flagellar lengths in MV2 did not differ significantly from those in wild type (Table 3.1), ~25% of the MV2 flagella that were measured were longer than the longest flagellum measured for wild type. Two of the motile variants, MV1 and MV2, produced significantly more flagella per cell than the original Δ*flhH* mutant, although flagella number was not restored to wild type levels in these motile variants (Fig. 3.4C). Cells of MV3 appeared to be slightly more flagellated than those of the original Δ*flhH* mutant, but the difference was just above the cutoff value for being statistically significant (*p*-value = 0.057).

Whole-genome sequencing was done to identify single nucleotide polymorphisms (SNPs) in the genomes of the motile variants that might have been responsible for restoring motility. Each of the motile variants contained a SNP in *faaA* (HPG27_570) that resulted in a frameshift mutation. FaaA is an autotransporter (Type V protein secretion pathway protein) that shares homology with the vacuolating toxin VacA. MV1 and MV3 shared the same mutation in *faaA* (deletion of a guanine residue at nucleotide position 623), while MV2 had a deletion of a G residue in a homopolymeric run of eight G residues at nucleotide position 4,493. In addition to having SNPs in *faaA*, all three Δ*flhH* motile variants contained a SNP in HPG27_708 (*flaG*-2; homolog of *B. subtilis yvyC*). MV1 and MV3 had the same mutation in *flaG*-2, a C to T transition at nucleotide position 313 that changed the CAA

codon for Gln to a TAA stop codon and truncated the encoded protein by 15 amino acids. The *flaG*-2 mutation in MV2 was a deletion of a T at nucleotide position 102 that results in a frameshift resulting in a predicted truncated protein that includes only the first 33 (out of 119) amino acid residues of FlaG-2. The mutations in *flaG*-2 were likely responsible for the longer flagella of the Δ*flhH* motile variants, as mutations in *flaG*-2 homologs in *P. fluorescens* and *V. anguillarum* result in longer than normal flagella [32, 33].

Each of the Δ*flhH* motile variants possessed a third unique SNP. MV1 had an A to G transition at nucleotide position 85 in HPG27_543 (*fliN*, a C-ring protein) that resulted in an Ala substitution at Thr-29. MV2 had a C to T transition at nucleotide position 149 in HPG27_1372 (HP1451 in *H. pylori* 22695) that changed Ala-50 to Val. A crystal structure was reported for a fragment of the protein (amino acid residues 92 to 264) bound to the N-terminal domains of the hexameric Cag HP0525 ATPase and HP1451 is thought to regulate the activity of HP0525 ATPase [37]. MV3 had a deletion of an A residue in a homopolymeric run of nine A residues at nucleotide position 952 in HPG27_261, which encodes a member of the Trk A_C protein family (pfam02080; regulator of K+ conductance).

Since all three of the motile variants had mutations in *faaA* and *flaG*-2, we reasoned that one or both of these mutations were responsible for rescuing motility in the Δ*flhH* mutant. To examine this hypothesis, we deleted *flaG*-2 in the Δ*flhH* mutant. Deletion of *flaG*-2 by itself in the Δ*flhH* mutant failed to rescue motility (Fig. 3.5), suggesting that mutations in both *flaG*-2 and *faaA* are needed to fully rescue motility in the Δ*flhH* mutant.

Localization of a FlhH-YFP fusion. Given the role of FlhH in flagellum function, we wished to determine if it localized to the flagellated cell pole. A *flhH-yfp* fusion was

constructed and introduced into the *flhH* locus in *H. pylori* G27. The strain expressing the FlhH-YFP fusion exhibited wild-type motility in soft agar medium, suggesting the YFP fused to the C-terminal end of FlhH did not interfere with FlhH function (mean swim halo diameter 49 ± 3.6 mm, *p*-value = 0.37). Fluorescence microscopy of the *H. pylori* strain expressing the FlhH-YFP fusion revealed that fluorescence was distributed uniformly for most of the cells, but fluorescent foci at a single cell pole was observed in a small proportion of the cells (Fig. 3.6). These findings suggest FlhH localizes transiently to one of the cell poles, which we postulate to be the flagellated cell pole.

DISCUSSION

We report here on the identification of a novel flagellar gene, which we designate as *flhH*, that is conserved in members of the subphylum Epsilonproteobacteria. The synteny of *flhF*, *flhG* and *flhH* across a wide range of genera suggested FlhH functions with FlhF or FlhG. The lack of epistasis between *flhG* and *flhH*, however, argued against FlhH having a role in regulating the activity of FlhG (Figs. 3.2 and 3.3). Activity of GTPases is often regulated by a guanine nucleotide exchange factor (GEF), which facilitates the exchange of GTP for GDP in the inactive GDP-bound form of the GTPase [38]. A GEF for FlhF has not been described in any bacterial species [18], and while it is possible that FlhH acts as a GEF for FlhF, we do not believe that is the case. If FlhH is a GEF, we would predict FlhF to exist in its inactive GDP-bound form at a higher frequency in the Δ*flhH* mutant and result in decreased initiation of flagellum assembly. While the Δ*flhH* mutant did have fewer flagella than wild-type cells, most of the Δ*flhH* mutant cells were flagellated and >40% of the cells possessed multiple flagella (Fig. 3.3), which was inconsistent with the severe

decrease in motility observed for the Δ*flhH* mutant (Fig. 3.2). Indeed, the Δ*flhF* mutant was more motile than the Δ*flhH* mutant in soft agar medium, even though the Δ*flhF* mutant was less flagellated than the Δ*flhH* mutant. These data suggest the flagella of the Δ*flhH* mutant do not function efficiently under the conditions in the soft agar motility assay.

Disruption of *flaG-2* resulted in significantly longer flagellar filaments, which we hypothesize is needed to restore motility in the Δ*flhH* mutant. Although deletion of *flaG-2* did not rescue motility of the Δ*flhH* mutant, we did not visualize the Δ*flhH*/Δ*flaG-2* strain by TEM to confirm the presence of long flagella. It is possible the truncated FlaG-2 variant produced in MV1 and MV3, which is missing 15 amino acid residues from the C-terminus, is necessary to produce the longer flagella and thus increased motility. Consistent with this hypothesis, the more severe truncation of the FlaG-2 variant expressed in MV2 failed to support the high proportion of abnormally long flagella that was observed in MV1 and MV3 (Table 3.1). We hypothesize that the longer flagellum increases the load on the motor, which allows for the motor to operate efficiently. In *E. coli*, stator units within the motor exchange readily with a pool of unbound stators in the membrane, and the number of stators that engage the rotor varies according to the load on the motor [15]. In contrast to *E. coli* or *S.* Typhimurium, the association of the stators with the motor is more stable in *H. pylori* as the stators are readily visible in cryo-electron microscopy tomograms [10, 11]. It possible that FlhH stabilizes association of the stators within the motor, either directly by interacting with the stator and/or rotor, or indirectly by facilitating assembly of motor embellishments required for recruiting or stabilizing the stator to the motor. Examination of the flagellar motors of the Δ*flhH* mutant and the Δ*flhH* motile variants by cryo-ET should provide valuable insight into the role of FlhH in flagellum function.

As reported for *P. fluorescens* and *V. anguillarum* [32, 33], the FlaG-2 homolog in *H. pylori* controls the length of the flagellar filament through an unknown mechanism. Using a combination of experimental and mathematical approaches, Renault and co-workers showed that growth of the flagellar filament in *S.* Typhimurium, which lacks a *flaG*-2 homolog, is controlled by an injection-diffusion mechanism [39]. In this model, flagellin subunits are transported into the lumen of the nascent flagellum by the flagellar protein export apparatus and diffuse to the tip of the filament where they are incorporated into the growing filament. The rate at which the filament elongates decreases with length due to diffusion limitations, until growth of the filament eventually stops. Why do *H. pylori* and other bacteria utilize FlaG-2 to control filament length instead of the injection-diffusion mechanism? One possibility is the flagellar motors in these bacteria generate greater torque than the *S.* Typhimurium motor, which enhances the diffusion of flagellins to the tip of the filament and results in longer filaments. Further investigation in the mechanism by which FlaG-2 controls filament length in *H. pylori* will provide clues in addressing this question.

MATERIALS AND METHODS

Bacterial strains and growth conditions. *E. coli* DH5α, which was used for cloning and plasmid construction, was grown in LB liquid or agar medium supplemented with ampicillin (100 μg/ml) or kanamycin (30 μg/ml) when appropriate. *H. pylori* strains were grown microaerobically under an atmosphere consisting of 10% CO_2, 4% O_2 and 86% N_2 at 37°C on tryptic soy agar (TSA) supplemented with 5% horse serum. Liquid cultures of *H. pylori* were grown in Brain Heart Infusion (BHI) medium supplemented with 5% heat-

inactivated horse serum with shaking in serum bottles under an atmosphere consisting of 5% CO_2, 10% H_2, 10% O_2 and 75% N_2. *H. pylori* growth medium was supplemented with kanamycin (30 μg/ml) or sucrose (2.5%) where appropriate.

Strain construction. All primers used for PCR in the construction of *H. pylori* mutants are listed in Supplemental Table S3.2. Plasmids and *H. pylori* stains used in the study are listed in Supplemental Table S3.3. Genomic DNA from *H. pylori* G27 was purified using the Wizard genomic DNA purification kit (Promega) and used as the PCR template to construct the suicide vectors used to generated deletion mutants. PCR was carried out using DNA polymerase (New England Biolabs) and the resulting amplicons were incubated with *Taq* polymerase (Promega) at 72^o C for 10 min to add 3'-A overhangs for T/A cloning with pGEM-T Easy plasmid (Promega). A 610 bp DNA fragment upstream of *flhH* was amplified using PCR primers 85 and 86, and a 600 bp downstream DNA fragment was amplified using PCR primers 87 and 88. PCR SOEing was used to join the upstream and downstream regions, and the resulting amplicon was cloned into pGEM-T Easy to generate the suicide plasmid pKHG25. Plasmid pKHG25 was cut at unique XhoI and NheI restriction sites and ligated with a *kan-sacB* cassette [40], generating plasmid pKHG26. pKHG26 was introduced into *H. pylori* G27 by natural transformation. Presence of the *kan-sacB* cassette in a kanamycin-resistant transformant (strain KG45) was confirmed by PCR. Plasmid pKHG25 was introduced into strain KG45 by natural transformation, and sucrose-resistant transformants that had lost the *kan-sacB* cassette were isolated by plating onto TSA supplemented with horse serum and sucrose. Deletion of *flhH* was confirmed by PCR generating strain KG48.

A 528 bp DNA fragment upstream of *flhGH* was amplified using PCR primers 62 and 63, and a 514 bp downstream DNA fragment was amplified using PCR primers 64 and 65. PCR SOEing was used to join the upstream and downstream regions, and the resulting amplicon was cloned into pGEM-T Easy to generate the suicide plasmid pKHG28. Plasmid pKHG28 was cut at unique XhoI and NheI restriction sites and ligated with the *kan-sacB* cassette to generate plasmid pKHG29 which was introduced into *H. pylori* G27 by natural transformation. Presence of the *kan-sacB* cassette in a kanamycin-resistant transformant (KG42) was confirmed by PCR. Plasmid pKHG28 was introduced to strain KG42 and sucrose-resistant transformants that had lost the *kan-sacB* cassette were isolated as described above. Deletion of *flhGH* was confirmed by PCR generating strain KG44.

PCR primers 85 and 74 amplified *flhH* and an upstream flanking region totaling 877 bp, omitting the *flhH* stop codon. Primers 75 and 76 were used to amplify YFP and added a flexible linker to the N-terminus of YFP (Gly-Ser-Ala-Gly-Ser-Gly). Primers 77 and 78 amplified a 512 bp downstream sequence of *flhH*. PCR SOEing was used to join the all three fragments, and the resulting amplicon was cloned into pGEM-T Easy to generate the suicide plasmid pKHG35. Plasmid pKHG35 was introduced to strain KG45 and sucrose-resistant transformants that lost the *kan-sacB* cassette were isolated as described above. Replacement of *flhH* with the *flhH-yfp* allele was confirmed by PCR generating strain KG58.

Transmission electron microscopy. *H. pylori* cultures were grown to late-log phase (A_{600} = ~1.0) in Brain Heart Infusion (BHI) supplemented with 10% heat-inactivated horse serum. Cells from the cultures were collected by centrifugation, fixed with formaldehyde and glutaraldehyde, and negatively stained with uranyl acetate as described [41]. Cells

were visualized using a JEOL JEM 1011 transmission electron microscope operated at 80 kV.

Fluorescence microscopy. *H. pylori* was grown on TSA supplemented with horse serum for 4 days. Cells were collected by centrifugation, resuspended in 1X phosphate buffered saline, then applied to a microscope slide and allowed to dry before heat fixation. One drop of ProLong Gold Antifade reagent (Thermo) was added to slides and allowed to cure overnight before sealing with a coverslip. FlhH-YFP was visualized on an Eclipse Ni fluorescence microscope (Nikon) using a YFP filter cube. Images were captured with a digital charge-coupled-device camera (Photometrics CoolSNAP MYO) and analyzed using NIS-Elements AR software version 4.20 (Nikon).

Motility assay. Motility of *H. pylori* strains in a soft agar medium consisting of Mueller-Hinton broth, 10% heat-inactivated horse serum, 20 mM 2-(N-morpholino)ethanesulfonic acid (MES; pH 6.0), 5 μM $FeSO_4$ and 0.4% Noble agar was done as described [41]. Diameters of the swim halos emanating from the point of inoculation in the soft agar medium were measured 7 days post-inoculation. At least three replicates were done for each strain. Mean values for the of the swim halo diameters were calculated and a two-sample *t* test was used to determine statistical significance.

Isolation of motile variants of Δ*flhH* mutant. Enrichment of motile variants of the *H. pylori* G27 Δ*flhH* mutant was accomplished by six rounds of inoculating the mutant in soft agar medium, allowing the bacteria to migrate from the point of inoculation, picking cells from the edge of the swim halo, and inoculating fresh soft agar medium. Following the last iteration, cells from the edge of the swim halo were streaked onto TSA supplemented with 10% horse serum to obtain single colonies, and motilities of cells from the isolated

colonies were examined in soft agar medium to verify they were more motile than the original Δ*flhH* mutant. Three independent enrichments were done and a single motile isolate from each enrichment was saved and characterized. Flagella lengths were measured from TEM images using Fiji software [42], and length profiles were compared using a Mann-Whitney U test.

DNA sequencing and analysis. Genomic libraries, prepared with the Illumina iTruSeq adaptor kit from 500 ng of gDNA from various *H. pylori* strains, were sequenced at the University of Georgia Genomics Facility by Illumina sequencing. Quality of the reads were assessed with FastQC and trimmed using Trimmomatic [43, 44]. Reads for *H. pylori* gDNA sequences were mapped using Bowtie2 with the published NCBI genome for *H. pylori* G27 (Accession no.: NC_011333.1) and visualized in Geneious. The gDNA sequence of the *H. pylori* Δ*flhH* mutant was aligned with that of *H. pylori* G27, which served as the backbone for aligning the gDNA sequences of the motile variants. SNPs were identified in the genome sequences of the motile variants using Geneious.

Replacement of *flaG*-2 in the *H. pylori* G27 Δ*flhH* mutant. For the following PCR and cloning steps, target DNA was amplified using Phusion polymerase and the resulting amplicons were incubated with *Taq* polymerase at 72^{o} C for 10 min to add 3'-A overhangs to facilitate T/A cloning into plasmid pGEM-T Easy. A 592 bp DNA sequence upstream of *flaG*-2 was amplified using PCR primers 107 and 108, and a 581 bp DNA sequence downstream of *flaG*-2 was amplified using PCR primers 109 and 110. PCR SOEing was used to join the upstream and downstream regions, and the resulting amplicon was cloned into pGEM-T Easy to generate the suicide plasmid pKHG52. Plasmid pKHG52 was cut at unique XhoI and NheI restriction sites and ligated with the *kan-sacB* cassette to generate

plasmid pKHG53 which was introduced into *H. pylori* strain KG48. Presence of the *kan-sacB* cassette in kanamycin-resistant transformants was confirmed by PCR generating strain KG60. Plasmid pKHG52 was introduced to strain KG60 and sucrose-resistant transformants in which the unmarked *flaG*-2 deletion had replaced the *kan-sacB* cassette were confirmed by PCR generating strain KG63.

AUTHOR CONTRIBUTIONS

TRH and KHG designed experiments and wrote the manuscript. KHG performed all experiments. VJS oversaw the fluorescence microscopy experiments.

ACKNOWLEDGEMENTS

We thank Winsen Wijaya for his technical assistance and Nathan Glueck for his assistance with the fluorescence microscopy. This work was supported by NIH grants AI140444 and AI146907 to T.R.H.

Table 3.1. Measurements of flagellum lengths of Δ*flhH* motile variants.

strain	**median flagellum length (μm)**	**mean flagellum length (μm)[a]**	**number measured**	***p*-value[b]**
wild type	3.28	3.16 ± 0.958	71	
MV1	8.72	7.61 ± 2.98	15	<0.00001
MV2	2.96	4.00 ± 2.70	34	0.78
MV3	8.74	8.16 ± 2.30	14	<0.00001

[a]Range indicates one standard deviation.

[b]Significant differences in flagellum length for the motile variants compared to wild type were determined using a Mann-Whitney U test.

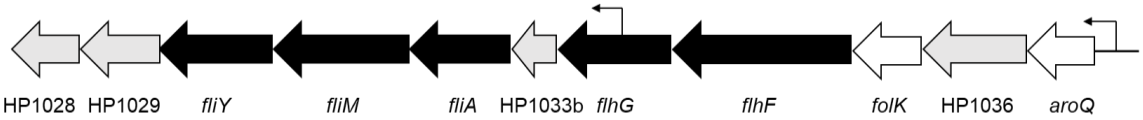

Figure 3.1. Organization of genes within operon containing *flhFG* in *H. pylori* 26695. Gray arrows indicate genes of unknown function, while black arrows indicate known flagellar genes. *fliA* encodes the sigma factor, σ^{28}, which is required for transcription of late flagellar genes, and *fliY* and *fliM* encode components of the C-ring. The smaller arrows upstream of *aroQ* and within *flhG* indicate identified transcriptional start sites [45]. The region corresponding to HP1033b was annotated originally as an open reading frame (ORF) in the opposite direction, but reassessment of the region between *flhF* and HP1028 identified a new ORF, HP1033b, which is in direct orientation to the upstream and downstream ORFs [36].

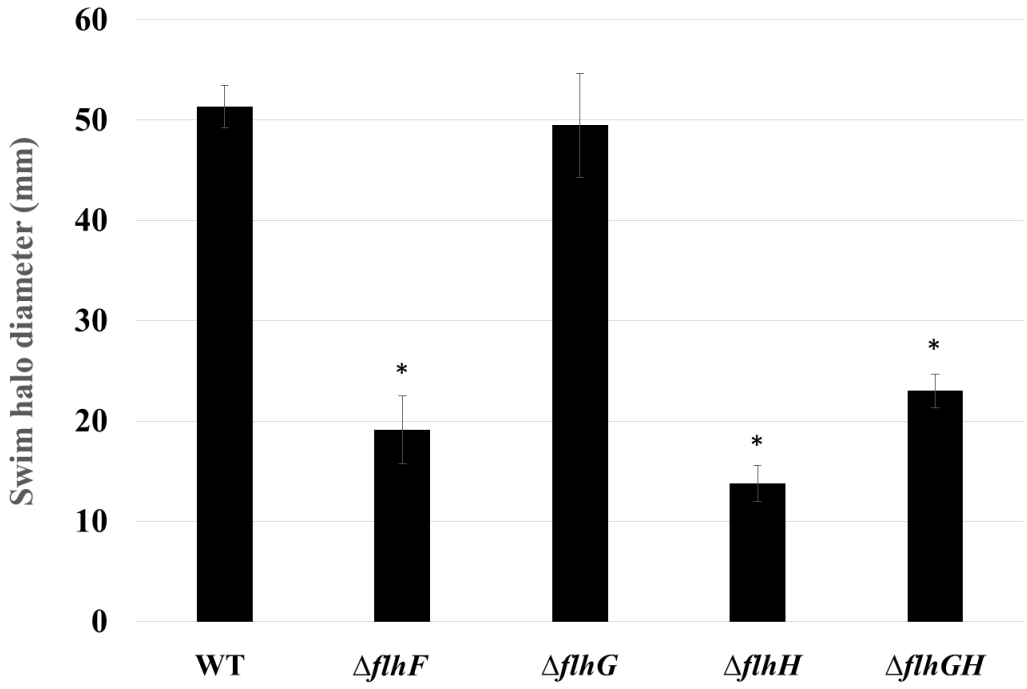

Figure 3.2. Motility of the *H. pylori* G27 Δ*flhH* mutant is impaired in soft agar medium. Motilities of the *H. pylori* G27 Δ*flhH*, Δ*flhGH* and Δ*flhF* mutants in soft agar medium, but not the Δ*flhG* mutant, were reduced significantly compared to the wild type (asterisk indicated swim halo diameter that differed significantly from wild type; *p*-value <0.00001). Black bars indicate mean values for the swim halo diameter (n = 8 for wild type; n = 9 for the Δ*flhF*, Δ*flhG* and Δ*flhH* mutants; n = 3 for Δ*flhGH* mutant). Error bars indicate one standard deviation. Statistical analysis of the data was done using a two-sample *t* test.

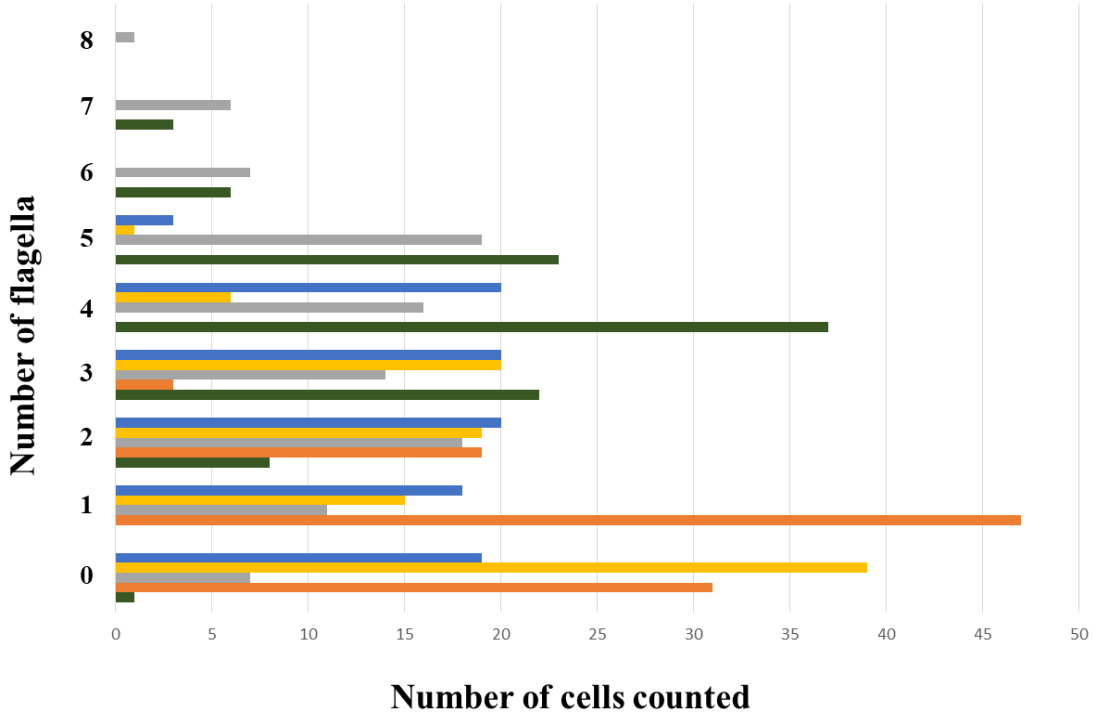

Figure 3.3. Flagella numbers for *H. pylori* WT, Δ*flhF*, Δ*flhG*, Δ*flhH*, Δ*flhGH* mutants. Flagella were counted for at least 100 cells for the wild type strain (dark green), the Δ*flhF* mutant (orange), Δ*flhG* mutant (grey), Δ*flhH* mutant (yellow), and Δ*flhGH* mutant (blue). The mode (i.e., most common number) and mean for the samples were: (wild type) 4 and 4.0, respectively, (Δ*flhF* mutant) 1 and 0.94, respectively, (Δ*flhG* mutant) 5 and 3.5, respectively, (Δ*flhH* mutant) 0 and 1.42, respectively, (Δ*flhGH* mutant) 3 and 2.13, respectively. Distribution of the number of flagella per cell for the Δ*flhF* (*p*-value <0.00001), Δ*flhG* mutant (*p*-value = 0.035), Δ*flhH* mutant (*p*-value <0.00001), and Δ*flhGH* mutant (*p*-value <0.00001) differed from that of wild type. Statistical significance was determined using a Mann-Whitney U test.

A

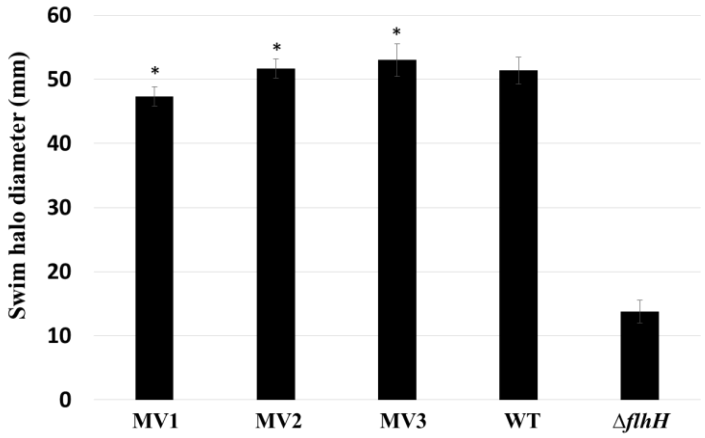
Swim halo diameter (mm)
60
50
40
30
20
10
0
*
*
*
MV1
MV2
MV3
WT
ΔflhH

B

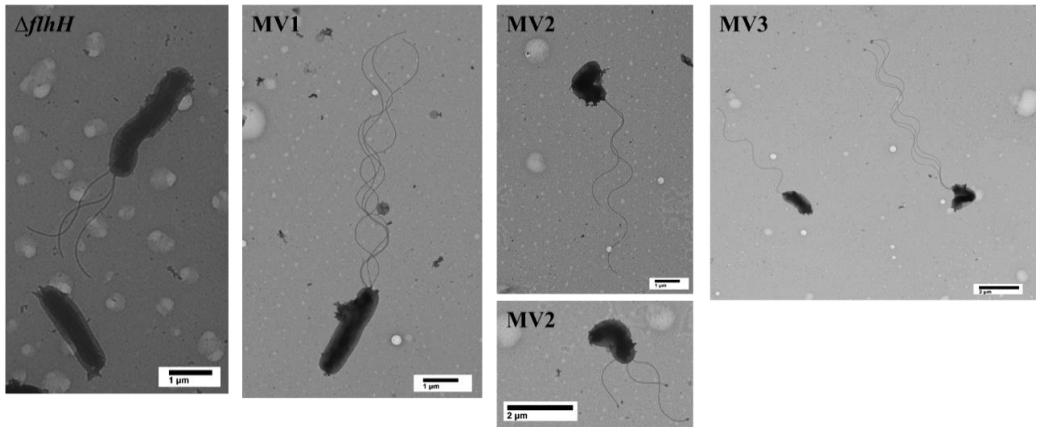
ΔflhH
MV1
MV2
MV3
MV2
1 µm
1 µm
1 µm
2 µm

C

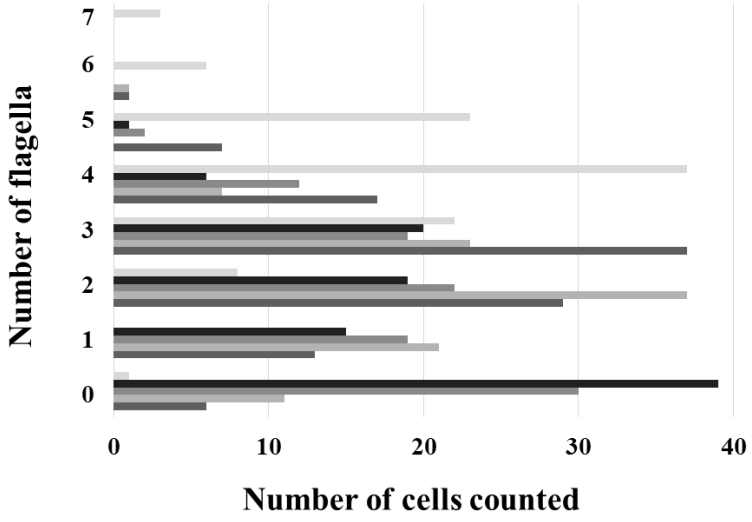
Number of flagella
7
6
5
4
3
2
1
0
0
10
20
30
40
Number of cells counted

Figure 3.4. Motility and flagellation patterns of the Δ*flhH* mutant and motile variants of the mutant. (**A**) Motility of the Δ*flhH* mutant and the motile variants derived from the Δ*flhH* mutant was assessed in soft agar medium. Bars indicate mean values for the diameters of the swim halos (n = 3), which were measured 7 days post-inoculation. Error bars indicate one standard deviation. Statistical analysis of the data was done using a two-sample *t* test. Motilities of the motile variants were significantly higher than that of the Δ*flhH* parent strain, which is indicated by asterisk (*p*-value <0.00001). (**B**) TEM of the Δ*flhH* parental strain and the Δ*flhH* motile variants. (**C**) Flagella were counted for at least 100 cells for the Δ*flhH* parent strain (black), the three motile variants (MV1, light gray; MV2, medium gray; MV3, dark gray), and G27 wild-type (palest grey). The mode (i.e., most common value) and mean for the number of flagella per cell for the strains were: Δ*flhH* parent strain, 0 and 1.4, respectively; MV1, 3 and 2.6, respectively; MV2, 2 and 2.0; and MV3, 2 and 1.7, respectively. Distribution of the number of flagella per cell for MV1 and MV2 differed from that of the Δ*flhH* parent strain (*p*-values <0.00001 and 0.00066, respectively), whereas the distribution of the number of flagella per cell for MV3 and the Δ*flhH* parent strain did not differ significantly (p-value = 0.057). Statistical significance for differences in the distribution of the number of flagella per cell were determined using a Mann-Whitney U test.

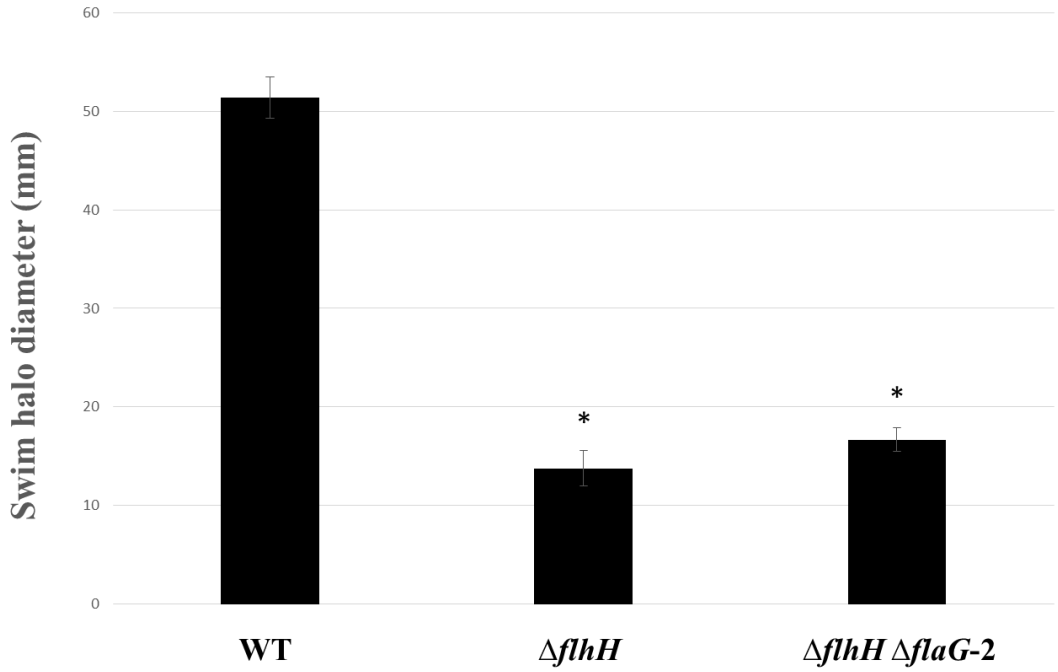

Figure 3.5. Motility profile of Δ*flhH* mutant versus Δ*flhH* Δ*flaG*-2 mutant. Motilities of the *H. pylori* G27 Δ*flhH* and Δ*flhH*/Δ*flaG* mutants in soft agar medium were reduced significantly compared to the wild type, which is indicated by asterisk (*p*-value <0.00001 for both). Motility of the Δ*flhH*/Δ*flaG*-2 mutant was about the cutoff value for significance when compared to the parent Δ*flhH* mutant (*p*-value = 0.02). Black bars indicate mean values for the swim halo diameter (n = 8 for wild type; n = 9 for the Δ*flhH* mutant; n = 3 for Δ*flhH*/Δ*flaG* mutant). Error bars indicate one standard deviation. Statistical analysis of the data was done using a two-sample *t* test.

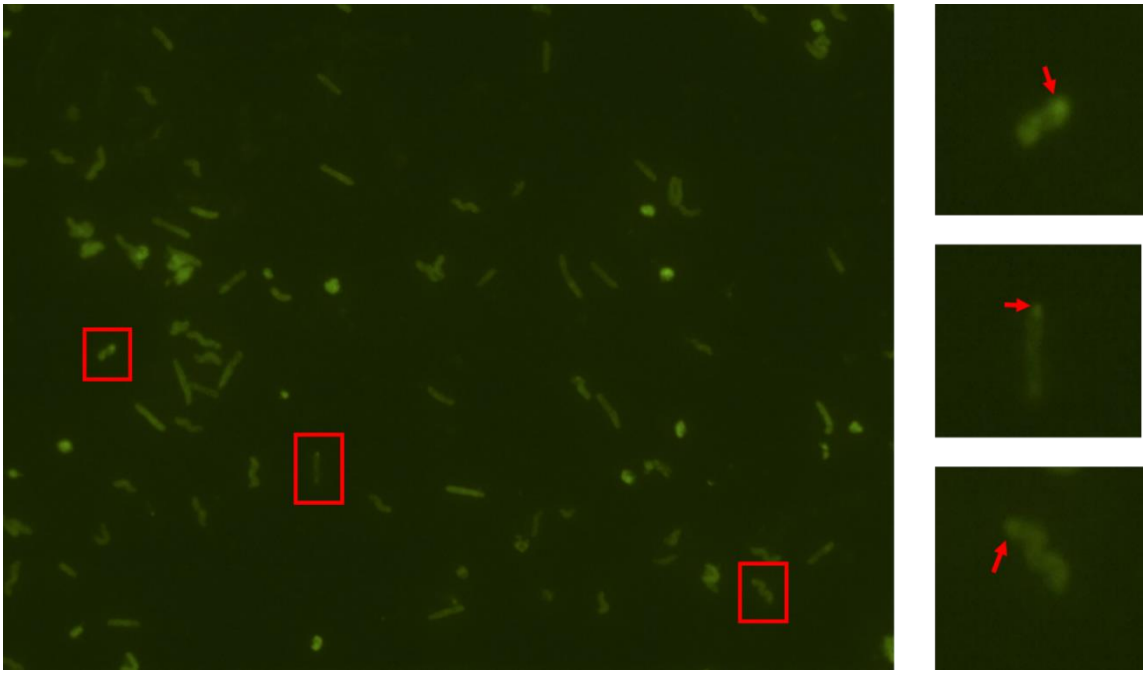

Figure 3.6. Fluorescent microscopy of FlhH-YFP. Fluorescent foci were observed at the cell pole in a small proportion of cells. Cells were viewed under 100X objective with immersion oil. Specific cells (red boxes) enlarged to show foci detail.

Table S3.1. Predicted *flhH* homologs in diverse representatives of Epsilonproteobacteria.

Species	**NCBI accession**	**[a]Identity/ similarity to *H. pylori* FlhH**
Helicobacter hepaticus 3B1	WP_011115985	43%/63% (102)
Campylobacter jejuni 81116	WP_002851727	30%/50% (93)
Wolinella succinogenes DSM 1740	WP_011139455	46%/66% (99)
Sulfurimonas autotrophica OK10	WP_013326520	31%/53% (87)
Sulfurospirillum multivorans DSM 12446	AHJ11662	41%/59% (95)
Sulfuricurvum kujiense YK-1	WP_013459341	35%/52% (86)
Hydrogenimonas thermophila EP1-55-1	WP_092910690	30%/55% (96)
Thiovulum sp. ES	EJF07001	33%/51% (88)
Arcobacter butzleri ED-1	BAK71473	no significant
Aliiarcobacter porcinus 117434	OCL82944	no significant
Pseudoarcobacter caeni RW17-10	WP_108559542	no significant

[a]Number in parentheses indicates the length over which the compared proteins share identity or similarity.

Table S3.2. Primers used in this study.

Primer	Name	Sequence
85	flhH US F	5’ GGG GAT AGC GGC GAA GAA ATT
86	flhH US R	5’ GCT AGC GAT AAT CGA ATT CCT CGA GAA ACC CTA CCA CAA CAG AAA AAT G
87	flhH DS F	5’ CTC GAG GAA TTC GAT TAT CGC TAG CAA GAA CAG AGA AAA AGA AGT GGC TAG T
88	flhH DS R	5’ GTG ATT TCA TCT TGC TCA ATC GCA TTG
74	flhH R + YFP linker	5' CCC GCT CCC AGC GCT CCC TTT TCC ATC ATC AAA ATC ATA ACT TCT A
75	YFP F + linker	5' GGG AGC GCT GGG AGC GGG ATG GTG AGC AAG GGC GA
76	YFP R + flhH overhang	5' TTT TTG ATT TCC TTT GGG CAT TTT ACT TGT ACA GCT CGT CCA
77	flhH DS F + YFP overhang	5' TGG ACG AGC TGT ACA AGT AAA ATG CCC AAA GGA ATT CAA AAA
78	flhH DS R	5' CAA TCG CAT TGA ATT GCT CAT
107	flaG US F	5' AAG AGA GGG TCA GTT TGA AAA
108	flaG US R + XhoI	5' GAA TTC GAT TAT CCT CGA GAA TCC CTT GAA CTT CAT TGA C
109	flaG DS F + NheI	5' GAT AAT CGA ATT CGC TAG CGC GAT GTG ATA GGC ATT ATC T
110	flaG DS R	5' TCA TTC CCT CCT GTT TTC A
62	flhGH US F	5' ACT TAA GAC AAT TAT CGC ATT GGG G
63	flhGH US R + XhoI	5' GAA TTC GAT TAT CCT CGA GAA TTA TCC AAG CGG CTC GC
64	flhGH DS F + NheI	5' CAT AAT CGA ATT CGC TAG CAA TGC CCA AAG GAA TTC AAA AAA CTG
65	flhGH DS R	5' CTC AAT CGC ATT GAA TTG CTC ATC

Table S3.3. Plasmids and *H. pylori* strains used in this study.

Plasmid name	**Description**	**Reference**
pKHG25	pGEM-T Easy *flhH* flanking regions	This study
pKHG26	pGEM-T Easy *flhH::kan-sacB*	This study
pKHG28	pGEM-T Easy *flhGH* flanking sequences	This study
pKHG29	pGEM-T Easy *flhGH::kan-sacB*	This study
pKHG35	pGEM-T Easy *flhH-yfp*	This study
pJC038	pGEM-T Easy with *kan-sacB* cassette	[40]
pKHG52	pGEM-T Easy *flaG* flanking sequences	This study
pKHG53	pGEM-T Easy *flaG::kan-sacB*	This study
H. pylori strain	**Relevant genotype**	
H. pylori G27	wild type	
KG45	*H. pylori* G27 *flhH::kan-sacB*	This study
KG48	*H. pylori* G27 Δ*flhH*	This study
KG42	*H. pylori* G27 *flhGH::kan-sacB*	This study
KH44	*H. pylori* G27 Δ*flhGH*	This study
KG58	*H. pylori* G27 *flhH-yfp*	This study
KG60	*H. pylori* G27 Δ*flhH flaG::kan-sacB*	This study
KG63	*H. pylori* G27 Δ*flhH* Δ*flaG*	This study
KG43	*H. pylori* G27 Δ*flhF*	K. Gibson, unpublished
KG47	*H. pylori* G27 Δ*flhG*	K. Gibson, unpublished

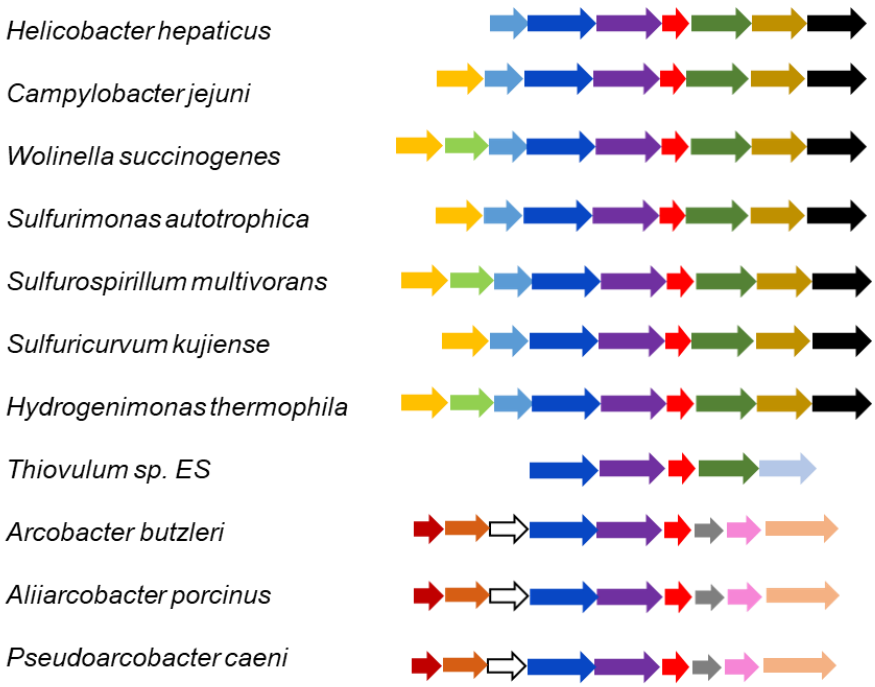

Figure S3.1. Synteny of *flhFGH* in the Epsilonproteobacteria. Genomic regions surrounding *flhH* homologs are shown for representatives from each genera of the Epsilonproteobacteria. Homologous genes are color coded as follows: *folK* (light blue), *flhF* (dark blue), *flhG* (purple), *flhH* (red), *fliA* (dark olive), *fliM* (brown), *fliY* (black), *aroQ* (gold), *pepQ* (light green), predicted lipoprotein gene (bluish gray), predicted rod-binding protein gene (dark red), hypothetical protein genes (orange and white), *fliE* (gray), *flgB* (pink), and *fliK* (peach). *Nitratifractor salsuginis* E9I37-1 (DSM 16511), a non-motile and aflagellated member of the subphylum Epsilonproteobacteria [46], and lacks homologs of several flagellar genes including *flhG*, *flhH*, and *fliA*. In *A. butzleri*, *A. porcinus* and *P. caeni*, *flhFGH* appear to be part of a large operon of ~30 genes encoding other flagellar and chemotaxis proteins.

REFERENCES

1. Berg, H.C., *The rotary motor of bacterial flagella.* Annu Rev Biochem, 2003. **72**: p. 19-54.

2. Chevance, F.F. and K.T. Hughes, *Coordinating assembly of a bacterial macromolecular machine.* Nat Rev Microbiol, 2008. **6**(6): p. 455-65.

3. Macnab, R.M., *How bacteria assemble flagella.* Annu Rev Microbiol, 2003. **57**: p. 77-100.

4. Manson, M.D., et al., *A protonmotive force drives bacterial flagella.* Proc Natl Acad Sci U S A, 1977. **74**(7): p. 3060-4.

5. Kojima, S. and D.F. Blair, *Solubilization and purification of the MotA/MotB complex of Escherichia coli.* Biochemistry, 2004. **43**(1): p. 26-34.

6. Hizukuri, Y., S. Kojima, and M. Homma, *Disulphide cross-linking between the stator and the bearing components in the bacterial flagellar motor.* J Biochem, 2010. **148**(3): p. 309-18.

7. Hizukuri, Y., et al., *The peptidoglycan-binding (PGB) domain of the Escherichia coli pal protein can also function as the PGB domain in E. coli flagellar motor protein MotB.* J Biochem, 2009. **146**(2): p. 219-29.

8. Blair, D.F. and H.C. Berg, *The MotA protein of E. coli is a proton-conducting component of the flagellar motor.* Cell, 1990. **60**(3): p. 439-49.

9. Stolz, B. and H.C. Berg, *Evidence for interactions between MotA and MotB, torque-generating elements of the flagellar motor of Escherichia coli.* J Bacteriol, 1991. **173**(21): p. 7033-7.

10. Chaban, B., I. Coleman, and M. Beeby, *Evolution of higher torque in Campylobacter-type bacterial flagellar motors.* Sci Rep, 2018. **8**(1): p. 97.

11. Qin, Z., et al., *Imaging the motility and chemotaxis machineries in Helicobacter pylori by cryo-electron tomography.* J Bacteriol, 2017. **199**(3): p. e00695-16.

12. Reid, S.W., et al., *The maximum number of torque-generating units in the flagellar motor of Escherichia coli is at least 11.* Proc Natl Acad Sci U S A, 2006. **103**(21): p. 8066-71.

13. Leake, M.C., et al., *Stoichiometry and turnover in single, functioning membrane protein complexes.* Nature, 2006. **443**(7109): p. 355-8.

14. Tipping, M.J., et al., *Load-dependent assembly of the bacterial flagellar motor.* mBio, 2013. **4**(4): p. e00551-13.

15. Lele, P.P., B.G. Hosu, and H.C. Berg, *Dynamics of mechanosensing in the bacterial flagellar motor.* Proc Natl Acad Sci U S A, 2013. **110**(29): p. 11839-44.

16. Eaton, K.A., D.R. Morgan, and S. Krakowka, *Motility as a factor in the colonisation of gnotobiotic piglets by Helicobacter pylori.* J. Med. Microbiol., 1992. **37**: p. 123-127.

17. Ottemann, K.M. and A.C. Lowenthal, *Helicobacter pylori uses motility for initial colonization and to attain robust infection.* Infect Immun, 2002. **70**(4): p. 1984-90.

18. Schuhmacher, J.S., K.M. Thormann, and G. Bange, *How bacteria maintain location and number of flagella?* FEMS Microbiol Rev, 2015. **39**(6): p. 812-22.

19. Halic, M. and R. Beckmann, *The signal recognition particle and its interactions during protein targeting.* Curr Opin Struct Biol, 2005. **15**(1): p. 116-25.

20. Balaban, M., S.N. Joslin, and D.R. Hendrixson, *FlhF and its GTPase activity are required for distinct processes in flagellar gene regulation and biosynthesis in Campylobacter jejuni.* J Bacteriol, 2009. **191**(21): p. 6602-11.

21. Green, J.C., et al., *Recruitment of the earliest component of the bacterial flagellum to the old cell division pole by a membrane-associated signal recognition particle family GTP-binding protein.* J Mol Biol, 2009. **391**(4): p. 679-90.

22. Murray, T.S. and B.I. Kazmierczak, *FlhF is required for swimming and swarming in Pseudomonas aeruginosa.* J Bacteriol, 2006. **188**(19): p. 6995-7004.

23. Pandza, S., et al., *The G-protein FlhF has a role in polar flagellar placement and general stress response induction in Pseudomonas putida.* Mol Microbiol, 2000. **36**(2): p. 414-23.

24. Balaban, M. and D.R. Hendrixson, *Polar flagellar biosynthesis and a regulator of flagellar number influence spatial parameters of cell division in Campylobacter jejuni.* PLoS Pathog, 2011. **7**(12): p. e1002420.

25. Campos-Garcia, J., et al., *The Pseudomonas aeruginosa motR gene involved in regulation of bacterial motility.* FEMS Microbiol Lett, 2000. **184**(1): p. 57-62.

26. Correa, N.E., F. Peng, and K.E. Klose, *Roles of the regulatory proteins FlhF and FlhG in the Vibrio cholerae flagellar transcription hierarchy.* J Bacteriol, 2005. **187**(18): p. 6324-32.

27. Dasgupta, N., S.K. Arora, and R. Ramphal, *fleN, a gene that regulates flagellar number in Pseudomonas aeruginosa.* J Bacteriol, 2000. **182**(2): p. 357-64.

28. Kusumoto, A., et al., *Regulation of polar flagellar number by the flhF and flhG genes in Vibrio alginolyticus.* J Biochem, 2006. **139**(1): p. 113-21.

29. Bange, G., et al., *Structural basis for the molecular evolution of SRP-GTPase activation by protein.* Nat Struct Mol Biol, 2011. **18**(12): p. 1376-80.

30. Gulbronson, C.J., et al., *FlhG employs diverse intrinsic domains and influences FlhF GTPase activity to numerically regulate polar flagellar biogenesis in Campylobacter jejuni.* Mol Microbiol, 2016. **99**(2): p. 291-306.

31. Schuhmacher, J.S., et al., *MinD-like ATPase FlhG effects location and number of bacterial flagella during C-ring assembly.* Proc Natl Acad Sci U S A, 2015. **112**(10): p. 3092-7.

32. Capdevila, S., et al., *Analysis of Pseudomonas fluorescens F113 genes implicated in flagellar filament synthesis and their role in competitive root colonization.* Microbiology, 2004. **150**(Pt 11): p. 3889-3897.

33. McGee, K., P. Horstedt, and D.L. Milton, *Identification and characterization of additional flagellin genes from Vibrio anguillarum.* J Bacteriol, 1996. **178**(17): p. 5188-98.

34. Radin, J.N., et al., *Flagellar localization of a Helicobacter pylori autotransporter protein.* mBio, 2013. **4**(2): p. e00613-12.

35. Tomb, J.-F., et al., *The complete genome sequence of the gastric pathogen Helicobacter pylori.* Nature, 1997. **388**: p. 539-547.

36. Niehus, E., et al., *Genome-wide analysis of transcriptional hierarchy and feedback regulation in the flagellar system of Helicobacter pylori.* Mol Microbiol, 2004. **52**(4): p. 947-61.

37. Hare, S., et al., *Identification, structure and mode of action of a new regulator of the Helicobacter pylori HP0525 ATPase.* EMBO J, 2007. **26**(23): p. 4926-34.

38. Bos, J.L., H. Rehmann, and A. Wittinghofer, *GEFs and GAPs: critical elements in the control of small G proteins.* Cell, 2007. **129**(5): p. 865-77.

39. Renault, T.T., et al., *Bacterial flagella grow through an injection-diffusion mechanism.* Elife, 2017. **6**.

40. Chu, J.K., et al., *Loss of a Cardiolipin Synthase in Helicobacter pylori G27 Blocks Flagellum Assembly.* J Bacteriol, 2019. **201**(21).

41. Chu, J.K., et al., *Loss of a cardiolipin synthase in Helicobacter pylori G27 blocks flagellum assembly.* J Bacteriol, 2019. **201**(21): p. e00372-19.

42. Schindelin, J., et al., *Fiji: an open-source platform for biological-image analysis.* Nat Methods, 2012. **9**(7): p. 676-82.

43. Andrews, S., *FastQC: A quality control tool for high throughput sequence data.* 2014.

44. Bolger, A.M., M. Lohse, and B. Usadel, *Trimmomatic: a flexible trimmer for Illumina sequence data.* Bioinformatics, 2014. **30**(15): p. 2114-20.

45. Sharma, C.M., et al., *The primary transcriptome of the major human pathogen Helicobacter pylori.* Nature, 2010. **464**(7286): p. 250-5.

46. Nakagawa, S., et al., *Nitratiruptor tergarcus gen. nov., sp. nov. and Nitratifractor salsuginis gen. nov., sp. nov., nitrate-reducing chemolithoautotrophs of the epsilon-Proteobacteria isolated from a deep-sea hydrothermal system in the Mid-Okinawa Trough.* Int J Syst Evol Microbiol, 2005. **55**(Pt 2): p. 925-33.

CHAPTER 4

A *HELICOBACTER PYLORI* TRIPARTITE EFFLUX SYSTEM WITH A ROLE IN FLAGELLUM BIOSYNTHESIS

Katherine H. Gibson, Joshua K. Chu, Shiwei Zhu, Jan Mrázek, Jun Liu and Timothy R. Hoover. To be submitted to Molecular Microbiology.

ABSTRACT

Helicobacter pylori is motile via a cluster of polar flagella, each of which is surrounded by a membranous sheath that is continuous with the outer membrane. To identify genes with possible roles in flagellar sheath biosynthesis or function, we searched for homologs of *H. pylori* genes conserved in genomes of *Helicobacter* species that possess flagellar sheaths, but were absent or underrepresented in *Helicobacter* species with unsheathed flagella. Four genes identified in the comparative genomics approach encode a predicted tripartite efflux system consisting of two inner membrane ATP-binding cassette transporters (HP1487 and HP1486), a periplasmic membrane fusion protein (HP1488), and a TolC-like outer membrane efflux protein (HP1489). Deleting the HP1486/HP1487 and HP1489 homologs in *H. pylori* B128 resulted in decreased motility and a reduction in the number of flagella per cell. Cryo-electron tomography revealed that many of the flagellar motors of the ΔHP1489 and ΔHP1486/ΔHP1487 mutants lacked a unique cage-like structure and other features present in the wild-type *H. pylori* motor. These findings indicate a role for the HP1486-HP1489 tripartite efflux system in flagellum assembly or stability, and we designate the genes encoding the efflux system as flagellum-associated efflux system ABCD (*faeABCD*).

INTRODUCTION

Helicobacter pylori, a member of the Epsilonproteobacteria, colonizes the human gastric mucosa where it can cause a variety of diseases, including chronic gastritis, peptic and duodenal ulcers, B cell MALT lymphoma and gastric adenocarcinoma [1]. *H. pylori* possesses 2 to 6 polar, sheathed flagella that it uses to migrate through the viscous mucus layer covering the stomach epithelium. Flagellar-mediated motility is required for host colonization, as non-motile *H. pylori* mutants are unable to colonize animal models [2, 3].

The bacterial flagellum consists of three distinct structures referred as the basal body, hook and filament. The basal body includes the flagellar motor and the flagellar protein export apparatus, which is a Type III secretion system that transports axial components of the flagellum (e.g., rod, hook and filament proteins) across the inner membrane [4, 5]. Core structures of the bacterial flagellar motor include the MS-ring (base for the motor), the C-ring (switch complex that regulates motor rotation), rod (connects the MS-ring to the hook), P- and L-rings (bushings that support the rod while allowing it to rotate freely), and a stator comprised by the membrane complex of MotA and MotB proteins. The stator is a torque generator for the flagellar motor and is powered by the proton motive force [6]. The *H. pylori* flagellar motor accommodates up to 18 stators [7], making it the largest bacterial flagellar motor described to date. Torque generated by the motor is transmitted via the rod and hook to the flagellar filament, which is a long, rigid, helical structure that propels the cell as it rotates. The *H. pylori* flagellar filament consists of a minor flagellin (FlaB) that localizes near the hook and a major flagellin (FlaA) that forms the distal portion of the filament [8].

In addition to the conserved core features of flagellar motors, the *H. pylori* flagellar motor contains several structures not found in the archetypical flagellar motors of *E. coli* and *S. enterica* serovar Typhimurium [7, 9, 10]. Unique features of the *H. pylori* flagellar motor include a large disk (referred to as the P-disk) located near the P- and L-rings, a smaller disk situated between the P-disk and the outer membrane, a cage-like periplasmic structure with 18-fold symmetry, and an additional ring between the MS-ring and the cage (Fig. 4.1). The additional ring was proposed to be a FliL ring based on its similarity with a FliL structure found the spirochete *Borrelia burgdorferi* [7, 11], however, the exact structure and function of FliL in *H. pylori* is unknown.

H. pylori is one of several bacterial species that possess a membranous sheath surrounding the flagellum [12]. The *H. pylori* flagellar sheath is continuous with the outer membrane [7], but the composition of the flagellar sheath and outer membrane varies [13-17]. Proposed roles for the *H. pylori* flagellar sheath include protecting the filament subunits from dissociation by gastric acid and adherence to host cells. In *Vibrio cholerae*, the flagellar sheath has been suggested to hide flagellin from Toll-like receptor 5 and thereby prevent triggering of the host innate immune system [18]. Such a role is not likely the case for the *H. pylori* flagellar sheath since the *H. pylori* flagellins lack the conserved region that is recognized by Toll-like receptor 5 [19, 20]. Another possible role of the *H. pylori* flagellar sheath is to generate outer membrane vesicles (OMVs) for communication with the host immune system or for innate bacterial defense. Rotation of the sheathed flagellum in *Vibrio* species releases OMVs that contain the potent immune response stimulant lipopolysaccharide (LPS) [21, 22]. In the symbiosis between *Vibrio fischeri* and the Hawaiian bobtail squid, *Euprymna scolopes*, LPS associated with the OMVs induces

apoptotic cell death in the epithelium of the squid light organ that is required for normal development of the organ [22]. OMVs can also bind bacteriophage, which appears to afford some protection against phage for bacteria [23, 24].

Our understanding of the proteins and other factors involved in flagellar sheath biosynthesis for any bacterial species is limited [25]. To address this gap in our knowledge, we compared the genomes of *Helicobacter* species that have flagellar sheaths with the genomes of *Helicobacter* species that have unsheathed flagella to identify genes with potential roles in flagellar sheath biosynthesis. Four candidate genes identified in the comparative genomics approach encode a predicted tripartite efflux system consisting of two inner membrane ATP-binding cassette (ABC) transporters (HP1487 and HP1486), a periplasmic membrane fusion protein (MFP; HP1488), and an outer membrane efflux protein (OEP; HP1489). Tripartite efflux systems transport a variety of substrates directly from the cytoplasm to the external medium, including proteins, oligosaccharides, antibiotics, metals, large cations, and other various xenobiotics [26, 27]. Deleting HP1486/HP1487 and HP1489 homologs in *H. pylori* B128 inhibited motility and reduced the number of flagella per cell. Visualization of the flagellar motors of the ΔHP1489 and ΔHP1486/ΔHP1487 mutants by cryo-electron tomography (cryo-ET) revealed aberrant structures for many of the motors. These findings suggest a role for the HP1486-HP1489 efflux system in flagellum assembly or stability, and we designate the genes encoding the efflux system as flagellum-associated efflux system ABCD (*faeABCD*).

RESULTS

Identification of Helicobacter genes correlated with the presence of a flagellar sheath.

The majority of *Helicobacter* species identified to date possess a flagellar sheath, but several *Helicobacter* species have unsheathed flagella. To identify genes that have potential roles in flagellar sheath biosynthesis or function, we searched for homologs of *H. pylori* genes that were present in the genomes of *Helicobacter* species that possess flagellar sheaths (FS^+), but were absent in *Helicobacter* species with unsheathed flagella (FS^-). Using blastp, predicted proteins encoded in the genomes of 35 FS^+ *Helicobacter* species and 9 FS^- *Helicobacter* species were examined for homologs of the 1458 predicted proteins encoded in the *H. pylori* G27 genome. The *H. pylori* G27 genome was chosen for the analysis since it is a finished genome sequence and G27 is a model for studies of motility and flagellum biosynthesis in *H. pylori*. *Helicobacter* species and strains analyzed are listed in Table S4.1. The blastp comparison was performed with two E-value cutoffs, $1e^{-20}$ and $1e^{-8}$. Proteins in other *Helicobacter* genomes that matched the *H. pylori* G27 query with E-value below the more stringent $1e^{-20}$ cutoff were considered homologs of the *H. pylori* G27 protein; those with E-value above $1e^{-20}$ but below $1e^{-8}$ were included if the match was supported by the protein functional annotation. Fisher's exact test was used to identify proteins that were significantly more prevalent in FS^+ *Helicobacter* species compared to FS^- *Helicobacter* species (p-value ≤ 0.0001). Results from the blastp analysis for all 1458 *H. pylori* G27 proteins are presented in Tables S4.2 and S4.3. Thirty-seven proteins were identified as occurring preferentially in FS^+ *Helicobacter* species (Table 4.1).

Most of the genes that appear to be specific to FS^+ *Helicobacter* species encode outer membrane proteins, transport proteins or enzymes involved in lipopolysaccharide (LPS)

biosynthesis or modification (Table 4.1). Several of the genes specific to FS^+ *Helicobacter* species, however, are of unknown function or encode proteins with miscellaneous, and seemingly unrelated, functions. Interestingly, one of the genes within this latter class is *clsC*, which encodes a cardiolipin synthase [28]. Cardiolipin is a phospholipid that accumulates at the cell pole and septal regions in rod-shaped bacteria due to its ability to form microdomains that exhibit a high intrinsic curvature and thus have a lower energy when localized to negatively curved regions of the membrane [29, 30]. Given the flagellar sheath has a considerable amount of negative curvature along its entire length, it is reasonable to predict that cardiolipin accumulates in the flagellar sheath. Consistent with this hypothesis, preparations of sheathed flagella from *H. pylori* G27 flagellar sheath have significant amounts of cardiolipin (J. Chu, University of Georgia PhD thesis). Thus, the presence of *clsC* in FS^+ *Helicobacter* species may reflect an increased requirement for cardiolipin during flagellar sheath biosynthesis.

Several genes that occur preferentially in FS^+ *Helicobacter* species are involved in LPS biosynthesis or modification. Compared with LPS from other Gram-negative bacteria, *H. pylori* LPS has low endotoxin and immunological activity [31-33]. Rotation of the sheathed flagellum in *Vibrio* species is a major source of OMVs containing LPS and other molecules that have key roles in host signaling in symbiosis and pathogenesis [21, 22]. If rotation of the sheathed flagellum in *Helicobacter* species similarly results in the release of OMVs, modification of LPS may be more important in FS^+ *Helicobacter* species than in FS^- *Helicobacter* species for avoiding the activation of the host innate immune response.

Seven *H. pylori* G27 genes specific to FS^+ *Helicobacter* species encode proteins belonging to the Sel1-like repeat (SLR) family (Table 4.1), members of which contain

multiple copies of a degenerate amino acid repeat motif that is characteristic of eukaryotic Sel1 proteins [34]. In the blastp analysis, SLR family members from *Helicobacter* species typically shared homology with multiple SLR proteins from *H. pylori* G27. The number of SLR homologs that FS^+ *Helicobacter* species possessed ranged from one (*H. fennelliae*) to five (*H. acinonychis*), with two homologs being the most common number. A single SLR protein homolog was found in two of the FS^- *Helicobacter* species (*H. pullorum* and *H. rodentium*) from the blastp analysis using the more stringent cutoff (E-value of $1e^{-20}$), and a third species (*H. ganmani*) when the less stringent cutoff was used (E-value of $1e^{-8}$). All three of the FS^- *Helicobacter* species proteins are predicted to be SLR family members. Although the functions of the *H. pylori* SLR proteins are not known, some of them bind β-lactam compounds [35, 36], and have been suggested to interact with immunomodulatory peptidoglycan fragments to affect the innate immune response [37].

Another seven *H. pylori* genes specific to FS^+ *Helicobacter* species encode proteins that belong to Hof family of outer membrane proteins (Table 4.1). Close homologs of Hof proteins are absent outside the genus *Helicobacter* [38]. Functions for the Hof proteins are unknown, except for HofE and HofF in *H. heilmannii*, which have apparent roles in adherence to human gastric mucin [39]. No Hof family homologs were identified in the FS^- *Helicobacter* species from the blastp analysis. The number of Hof family homologs in the FS^+ *Helicobacter* species ranged from zero (*H. brantae*, *H. cholecytus*, and *H. pametensis*) to seven (*H. cetorum*), and about half of the FS^+ *Helicobacter* species examined possess multiple Hof protein homologs with most species having at least five Hof family homologs.

Many of *H. pylori* proteins that occur preferentially in FS^+ *Helicobacter* species have roles in transport (Table 4.1). One of these proteins is a predicted outer membrane protein proposed to be involved in fatty acid transport (HP0839), while another protein is a predicted lipocalin (HP1028). Lipocalins occur in all domains of life and have varied functions, but in general, they bind hydrophobic ligands to chaperone them through aqueous compartments of the cell [40]. Some bacterial lipocalins bind antibiotics and contribute to antibiotic resistance [41]. Bacterial lipocalins are suggested to have originated in association with the development of bacterial outer membrane and to function in maintenance of the outer membrane [42]. HP0839 and HP1028 are in operons with flagellar or flagellum-associated genes - HP0839 is in an operon with *flgP* and *pseH*, while HP1028 is in an operon with *fliAMY* [43]. The occurrence of HP0839 and HP1028 in operons with flagellar genes suggests roles for these genes in flagellum biosynthesis or function. The remaining transport proteins that occur preferentially in FS^+ *Helicobacter* species are components of tripartite efflux systems. Two of these genes encode components of an efflux system (*cznB* and *cznC*) required for cadmium, zinc, and nickel resistance in *H. pylori* [44]. The other component of this efflux system, CznA, has limited homology with related proteins in several of the FS^- *Helicobacter* species, which explains why it was not identified as being preferentially conserved in FS^+ *Helicobacter* species. The remaining transport genes (*faeABCD*) encode components of another tripartite efflux system that appears to occur specifically in FS^+ *Helicobacter* species.

***faeABCD* are required for wild type motility in H. pylori B128.** Homologs of *faeABCD* were present in all of the FS^+ *Helicobacter* species and absent in the FS^- *Helicobacter* species examined (Tables S4.2 and S4.3), which suggested a role for these genes in the

biosynthesis or function of the sheathed flagella in *Helicobacter*. To determine if *faeABCD* are involved in biosynthesis or function of the *H. pylori* flagellum, we deleted *faeA* and *faeCD* in *H. pylori* B128 using a sucrose-based counter-selection method [45]. *H. pylori* B128 was used for the study since it is very amendable for cryo-ET imaging [7]. Since *faeC* and *faeD* are predicted to encode subunits of the same ABC transporter, we deleted both genes together. The motility of the *H. pylori* B128 Δ*faeC*/Δ*faeD* mutant was ~60% of that of the wild-type parental strain (Fig. 4.2). Examination of the Δ*faeC*/Δ*faeD* double mutant by transmission electron microscopy (TEM) revealed it possessed fewer flagella per cell than wild type, and compared to wild type, a higher proportion of the Δ*faeC*/Δ*faeD* mutant cells either lacked flagella or possessed a single flagellum (~25% for the mutant versus ~15% for wild type) (Fig. 4.3). Deleting *faeA* in *H. pylori* B128 similarly reduced motility (Fig. 4.2) and reduced the number of flagella per cell (Fig. 4.3). Taken together, these observations suggest the FaeABCD efflux system is required for normal flagellum biosynthesis and motility. Disrupting *faeA* in *H. pylori* G27 with the *kan-sacB* cassette reduced motility of the strain by more than 60% (data not shown), indicating the FaeABCD efflux system is required for wild-type motility in *H. pylori* G27 as it is in *H. pylori* B128.

Visualization of the flagellar motors of the FaeABCD efflux system mutants. The decreased motility and reduced number of flagella in the Δ*faeA* and Δ*faeCD* mutants suggests a role for the FaeABCD efflux system in the assembly, stability or function of the flagellar motor. To determine the structure of the flagellar motors of the Δ*faeA* and Δ*faeCD* mutants in detail, we selected 77 subtomograms of motors from 48 reconstructions of Δ*faeA* cells and 137 subtomograms of motors from 70 reconstructions of Δ*faeCD* mutants,

which we analyzed by subtomogram averaging and classification. The resulting flagellar motor structures are presented in Figure 4.4.

Many of the motors of the Δ*faeA* and Δ*faeCD* mutants appeared similar to the wild-type flagellar motor, with the notable exception that the cage did not span the periplasm and contact the P-disk (Fig. 4.4A). We assume that these motors were functional and responsible for the motility observed for the Δ*faeA* and Δ*faeCD* mutants. Some of the flagellar motors of the Δ*faeA* and Δ*faeCD* mutants lacked a visible hook and filament, as well as some of the structures associated with the motor. Other flagellar motors possessed a hook and filament, but lacked some motor structures. To gain a better understanding of these aberrant flagellar motors, we generated three specific class averages for these motors. For one class of motor, the hook, filament and flagellar sheath were evident, but the cage and other motor embellishments normally found near the inner membrane were missing (Fig. 4.4B). This class of motor was observed for the Δ*faeA* mutant, but not the Δ*faeCD* mutant. Another class of motor lacked the hook and filament, and the outer membrane above the rod is deformed slightly (Fig. 4.4C). The only motor embellishment that was apparent in this second class of motor was the P-disk. As with the first class, this second class of motor was only observed for the Δ*faeA* mutant. The third class of motor consists of only the P-disk with the outer membrane above the disk exhibiting some deformation (Fig. 4.4D), and was observed for both the Δ*faeA* and Δ*faeCD* mutants. The aberrant flagellar motors do not appear to be flagellum assembly intermediates since the cage and other motor embellishments were present in a wild-type *H. pylori* flagellar motor assembly intermediate that possessed a rod, but not the hook or filament [7]. Taken together, these observations suggest the Fae efflux system forms part of the cage that surrounds the *H.*

pylori flagellar motor, and is required for assembly of other motor components, such as the outer disk and ring located between the cage and MS-ring.

DISCUSSION

Despite there being a number of bacterial pathogens that possess flagellar sheaths, proteins and other factors that contribute to flagellar sheath biosynthesis in any bacterial species remain unknown. To address this critical gap in our knowledge, we searched for *H. pylori* genes that are conserved in FS^+ *Helicobacter* species but are absent or underrepresented in FS^- *Helicobacter* species assuming that some of these genes have roles in flagellar sheath biosynthesis or function. A caveat of the comparative genomics approach is the FS^+ and FS^- *Helicobacter* species, in general, segregate into distinct phylogenic groups based on alignments of *gyrA* or 16s rRNA sequences [46], which means that some of the genes identified as specifically occurring in FS^+ *Helicobacter* species likely have roles unrelated to the flagellar sheath, flagellum or motility. There are also intrinsic imitations to identification of orthologous proteins from sequence comparisons, particularly with respect to distinguishing orthologs and paralogs. This problem was most evident for the SLR family members and Hof outer membrane proteins as single members of these protein families were identified as homologs for multiple *H. pylori* proteins (Table 4.1).

Despite these limitations, the comparative genomics approach allowed for the identification of likely candidates for genes with roles in flagellar sheath biosynthesis, which was supported by additional evidence. One such candidate is *clsC*, which we postulate is needed to satisfy an increased demand for cardiolipin during flagellar sheath

biosynthesis. Another reasonable candidate encodes a predicted lipocalin (HP1028). Further circumstantial evidence for HP1028 playing a role in flagellar sheath biosynthesis is its association in an operon with several flagellar genes, which includes *flhFG* and *fliAMY*. Given that some bacterial lipocalins are believed to play a role in maintenance of the outer membrane [42], we hypothesize the lipocalin encoded by HP1028 transports cardiolipin or other phospholipids across the cell envelope for flagellar sheath biosynthesis. Future experiments will examine potential roles for *clsC* and HP1028, as well as other genes identified here, in biosynthesis of the *H. pylori* flagellar sheath or flagellum.

We postulate that some of the genes found predominantly in FS^+ *Helicobacter* species assist in mitigating the action of the sheathed flagellum. Rotation of the sheathed flagellum in *Vibrio* species is a major source of OMVs [21, 22], and it is likely that such is the case in *Helicobacter* species as well. Six of the proteins conserved in FS^+ *Helicobacter* species encode enzymes involved in LPS biosynthesis or modification (Table 4.1), and these modifications contribute to the low endotoxin and immunological activity of *H. pylori* LPS [31-33]. Moreover, some of the SLR proteins conserved in FS^+ *Helicobacter* species are proposed to affect the innate immune response by binding peptidoglycan fragments released from the bacterial cells [37]. It is possible that in addition to releasing OMVs, rotation of the *H. pylori* sheathed flagellum releases peptidoglycan fragments present in the periplasmic space. Thus, the LPS modification enzymes and peptidoglycan-binding SLR proteins may be strategies *Helicobacter* species evolved to avoid activating the host innate immune response by LPS and peptidoglycan fragments released due to rotation of the sheathed flagellum.

Four of the genes conserved in FS^+ *Helicobacter* species but absent in FS^- *Helicobacter* species, which we designated as *faeABCD*, encode a putative tripartite efflux system that is required for flagellar biosynthesis and motility in *H. pylori* B128. Tripartite efflux systems in Gram-negative bacteria consists of an inner membrane ABC transporter, and TolC-like OEP, and a periplasmic MFP that connects the ABC transporter and OEP. Tripartite efflux systems transport a diverse range of proteins, xenobiotics, antibiotics, metal ions and other small molecules [26, 27]. The substrates that are transported by the FaeABCD efflux system are not known, although van Amsterdam and co-workers reported disruption of *faeA* (HP1489) in *H. pylori* 1061 resulted in increased sensitivity to ethidium bromide [47].

The *H. pylori* flagellar motor has 18 MotA/MotB stator units making it the largest bacterial flagellar motor described to date [7]. A unique feature of the *H. pylori* flagellar motor is a cage-like structure with 18-fold symmetry that surrounds it [7]. The proximity of the cage and stator units, together with the identical symmetries of these structures, suggest an interaction between these two flagellar motor components. In *E. coli* and *S. enterica* serovar Typhimurium, the stator units transiently associate with the flagellar motor [9, 48], whereas the stators are stably associated with the flagellar motor in *H. pylori* [7]. Qin and co-workers proposed the cage provides a stable platform to recruit and stabilize stator units at the motor [7]. Deletion of *faeA* or *faeCD* in *H. pylori* B128 resulted in a partial or complete loss of the periplasmic cage surrounding the flagellar motor (Fig. 4.4), which suggests the FaeABCD efflux system constitutes part of the motor cage. In support of this hypothesis, the MFP and OEP components of tripartite efflux systems span

the periplasmic space and connect the inner and outer membranes [49], forming a structure that is consistent with cage that surrounds the *H. pylori* flagellar motor.

In addition to loss of the periplasmic cage, deletion of *faeA* or *faeCD* in *H. pylori* B128 resulted in the loss of other flagellar motor components (Figs. 4.4J-L). Flagellum assembly is a highly ordered process with assembly the axial components proceeding from the rod to the hook and finally to the filament [4, 5]. Qin and co-workers examined the ultrastructure of flagellum assembly intermediates in *H. pylori* using high-throughput cryo-ET to visualize over 300 flagellar motors, and the earliest flagellum assembly intermediate they were able to observe had progressed through rod assembly [7]. The rod assembly intermediate contained the cage and the other motor components present in the mature *H. pylori* flagellum [7], suggesting the aberrant flagellar motors observed in the *faeA* and *faeCD* mutants are not assembly intermediates. A recent cryo-ET study by Kaplan and co-workers examined cells of *Legionella pneumophila*, *Pseudomonas aeruginosa* and *Shewanella oneidensis* and reported disassembly of the flagellar motor results in stable sub-complexes embedded in the outer membrane that consist of embellished P- and L-rings [65]. The averaged structure for the *H. pylori faeA* and *faeCD* mutants shown in Figure 4.4H is reminiscent of the disassembly intermediate observed by Kaplan and co-workers. Thus, the FaeABCD efflux system and/or periplasmic cage surrounding the *H. pylori* flagellar motor may be essential for the stability of the flagellum, and the aberrant motors observed in the *faeA* and *faeCD* mutants are likely flagellum disassembly products.

MATERIALS AND METHODS

Bacterial strains and growth conditions. *Escherichia coli* DH5α was used for cloning and plasmid construction, and was grown in Luria-Bertani broth or agar medium. Medium was supplemented with ampicillin (100 μg/ml), chloramphenicol (30 μg/mL) or kanamycin (30 μg/ml) when appropriate. *H. pylori* B128 and its derivatives were grown at 37ºC on tryptic soy agar (TSA) supplemented with 5% heat-inactivated horse serum under an atmosphere consisting of 10% CO_2, 4% O_2, and 86% N_2. For liquid cultures, *H. pylori* strains were grown at 37ºC with shaking in Mueller-Hinton broth (MHB) supplemented with 5% heat-inactivated horse serum under an atmosphere consisting of 5% CO_2, 10% H_2, 10% O_2 and 75% N_2. Kanamycin (30 μg/ml) or chloramphenicol (30 μg/ml) was added to the medium used to culture *H. pylori* when appropriate.

Strain construction. Primers used for PCR are listed in Table S4.4 and strains used in this study are listed in Table 4.2. Genomic DNA (gDNA) from *H. pylori* B128 was purified using the Wizard genomic DNA purification kit (Promega) and used as the template to construct all deletion mutants. Target sequences from gDNA were amplified using Phusion polymerase (New England Biolabs). To facilitate cloning into the pGEM-T Easy vector (Promega) amplicons were incubated with *Taq* polymerase (Promega) at 72º C for 10 min to add 3'-A overhangs.

H. pylori B128 HPB128_199g42 (HP1489 homolog; *faeA*) and HPB128_199g40 along with HPB128_199g39 (HP1487 and HP1486 homologs, respectively; *faeC* and *faeD*) were deleted as follows. Regions flanking the target genes were amplified from *H. pylori* B128 gDNA using primer pairs P117/P118 plus P119/P120 for *faeA*, and P177/P178 plus P179/P180 for *faeC*/*faeD*. The primer pairs introduced 24 bp of complementary sequence

to the ends of the amplicons used for overlapping PCR. The complementary sequences also included NheI and XhoI restriction sites for a subsequent cloning step. After joining the flanking regions for each target gene by PCR SOEing, the resulting amplicons were cloned into pGEM-T Easy to generate the plasmids pJC049 (carried flanking sequences for *faeA*), and pJC076 (carried flanking sequences for *faeC*/*faeD*). Plasmid pJC038 carries a kan^R-*sacB* cassette in which *sacB* was under control of the *H. pylori ureA* promoter [28]. The kan^R-*sacB* cassette from pJC038 was introduced into unique NheI and XhoI sites in plasmids pJC049 and pJC076 to generate the suicide plasmids pJC051 and pJC080, respectively. The suicide plasmids were introduced by natural transformation into *H. pylori* B128 and transformants were screened for kanamycin resistance. The kan^R-*sacB* cassette in the target genes was removed by transforming the kanamycin-resistant isolates with plasmids pJC049 or pJC076, and transformants in which the *kan-sacB* cassette was replaced with the unmarked deletion were isolated following a sucrose-based counter-selection [45]. Regions flanking the targeted genes were amplified by PCR to confirm the target genes were deleted.

Motility assay. Motility was evaluated using a semisolid medium containing Mueller-Hinton broth, 10% heat-inactivated horse serum, 20 mM MES (2-(4-morpholino)-ethane sulfonic acid) (pH 6.0), 5 μM $FeSO_4$ and 0.4 % Noble agar. A minimum of three biological samples and three technical replicates were used to assess the motility of each strain. *H. pylori* strains grown on TSA supplemented with 10% heat-inactivated horse serum for 4 days were stab-inoculated into the motility agar and incubated at 37° C under an atmospheric condition consisting of 10% CO_2, 4% O_2 and 86% N_2. The diameters of the

resulting swim halos were measured 7 d post-inoculation. The two-sample *t* test was used to determine statistical significance for the results.

Transmission electron microscopy. *H. pylori* strains were grown to late-log phase (OD_{600} ~1.0) in MHB supplemented with 10% heat-inactivated horse serum. Cells from 1 mL of culture were pelleted by centrifugation (550 x g) then resuspended in 125 μL of 0.1 M phosphate-buffered saline. Cells were fixed by adding 50 μL of 16% EM grade formaldehyde and 25 μL of 8% EM grade glutaraldehyde to the cell resuspension. Following incubation at room temperature for 5 min, 10 μL of the cell suspension were applied to a 300 mesh, formvar-coated copper grid and incubated at room temperature for 5 min. The cell suspension was wicked off the grids using a filter paper, and the grids were washed 3 times with 10 μL of water. Cells were stained by applying 10 μL of 1% uranyl acetate to the grids for 30 s. After removing the stain with filter paper, the grids were washed three times with 10 μL of water and then air-dried. Cells were visualized using a JEOL JEM 1011 transmission electron microscope. The number of flagella per cell (n=50) were determined for each strain. The Mann-Whitney U test was used to identify statistically significant differences in number of flagella per cell for the various *H. pylori* strains.

Sample preparation for cryo-EM observation. *H. pylori* strains were cultured on plates for 4 d. The cells on the agar surface were collected then washed with PBS buffer. Colloidal gold solution (10 nm diameter) was added to the diluted *H. pylori* samples and then deposited on a freshly glow-discharged EM grid for 30 seconds. The grid was blotted with filter paper and rapidly plunge-frozen in liquid ethane in a homemade plunger apparatus as described [50].

Cryo-ET data collection and image processing. The frozen-hydrated specimens of *H. pylori* B128 wild type, Δ*faeA* and Δ*faeC*/Δ*faeD* mutants were transferred to Titan Krios electron microscope (Thermo Fisher) equipped with a 300kV field emission gun and a Direct Electron Detector. The data was acquired automatically with Tomography from Thermo Fisher. A total dose of 50 $e^{-}/Å^{2}$ is distributed among 35 tilt images covering angles from −51° to +51° at tilt steps of 3°. The tilt series were aligned using gold fiducial markers and volumes reconstructed by the weighted back-projection method using IMOD and Tomo3d software to generate tomograms [51, 52]. In total, 207 tomograms from *H. pylori* B128 WT cells, 48 tomograms from *H. pylori* B128 Δ*faeA* cells and 70 tomograms from the *H. pylori* B128 Δ*faeC*/Δ*faeD* double mutant cells were generated.

Sub-tomogram analysis with i3 packages. Bacterial flagellar motors were detected manually using the i3 program [53, 54]. The orientation and geographic coordinates of selected particles were then estimated. In total, 511, sub-tomograms of *H. pylori* B128 WT, 77 sub-tomograms of *H. pylori* B128 Δ*faeA* mutant and 137 sub-tomograms of the *H. pylori* B128 Δ*faeC*/Δ*faeD* double mutant flagellar motors were used to sub-tomogram averaging analysis. The i3 tomographic package was used on the basis of the "alignment by classification" method with missing wedge compensation for generating the averaged structure of the motor as described [50].

AUTHOR CONTRIBUTIONS

JKC constructed and characterized the phenotypes of the *H. pylori faeABCD* mutants; KHG, JL, and SZ acquired, analyzed and interpreted the cryo-ET data; JM and TRH acquired, analyzed and interpreted the comparative genomics data; JL and TRH contributed to the design of the study; and KHG, JKC, JM, JL and TRH contributed to the writing of the manuscript.

ACKNOWLEDGEMENTS

We thank Samuel Morris for his assistance in TEM examination of the *H. pylori* strains. This work was supported by NIH grant AI140444 to T.R.H. and NIH grants GM107629 and AI087946 to J.L.

Table 4.1. Genes conserved in *Helicobacter* species that possess flagellar sheaths.

NCBI reference sequence	Locus number *H. pylori* 26695	Locus number *H. pylori* G27	Gene	Known or proposed function	Reference
LPS biosynthesis					
WP_000487418.1	HP0329	HPG27_1018	*futA*	fucosylation of LPS	[55]
WP_000433778.1	HP0580	HPG27_539	*kdhA*	Kdo-lipid A hydrolase	[56]
WP_000487458.1	HP0651	HPG27_613	*futB*	fucosylation of LPS	[55]
WP_000465224.1	HP0694	HPG27_650	*lpxR*	lipid A deacylase	[57]
WP_000898474.1	HP1580	HPG27_1517	*lpxF*	lipid A 4'-phosphatase	[58]
WP_041201341.1	HP1581	HPG27_1518	*wecA*	O-antigen assembly	[59]
Sel1-like proteins					
WP_000597817.1	HP0160	HPG27_147	*hcpD*	penicillin-binding protein	[35]
WP_000901623.1	HP0211	HPG27_193	*hcpA*	penicillin-binding protein	[36]
WP_000111740.1	HP0235	HPG27_215	*hcpE*		
WP_000917816.1	HP0628	HPG27_588	*hcpF*		
WP_000892789.1	HP1098	HPG27_1039	*hcpC*		
WP_000540103.1	HP1117	HPG27_1061			

WP_000943858.1		HPG27_1469	*hcpG*		
outer membrane proteins					
WP_041201349.1	HP0209	HPG27_191	*hofA*		[60]
WP_000768629.1	HP0486	HPG27_445	*hofC*		[60]
WP_012552416.1	HP0487	HPG27_446	*hofD*		[60]
WP_000911466.1	HP0782	HPG27_739	*hofE*		[60]
WP_001108270.1	HP0788	HPG27_744	*hofF*		[60]
WP_041201373.1	HP0914	HPG27_865	*hofG*		[60]
WP_000797787.1	HP1083	HPG27_347	*hofB*		[60]
transport proteins					
WP_000788001.1	HP0839	HPG27_797		putative fatty acid transport protein	[60]
WP_000816869.1	HP0970	HPG27_917	*cznB*	metal efflux pump	[44]
WP_079990419.1	HP0971	HPG27_918	*cznC*	metal efflux pump	[44]
WP_000780237.1	HP1028	HPG27_400		lipocalin	[61]
WP_001008850.1	HP1486	HPG27_1409	*faeD*	ABC-2 family transporter protein	this study

WP_000489110.1	HP1487	HPG27_1410	*faeC*	ABC-2 family transporter protein	this study
WP_012552579.1	HP1488	HPG27_1411	*faeB*	membrane fusion protein	this study
WP_000754037.1	HP1489	HPG27_1412	*faeA*	outer membrane efflux protein	this study
miscellaneous functions					
WP_000820014.1	HP0018	HPG27_17		predicted lipoprotein	
WP_041201345.1	HP0097	HPG27_89		predicted lipoprotein	
WP_000233964.1	HP0111	HPG27_0103	*hrcA*	heat-inducible repressor	[62]
WP_000689112.1	HP0190	HPG27_174	*clsC*	cardiolipin synthase	[28]
WP_000949206.1	HP0653	HPG27_615	*ftnA*	bacterial non-heme ferritin	[63]
WP_000790557.1	HP0827	HPG27_786		RNA or ssDNA-binding protein	
WP_001268507.1	HP0838	HPG27_796		putative lipoprotein	
WP_000896338.1	HP1440	HPG27_1362	*ispDF*	isoprenoid biosynthesis	[64]
WP_000925195.1	HP1457	HPG27_1380		potential PBP1b activator	

Table 4.2. *H. pylori* strains and plasmids used in this study.

Strain	Relevant Genotype	Source
B128	wild-type	R. Peek, Jr.
HP116	B128 HPB128_199g42 (HP1489):: kan^R-P_{ureA}-*sacB*	this study
HP119	HP116 ΔHPB128_199g42 (HP1489)	this study
HP174	B128 HPB128_199g40/39 (HP1487/HP1486):: *kan^R-P_{ureA}-sacB*	this study
HP185	HP174 ΔHPB128_199g40/39 (HP1487/HP1486)	this study

Plasmid	Description	Source
pJC038	pGEM-T Easy carrying kan^R-P_{ureA}-*sacB*	[28]
pJC049	pGEM-T Easy carrying flanking regions of HPB128_199g42	this study
pJC051	pJC049 with *kan^R-P_{ureA}-sacB* insert	this study
pJC076	pGEM-T Easy carrying flanking regions HPB128_199g40/39	this study
pJC080	pJC076 with *kan^R-P_{ureA}-sacB* insert	this study

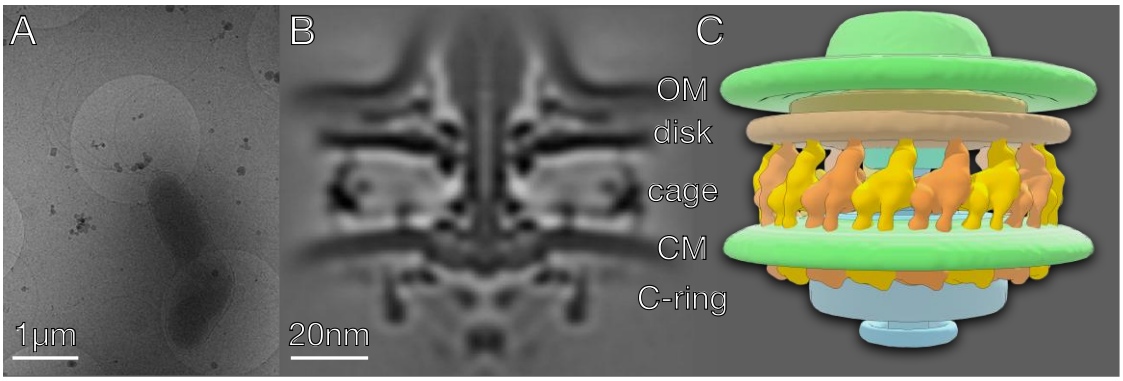

Figure 4.1. Structure of the *H. pylori* flagellar motor. (A) A low magnification cryo-EM image shows a cell with four flagella at the pole. (B) A central slice and (C) a surface view of the basal body structure. The cage subunits colored in yellow and orange are clearly visiable in the averaged structure.

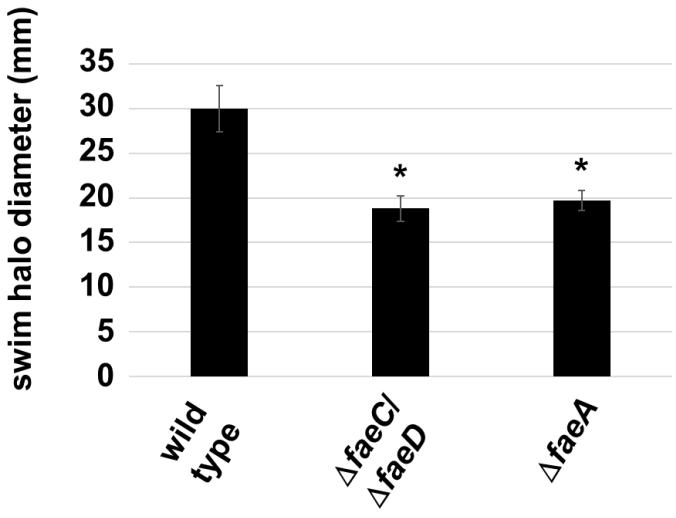

Figure 4.2. Motility of *H. pylori* B128 wild type and *fae* efflux system mutants. Motility was assessed by inoculating *H. pylori* strains into soft agar medium and allowing the cells to migrate from the point of inoculation. Bars indicate the mean of swim halo diameters measured 7 d post-inoculation (n= 12 to 16). Error bars correspond to one standard deviation. Asterisks indicate a significant difference between the mutant and wild type (*p*-value < 0.0001). Statistical significance was determined using a two-sample *t* test.

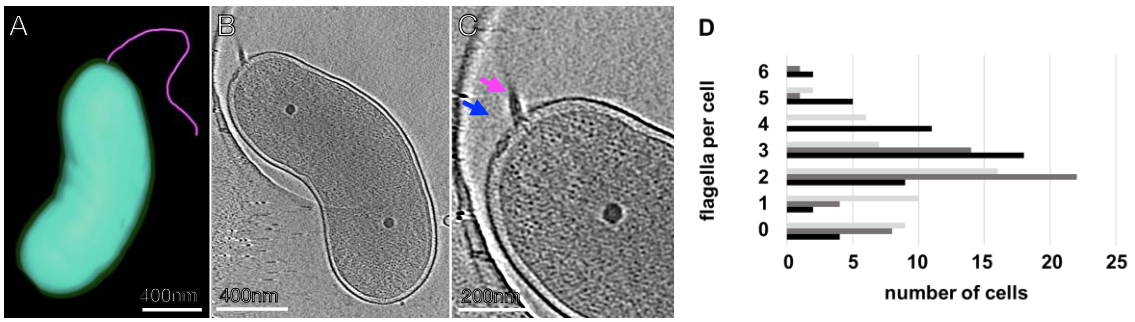

Figure 4.3. Flagella counts for *H. pylori* B128 wild type and *fae* mutants. (A) A 3D view of a Δ*faeA* cell. There is one flagellum (purple) visible at a cell pole. (B) A slice from the reconstruction of the Δ*faeA* cell. (C) A zoom-in view of the cell pole shows the flagellar basal body (purple arrow). In addition, there is a sub-assembly lacking filament (blue arrow). (D) For each *H. pylori* strain, cells were visualized by TEM and flagella were counted for 50 cells. The x-axis indicates the number of cells counted with the number of flagella per cell indicated in the y-axis. Data for the various *H. pylori* strains are indicated as follows: wild type (black bars), Δ*faeCD* mutant (dark gray bars), and Δ*faeA* (light gray bars). Both mutants produced fewer flagella per cell than wild type (*p*-values <0.01). Statistical significance was determined using a Mann-Whitney U test.

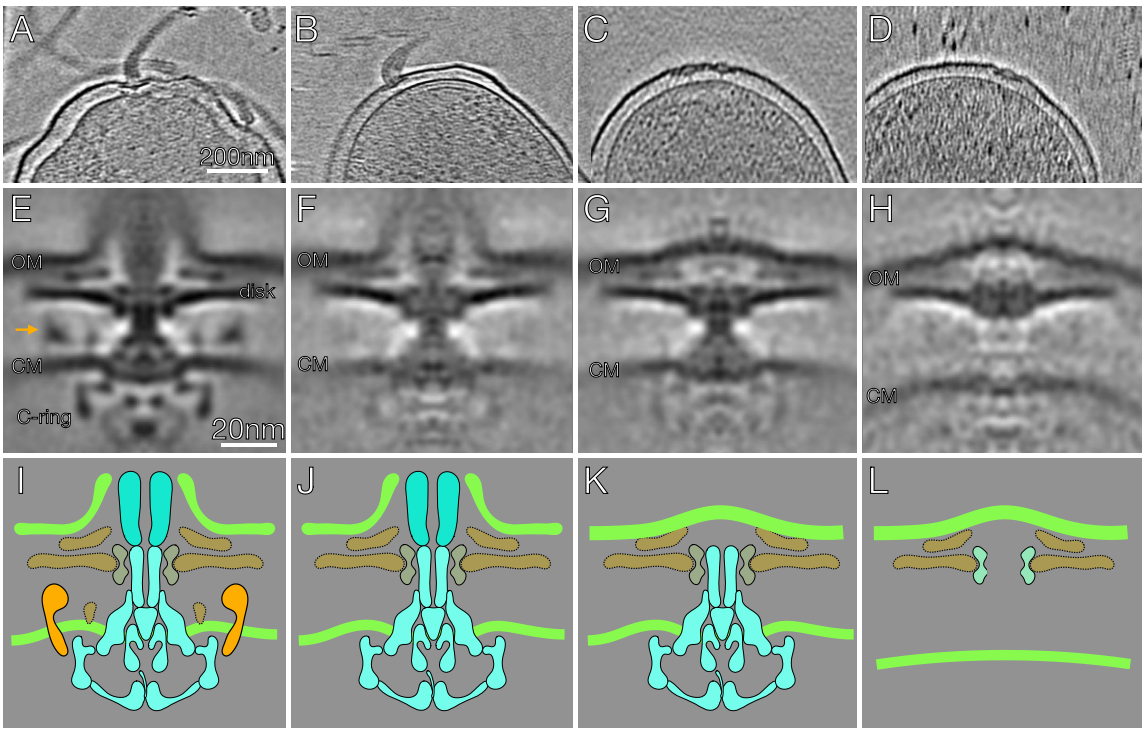

Figure 4.4. Flagellar motors of the *H. pylori* B128 Δ*faeA* and Δ*faeCD* mutants. (A to D) Representative slices of cryo-ET reconstructions show various aberrant forms of flagellar motor from the mutants. (E to H) Central slices of the averaged structures of the specific classes of flagellar motors. Each averaged structure is below the representative slice for the specific class of motor. (I to L) The corresponding cartoon illustrations for the various classes of motor structures. The color scheme is: orange, cage; brown, putative FliL ring, P-disk and outer disk; gray, L- and P-rings; cyan, C-ring, MS-ring, export apparatus, rod, and hook; green, outer membrane, flagellar sheath, inner membrane.

REFERENCES

1. Atherton, J.C. and M.J. Blaser, *Coadaptation of Helicobacter pylori and humans: ancient history, modern implications.* J Clin Invest, 2009. **119**(9): p. 2475-87.

2. Eaton, K.A., D.R. Morgan, and S. Krakowka, *Motility as a factor in the colonisation of gnotobiotic piglets by Helicobacter pylori.* J. Med. Microbiol., 1992. **37**: p. 123-127.

3. Ottemann, K.M. and A.C. Lowenthal, *Helicobacter pylori uses motility for initial colonization and to attain robust infection.* Infect Immun, 2002. **70**(4): p. 1984-90.

4. Chevance, F.F. and K.T. Hughes, *Coordinating assembly of a bacterial macromolecular machine.* Nat Rev Microbiol, 2008. **6**(6): p. 455-65.

5. Macnab, R.M., *How bacteria assemble flagella.* Annu Rev Microbiol, 2003. **57**: p. 77-100.

6. Manson, M.D., et al., *A protonmotive force drives bacterial flagella.* Proc Natl Acad Sci U S A, 1977. **74**(7): p. 3060-4.

7. Qin, Z., et al., *Imaging the motility and chemotaxis machineries in Helicobacter pylori by cryo-electron tomography.* J Bacteriol, 2017. **199**(3): p. e00695-16.

8. Kostrzynska, M., et al., *Identification, characterization, and spatial localization of two flagellin species in Helicobacter pylori flagella.* J Bacteriol, 1991. **173**(3): p. 937-46.

9. Beeby, M., et al., *Diverse high-torque bacterial flagellar motors assemble wider stator rings using a conserved protein scaffold.* Proc Natl Acad Sci U S A, 2016. **113**(13): p. E1917-26.

10. Chen, S., et al., *Structural diversity of bacterial flagellar motors.* EMBO J, 2011. **30**(14): p. 2972-81.

11. Motaleb, M.A., et al., *A novel gene inactivation system reveals altered periplasmic flagellar orientation in a Borrelia burgdorferi fliL mutant.* J Bacteriol, 2011. **193**(13): p. 3324-31.

12. Geis, G., et al., *Ultrastructure and chemical analysis of Campylobacter pylori flagella.* J Clin Microbiol, 1989. **27**(3): p. 436-41.

13. Doig, P. and T.J. Trust, *Identification of surface-exposed outer membrane antigens of Helicobacter pylori.* Infect Immun, 1994. **62**(10): p. 4526-33.

14. Jones, A.C., et al., *A flagellar sheath protein of Helicobacter pylori is identical to HpaA, a putative N-acetylneuraminyllactose-binding hemagglutinin, but is not an adhesin for AGS cells.* J. Bacteriol., 1997. **179**: p. 5643-5647.

15. Luke, C.J. and C.W. Penn, *Identification of a 29 kDa flagellar sheath protein in Helicobacter pylori using a murine monoclonal antibody.* Microbiology, 1995. **141 (Pt 3)**: p. 597-604.

16. Lundstrom, A.M., et al., *HpaA shows variable surface localization but the gene expression is similar in different Helicobacter pylori strains.* Microb Pathog, 2001. **31**(5): p. 243-53.

17. Radin, J.N., et al., *Flagellar localization of a Helicobacter pylori autotransporter protein.* mBio, 2013. **4**(2): p. e00613-12.

18. Yoon, S.S. and J.J. Mekalanos, *Decreased potency of the Vibrio cholerae sheathed flagellum to trigger host innate immunity.* Infect Immun, 2008. **76**(3): p. 1282-8.

19. Lee, S.K., et al., *Helicobacter pylori flagellins have very low intrinsic activity to stimulate human gastric epithelial cells via TLR5.* Microbes Infect, 2003. **5**(15): p. 1345-56.

20. Smith, K.D., et al., *Toll-like receptor 5 recognizes a conserved site on flagellin required for protofilament formation and bacterial motility.* Nat Immunol, 2003. **4**(12): p. 1247-53.

21. Aschtgen, M.S., et al., *Rotation of Vibrio fischeri Flagella Produces Outer Membrane Vesicles That Induce Host Development.* J Bacteriol, 2016. **198**(16): p. 2156-65.

22. Brennan, C.A., et al., *A model symbiosis reveals a role for sheathed-flagellum rotation in the release of immunogenic lipopolysaccharide.* Elife, 2014. **3**: p. e01579.

23. Manning, A.J. and M.J. Kuehn, *Contribution of bacterial outer membrane vesicles to innate bacterial defense.* BMC Microbiol, 2011. **11**: p. 258.

24. Zhang, H., et al., *Polar flagella rotation in Vibrio parahaemolyticus confers resistance to bacteriophage infection.* Sci Rep, 2016. **6**: p. 26147.

25. Chu, J., J. Liu, and T.R. Hoover, *Phylogenetic Distribution, Ultrastructure, and Function of Bacterial Flagellar Sheaths.* Biomolecules, 2020. **10**(3).

26. Hinchliffe, P., et al., *Structure and operation of bacterial tripartite pumps.* Annu Rev Microbiol, 2013. **67**: p. 221-42.

27. Pasqua, M., et al., *The varied role of efflux pumps of the MFS family in the interplay of bacteria with animal and plant cells.* Microorganisms, 2019. **7**(9).

28. Chu, J.K., et al., *Loss of a Cardiolipin Synthase in Helicobacter pylori G27 Blocks Flagellum Assembly.* J Bacteriol, 2019. **201**(21).

29. Huang, K.C., R. Mukhopadhyay, and N.S. Wingreen, *A curvature-mediated mechanism for localization of lipids to bacterial poles.* PLoS Comput Biol, 2006. **2**(11): p. e151.

30. Renner, L.D. and D.B. Weibel, *Cardiolipin microdomains localize to negatively curved regions of Escherichia coli membranes.* Proc Natl Acad Sci U S A, 2011. **108**(15): p. 6264-9.

31. Birkholz, S., et al., *Immunological activity of lipopolysaccharide of Helicobacter pylori on human peripheral mononuclear blood cells in comparison to lipopolysaccharides of other intestinal bacteria.* FEMS Immunol Med Microbiol, 1993. **6**(4): p. 317-24.

32. Muotiala, A., et al., *Low biological activity of Helicobacter pylori lipopolysaccharide.* Infect Immun, 1992. **60**(4): p. 1714-6.

33. Perez-Perez, G.I., et al., *Activation of human THP-1 cells and rat bone marrow-derived macrophages by Helicobacter pylori lipopolysaccharide.* Infect Immun, 1995. **63**(4): p. 1183-7.

34. Mittl, P.R. and W. Schneider-Brachert, *Sel1-like repeat proteins in signal transduction.* Cell Signal, 2007. **19**(1): p. 20-31.

35. Krishnamurthy, P., et al., *Identification of a novel penicillin-binding protein from Helicobacter pylori.* J Bacteriol, 1999. **181**(16): p. 5107-10.

36. Mittl, P.R., et al., *The cysteine-rich protein A from Helicobacter pylori is a beta-lactamase.* J Biol Chem, 2000. **275**(23): p. 17693-9.

37. Deml, L., et al., *Characterization of the Helicobacter pylori cysteine-rich protein A as a T-helper cell type 1 polarizing agent.* Infect Immun, 2005. **73**(8): p. 4732-42.

38. Bauwens, E., et al., *In silico proteomic and phylogenetic analysis of the outer membrane protein repertoire of gastric Helicobacter species.* Sci Rep, 2018. **8**(1): p. 15453.

39. Cheng, L., et al., *The Helicobacter heilmannii hofE and hofF genes are essential for colonization of the gastric mucosa and play a role in IL-1b-induced gastric MUC13 expression.* Helicobacter, 2016. **21**(6): p. 504-522.

40. Flower, D.R., A.C. North, and C.E. Sansom, *The lipocalin protein family: structural and sequence overview.* Biochim Biophys Acta, 2000. **1482**(1-2): p. 9-24.

41. El-Halfawy, O.M., et al., *Antibiotic capture by bacterial lipocalins uncovers an extracellular mechanism of intrinsic antibiotic resistance.* mBio, 2017. **8**(2).

42. Bishop, R.E., et al., *Bacterial lipocalins: origin, structure, and function*, in *Madame Curie Bioscience Database [Internet]*. Landes Bioscience: Austin, TX.

43. Sharma, C.M., et al., *The primary transcriptome of the major human pathogen Helicobacter pylori.* Nature, 2010. **464**(7286): p. 250-5.

44. Stahler, F.N., et al., *The novel Helicobacter pylori CznABC metal efflux pump is required for cadmium, zinc, and nickel resistance, urease modulation, and gastric colonization.* Infect Immun, 2006. **74**(7): p. 3845-52.

45. Copass, M., G. Grandi, and R. Rappuoli, *Introduction of unmarked mutations in the Helicobacter pylori vacA gene with a sucrose sensitivity marker.* Infect Immun, 1997. **65**(5): p. 1949-52.

46. Berthenet, E., et al., *Whole-genome sequencing and bioinformatics as pertinent tools to support Helicobacteracae taxonomy, based on three strains suspected to belong to novel Helicobacter species.* Front Microbiol, 2019. **10**: p. 2820.

47. van Amsterdam, K., A. Bart, and A. van der Ende, *A Helicobacter pylori TolC Efflux Pump Confers Resistance to Metronidazole.* Antimicrobial Agents and Chemotherapy, 2005. **49**: p. 1477-1482.

48. Tipping, M.J., et al., *Load-dependent assembly of the bacterial flagellar motor.* mBio, 2013. **4**(4): p. e00551-13.

49. Jo, I., et al., *Recent paradigm shift in the assembly of bacterial tripartite efflux pumps and the type I secretion system.* J Microbiol, 2019. **57**(3): p. 185-194.

50. Zhu, S., et al., *In situ structural analysis of the spirochetal flagellar motor by cryo-electron tomography.* Methods Mol Biol, 2017. **1593**: p. 229-242.

51. Agulleiro, J.I. and J.J. Fernandez, *Tomo3D 2.0--exploitation of advanced vector extensions (AVX) for 3D reconstruction.* J Struct Biol, 2015. **189**(2): p. 147-52.

52. Kremer, J.R., D.N. Mastronarde, and J.R. McIntosh, *Computer visualization of three-dimensional image data using IMOD.* J Struct Biol, 1996. **116**(1): p. 71-6.

53. Winkler, H., *3D reconstruction and processing of volumetric data in cryo-electron tomography.* J Struct Biol, 2007. **157**(1): p. 126-37.

54. Winkler, H., et al., *Tomographic subvolume alignment and subvolume classification applied to myosin V and SIV envelope spikes.* J Struct Biol, 2009. **165**(2): p. 64-77.

55. Appelmelk, B.J., et al., *Phase variation in Helicobacter pylori lipopolysaccharide due to changes in the lengths of poly(C) tracts in alpha3-fucosyltransferase genes.* Infect Immun, 1999. **67**(10): p. 5361-6.

56. Stead, C.M., et al., *Removal of the outer Kdo from Helicobacter pylori lipopolysaccharide and its impact on the bacterial surface.* Mol Microbiol, 2010. **78**(4): p. 837-52.

57. Stead, C.M., et al., *Deciphering the unusual acylation pattern of Helicobacter pylori lipid A.* J Bacteriol, 2008. **190**(21): p. 7012-21.

58. Cullen, T.W., et al., *Helicobacter pylori versus the host: remodeling of the bacterial outer membrane is required for survival in the gastric mucosa.* PLoS Pathog, 2011. **7**(12): p. e1002454.

59. Hug, I., et al., *Helicobacter pylori lipopolysaccharide is synthesized via a novel pathway with an evolutionary connection to protein N-glycosylation.* PLoS Pathog, 2010. **6**(3): p. e1000819.

60. Alm, R.A., et al., *Comparative genomics of Helicobacter pylori: analysis of the outer membrane protein families.* Infect Immun, 2000. **68**(7): p. 4155-68.

61. Barison, N., et al., *Protein HP1028 from the human pathogen Helicobacter pylori belongs to the lipocalin family.* Acta Crystallogr D Biol Crystallogr, 2013. **69**(Pt 8): p. 1387-94.

62. Homuth, G., et al., *Transcriptional analysis of major heat shock genes of Helicobacter pylori.* J Bacteriol, 2000. **182**(15): p. 4257-63.

63. Doig, P., J.W. Austin, and T.J. Trust, *The Helicobacter pylori 19.6-kilodalton protein is an iron-containing protein resembling ferritin.* J Bacteriol, 1993. **175**(2): p. 557-60.

64. Perez-Gil, J., et al., *Cloning and functional characterization of an enzyme from Helicobacter pylori that catalyzes two steps of the methylerythritol phosphate*

pathway for isoprenoid biosynthesis. Biochim Biophys Acta, 2010. **1800**(9): p. 919-28.

65. Kaplan, M., et al., *In situ imaging of the bacterial flagellar motor disassembly and assembly processes.* EMBO J, 2019. **38**(14): p. e100957.

SUPPLEMENTAL DATA

Table S4.1. Primers used in this study.

primer ID #	primer name	sequence
P117	HP1489 US_F	5’-CATCAAAAACGCGGTGGA-3’
P118	HP1489 US_R	5’-GCTAGCATAATCGAATTCCTCGAGAGGAACTCCATCAACAGCGCT-3’
P119	HP1489 DS_F	5’-CTCGAGGAATTCGATTATGCTAGCGCTTATAAATACATTGTTTCATTAGCG-3’
P120	HP1489 DS_R	5’-CTTAGGGCTAAGCTCACCACC-3’
P139	HP1488 US F	5’-GAAGACATGATCCCTAGTTGGTTT-3’
P140	HP1488 US R	5’-GCTAGCGATTCGATCCTCGAGCACTTCAGCCTTAGGGCG-3’
P141	HP1488 DS F	5’-CTCGAGGATCGAATCGCTAGCGAGTTTAGGGTGGGTAAGGAATTT-3’
P142	HP1488 DS R	5’-CCACTTGGTATTTGATTTGAAGTG-3’
P177	1487 US F	5’-AAGCGCGATGAAGCCTAT-3’
P178	1487 US R	5’-GCTAGCGATTCGATCCTCGAGCTTGTCTTGTAAAACCCATGC-3’
P179	1486 DS F	5’-CTCGAGGATCGAATCGCTAGCTTGAATCAAATGCATGCG-3’
P180	1486 DS R	5’-AAAAACGCTTGCAAATTTTC-3’

Table S4.2. *Helicobacter* genomes examined for homologs of *H. pylori* G27 genes.

***Helicobacter* species with flagellar sheaths**		
species and strain	**sequence status**	**reference**
Helicobacter acinonychis Sheeba	finished	(1)
Helicobacter ailurogastricus ASB7	incomplete	(2)
Helicobacter anseris MIT 04-9362	incomplete	
Helicobacter aurati isolate 137778_3	incomplete	(3)
Helicobacter baculiformis isolate 427351_3	incomplete	(4)
Helicobacter bilis AAQJH	finished	(5)
Helicobacter bizzozeronii CIII-1	finished	(6)
Helicobacter brantae MIT 04-9366	incomplete	(7)
Helicobacter canis NCTC 12740	finished	(8)
Helicobacter cetorum MIT 99-5656	finished	(9)
Helicobacter cholecystus ERZ467480	incomplete	(10)
Helicobacter cinaedi ATCC BAA-847	finished	(11)
Helicobacter cynogastricus 329937_4	incomplete	(12)
Helicobacter equorum 361872_4	incomplete	(13)
Helicobacter felis ATCC 49179	finished	(14)
Helicobacter fennelliae MRY-12-0050	finished	(11)
Helicobacter heilmannii ASB1.4	finished	(15)
Helicobacter hepaticus ATCC 51449	finished	(16)
Helicobacter himalayensis YS1	finished	(17)
Helicobacter jaachi MIT 09-6949	finished	(18)
Helicobacter japonicus MIT 01-6451	incomplete	(19)
Helicobacter labetoulli 48519	incomplete	(7)
Helicobacter macacae MIT 99-5501	finished	(20)
Helicobacter magdeburgensis MIT 96-1001	finished	(21)
Helicobacter marmotae 152490_3	incomplete	(22)
Helicobacter muridarum ST1	incomplete	(23)
Helicobacter mustelae 12198	finished	(24)
Helicobacter pametensis ATCC 51478	incomplete	(25)
Helicobacter rappini 95150_3	incomplete	(26)
Helicobacter saguini MIT 97-6194	finished	(27)
Helicobacter salomonis 56878_5	incomplete	(28)
Helicobacter suis HS1	incomplete	(29)
Helicobacter trogontum ATCC 700114	finished	(30)
Helicobacter typhlonius MIT 97-6810	finished	(31)

***Helicobacter* species with unsheathed flagella**		
species and strain	**sequence status**	**(7)**
Helicobacter apodemus SCJK1	finished	(32)
Helicobacter burdigaliensis CNRCH 2005/566H	incomplete	(7)
Helicobacter canadensis MIT 98-5491	finished	(33)

Helicobacter ganmani MIT 99-5101	incomplete	(7)
Helicobacter mesocricetorum 87012_3	incomplete	(34)
Helicobacter pullorum MIT 98-5489	incomplete	(35)
Helicobacter rodentium ATCC 700285	incomplete	(36)
Helicobacter valdiviensis WBE14	incomplete	(37)
Helicobacter winghamensis ATCC BAA-430	finished	(38)

SUPPLEMENTAL REFERENCES

1. Eppinger M, Baar C, Linz B, Raddatz G, Lanz C, Keller H, Morelli G, Gressmann H, Achtman M, Schuster SC**.** 2006. Who ate whom? Adaptive Helicobacter genomic changes that accompanied a host jump from early humans to large felines. PLoS Genet 2**:**e120.

2. Joosten M, Linden S, Rossi M, Tay AC, Skoog E, Padra M, Peters F, Perkins T, Vandamme P, Van Nieuwerburgh F, D'Herde K, Van den Broeck W, Flahou B, Deforce D, Ducatelle R, Marshall B, Haesebrouck F, Smet A**.** 2016. *Divergence between the highly virulent zoonotic pathogen Helicobacter heilmannii and its closest relative, the low-virulence "Helicobacter ailurogastricus" sp. nov*. Infect Immun 84**:**293-306.

3. Patterson MM, Schrenzel MD, Feng Y, Xu S, Dewhirst FE, Paster BJ, Thibodeau SA, Versalovic J, Fox JG**.** 2000. *Helicobacter aurati sp. nov., a urease-positive Helicobacter species cultured from gastrointestinal tissues of Syrian hamsters*. J Clin Microbiol 38**:**3722-3728.

4. Baele M, Decostere A, Vandamme P, Van den Bulck K, Gruntar I, Mehle J, Mast J, Ducatelle R, Haesebrouck F**.** 2008. *Helicobacter baculiformis sp. nov., isolated from feline stomach mucosa*. Int J Syst Evol Microbiol 58**:**357-364.

5. Fox JG, Yan LL, Dewhirst FE, Paster BJ, Shames B, Murphy JC, Hayward A, Belcher JC, Mendes EN**.** 1995. *Helicobacter bilis sp. nov., a novel Helicobacter species isolated from bile, livers, and intestines of aged, inbred mice.* J Clin Microbiol 33**:**445-454.

6. Schott T, Rossi M, Hanninen ML**.** 2011. *Genome sequence of Helicobacter bizzozeronii strain CIII-1, an isolate from human gastric mucosa.* J Bacteriol 193**:**4565-4566.

7. Berthenet E, Benejat L, Menard A, Varon C, Lacomme S, Gontier E, Raymond J, Boussaba O, Toulza O, Ducournau A, Buissonniere A, Giese A, Megraud F, Bessede E, Jehanne Q, Lehours P**.** 2019. *Whole-genome sequencing and bioinformatics as pertinent tools to support Helicobacteracae taxonomy, based on three strains suspected to belong to novel Helicobacter species.* Front Microbiol 10**:**2820.

8. Stanley J, Linton D, Burnens AP, Dewhirst FE, Owen RJ, Porter A, On SL, Costas M**.** 1993. *Helicobacter canis sp. nov., a new species from dogs: an integrated study of phenotype and genotype.* J Gen Microbiol 139**:**2495-2504.

9. Harper CG, Feng Y, Xu S, Taylor NS, Kinsel M, Dewhirst FE, Paster BJ, Greenwell M, Levine G, Rogers A, Fox JG**.** 2002. *Helicobacter cetorum sp. nov.,*

a urease-positive Helicobacter species isolated from dolphins and whales. J Clin Microbiol 40**:**4536-4543.

10. Franklin CL, Beckwith CS, Livingston RS, Riley LK, Gibson SV, Besch-Williford CL, Hook RR, Jr. 1996. *Isolation of a novel Helicobacter species, Helicobacter cholecystus sp. nov., from the gallbladders of Syrian hamsters with cholangiofibrosis and centrilobular pancreatitis*. J Clin Microbiol 34**:**2952-2958.

11. Totten PA, Fennell CL, Tenover FC, Wezenberg JM, Perine PL, Stamm WE, Holmes KK**.** 1985. *Campylobacter cinaedi (sp. nov.) and Campylobacter fennelliae (sp. nov.): two new Campylobacter species associated with enteric disease in homosexual men*. J Infect Dis 151**:**131-139.

12. Van den Bulck K, Decostere A, Baele M, Vandamme P, Mast J, Ducatelle R, Haesebrouck F**.** 2006. *Helicobacter cynogastricus sp. nov., isolated from the canine gastric mucosa.* Int J Syst Evol Microbiol 56**:**1559-1564.

13. Moyaert H, Decostere A, Vandamme P, Debruyne L, Mast J, Baele M, Ceelen L, Ducatelle R, Haesebrouck F**.** 2007. *Helicobacter equorum sp. nov., a urease-negative Helicobacter species isolated from horse faeces.* Int J Syst Evol Microbiol 57**:**213-218.

14. Arnold IC, Zigova Z, Holden M, Lawley TD, Rad R, Dougan G, Falkow S, Bentley SD, Muller A**.** 2011. *Comparative whole genome sequence analysis of the carcinogenic bacterial model pathogen Helicobacter felis*. Genome Biol Evol 3**:**302-308.

15. Smet A, Flahou B, D'Herde K, Vandamme P, Cleenwerck I, Ducatelle R, Pasmans F, Haesebrouck F**.** 2012. *Helicobacter heilmannii sp. nov., isolated from feline gastric mucosa*. Int J Syst Evol Microbiol 62**:**299-306.

16. Suerbaum S, Josenhans C, Sterzenbach T, Drescher B, Brandt P, Bell M, Droge M, Fartmann B, Fischer HP, Ge Z, Horster A, Holland R, Klein K, Konig J, Macko L, Mendz GL, Nyakatura G, Schauer DB, Shen Z, Weber J, Frosch M, Fox JG**.** 2003. *The complete genome sequence of the carcinogenic bacterium Helicobacter hepaticus.* Proc Natl Acad Sci U S A 100**:**7901-7906.

17. Hu S, Jin D, Lu S, Liu S, Zhang J, Wang Y, Bai X, Xiong Y, Huang Y, Xu H, Wang Y, Du X, Ye C, Hanninen ML, Xu J**.** 2015. *Helicobacter himalayensis sp. nov. isolated from gastric mucosa of Marmota himalayana.* Int J Syst Evol Microbiol 65**:**1719-1725.

18. Shen Z, Feng Y, Sheh A, Everitt J, Bertram F, Paster BJ, Fox JG**.** 2015. *Isolation and characterization of a novel Helicobacter species, Helicobacter jaachi sp. nov., from common marmosets (Callithrix jaachus).* J Med Microbiol 64**:**1063-1073.

19. Shen Z, Feng Y, Muthupalani S, Sheh A, Cheaney LE, Kaufman CA, Gong G, Paster BJ, Fox JG**.** 2016. *Novel Helicobacter species H.japonicum isolated from laboratory mice from Japan induces typhlocolitis and lower bowel carcinoma in C57BL/129 IL10-/- mice.* Carcinogenesis 37**:**1190-1198.

20. Fox JG, Boutin SR, Handt LK, Taylor NS, Xu S, Rickman B, Marini RP, Dewhirst FE, Paster BJ, Motzel S, Klein HJ**.** 2007. I*solation and characterization of a novel helicobacter species, "Helicobacter macacae," from rhesus monkeys with and without chronic idiopathic colitis.* J Clin Microbiol 45**:**4061-4063.

21. Traverso FR, Bohr UR, Oyarzabal OA, Rohde M, Clarici A, Wex T, Kuester D, Malfertheiner P, Fox JG, Backert S**.** 2010. *Morphologic, genetic, and biochemical characterization of Helicobacter magdeburgensis, a novel species isolated from the intestine of laboratory mice*. Helicobacter 15**:**403-415.

22. Fox JG, Shen Z, Xu S, Feng Y, Dangler CA, Dewhirst FE, Paster BJ, Cullen JM**.** 2002. *Helicobacter marmotae sp. nov. isolated from livers of woodchucks and intestines of cats*. J Clin Microbiol 40**:**2513-2519.

23. Lee A, Phillips MW, O'Rourke JL, Paster BJ, Dewhirst FE, Fraser GJ, Fox JG, Sly LI, Romaniuk PJ, Trust TJ, et al. 1992. *Helicobacter muridarum sp. nov., a microaerophilic helical bacterium with a novel ultrastructure isolated from the intestinal mucosa of rodents.* Int J Syst Bacteriol 42**:**27-36.

24. Fox JG, Cabot EB, Taylor NS, Laraway R**.** 1988. *Gastric colonization by Campylobacter pylori subsp. mustelae in ferrets.* Infect Immun 56**:**2994-2996.

25. Dewhirst FE, Seymour C, Fraser GJ, Paster BJ, Fox JG**.** 1994. *Phylogeny of Helicobacter isolates from bird and swine feces and description of Helicobacter pametensis sp. nov*. Int J Syst Bacteriol 44**:**553-560.

26. Dewhirst FE, Fox JG, Mendes EN, Paster BJ, Gates CE, Kirkbride CA, Eaton KA**.** 2000. *'Flexispira rappini' strains represent at least 10 Helicobacter taxa*. Int J Syst Evol Microbiol 50 Pt 5**:**1781-1787.

27. Shen Z, Mannion A, Whary MT, Muthupalani S, Sheh A, Feng Y, Gong G, Vandamme P, Holcombe HR, Paster BJ, Fox JG**.** 2016. *Helicobacter saguini, a Novel Helicobacter Isolated from Cotton-Top Tamarins with Ulcerative Colitis, Has Proinflammatory Properties and Induces Typhlocolitis and Dysplasia in Gnotobiotic IL-10-/- Mice.* Infect Immun 84**:**2307-2316.

28. Jalava K, Kaartinen M, Utriainen M, Happonen I, Hanninen ML**.** 1997. *Helicobacter salomonis sp. nov., a canine gastric Helicobacter sp. related to Helicobacter felis and Helicobacter bizzozeronii*. Int J Syst Bacteriol 47**:**975-982.

29. Baele M, Decostere A, Vandamme P, Ceelen L, Hellemans A, Mast J, Chiers K, Ducatelle R, Haesebrouck F**.** 2008. *Isolation and characterization of Helicobacter suis sp. nov. from pig stomachs.* Int J Syst Evol Microbiol 58**:**1350-1358.

30. Mendes EN, Queiroz DM, Dewhirst FE, Paster BJ, Moura SB, Fox JG**.** 1996. *Helicobacter trogontum sp. nov., isolated from the rat intestine.* Int J Syst Bacteriol 46**:**916-921.

31. Frank J, Dingemanse C, Schmitz AM, Vossen RH, van Ommen GJ, den Dunnen JT, Robanus-Maandag EC, Anvar SY**.** 2015. *The Complete Genome Sequence of the Murine Pathobiont Helicobacter typhlonius.* Front Microbiol 6**:**1549.

32. Jeon WJ, Dong HJ, Shin JH, Kim IY, Ho H, Oh SH, Yoon YM, Choi YK, Suh JG, Nam KH, Kim HC, Cho S, Seong JK**.** 2015. *Helicobacter apodemus sp. nov., a new Helicobacter species identified from the gastrointestinal tract of striped field mice in Korea*. J Vet Sci 16**:**475-481.

33. Loman NJ, Snyder LA, Linton JD, Langdon R, Lawson AJ, Weinstock GM, Wren BW, Pallen MJ**.** 2009. *Genome sequence of the emerging pathogen Helicobacter canadensis.* J Bacteriol 191**:**5566-5567.

34. Simmons JH, Riley LK, Besch-Williford CL, Franklin CL**.** 2000. *Helicobacter mesocricetorum sp. nov., A novel Helicobacter isolated from the feces of Syrian hamsters.* J Clin Microbiol 38**:**1811-1817.

35. Stanley J, Linton D, Burnens AP, Dewhirst FE, On SL, Porter A, Owen RJ, Costas M**.** 1994. *Helicobacter pullorum sp. nov.-genotype and phenotype of a new species isolated from poultry and from human patients with gastroenteritis.* Microbiology 140 (Pt 12)**:**3441-3449.

36. Shen Z, Fox JG, Dewhirst FE, Paster BJ, Foltz CJ, Yan L, Shames B, Perry L**.** 1997. *Helicobacter rodentium sp. nov., a urease-negative Helicobacter species isolated from laboratory mice*. Int J Syst Bacteriol 47**:**627-634.

37. Collado L, Jara R, Gonzalez S**.** 2014. *Description of Helicobacter valdiviensis sp. nov., an Epsilonproteobacteria isolated from wild bird faecal samples.* Int J Syst Evol Microbiol 64**:**1913-1919.

38. Melito PL, Munro C, Chipman PR, Woodward DL, Booth TF, Rodgers FG**.** 2001. *Helicobacter winghamensis sp. nov., a novel Helicobacter sp. isolated from patients with gastroenteritis*. J Clin Microbiol 39**:**2412-2417.

CHAPTER 5

EXAMINATION OF THE FLAGELLAR MOTOR STATOR COMPLEX IN *HELICOBACTER PYLORI*

Katherine H. Gibson, Shiwei Zhu, Timothy R. Hoover, and Jun Liu. To be submitted to Proceedings of the National Academy of Sciences, U.S.A.

ABSTRACT

Helicobacter pylori is a bacterial pathogen that colonizes the human gastric mucosa where it can cause a variety of diseases. *H. pylori* cells use a cluster of polar flagella to achieve robust motility in the viscous environment of the mucus layer that covers the gastric epithelium. The flagellar motor of *H. pylori* is predicted to have 18 torque-generating stator complexes, making it the largest bacterial flagellar motor described to date. Cryo-electron tomography (cryo-ET) of the *H. pylori* flagellar motor revealed the conserved core structure of the bacterial motor as well as additional embellishments, some of which may enhance the high torque generation required by the bacterium for motility in viscous environments. The motor embellishments include various disks and a periplasmic cage-like structure. The cryo-ET imaging was unable to clearly identify the location of the stator relative to other motor structures. We report here on the visualization of the flagellar motor of a *motAB* deletion mutant in *H. pylori* B128 by cryo-ET, which confirmed the location of the stator in the *H. pylori* flagellar motor and its proximity to the periplasmic cage, putative L-ring and the C-ring. These findings support the proposed role for the periplasmic cage in recruitment and/or stabilization of the stator within the *H. pylori* flagellar motor.

INTRODUCTION

Helicobacter pylori is a highly motile bacterial pathogen that colonizes the human gastric mucosa where it causes a variety of diseases, including chronic gastritis, peptic and duodenal ulcers, B cell MALT lymphoma and gastric adenocarcinoma [1]. *H. pylori* is motile via a cluster of polar, sheathed flagella. Motility of *H. pylori* cells is essential for host colonization as non-motile *H. pylori* mutants fail to colonize animal models [2, 3]. *H. pylori* cells are able to swim rapidly within the viscous mucus layer covering the stomach epithelium, and a couple of factors contribute to this robust swimming behavior. First, *H. pylori* uses urease to hydrolyze urea, which elevates the pH and triggers a transition of mucin from a soft viscoelastic gel to a viscous solution [4]. Second, the helical shape of *H. pylori* cells contributes to the robust motility of the bacterium in viscous medium [5]. Third, the *H. pylori* flagellar motor has 18 torque generating stator units, making it the largest bacterial flagellar motor described to date [6]. The large *H. pylori* flagellar motor is thought to provide the high torque needed for motility of the bacterium in viscous environments [6].

The general structure of the *H. pylori* flagellum is similar to that of the model organisms *Escherichia coli* and *Salmonella enterica* serovar Typhimurium (*S.* Typhimurium) [7-9]. The flagellum consists of three major structures: a basal body that contains a rotary motor embedded in the cell envelope, a filament that functions as a helical propeller, and a hook that acts as a flexible joint between the motor and the filament. The basal body is the most complex of these structures, and in addition to the rotary motor, contains a Type III secretion system that transports the axial components of the flagellum (e.g., rod, hook and filament subunits) across the cell membrane. The flagellar motor of Gram-negative

bacteria is comprised of the following features: MS-ring (forms base for the rotor), C-ring (contains rotor and switch complex that regulates motor rotation), rod (motor driveshaft), P- and L-rings (bushing for motor), and MotA/MotB stator [7-9]. The stator is the torque generator for the flagellar motor and is powered by the proton motive force [10].

Recent studies of the structures of flagellar motors from *H. pylori* and other bacteria by cryo-electron tomography (cryo-ET) have shown that while the core structure of the motor is highly conserved, motors of bacteria often have embellishments not found in the *E. coli* and *S.* Typhimurium paradigms [6, 11-13]. The *H. pylori* flagellar motor includes several disks and a cage-like periplasmic structure that are not found in the flagellar motors of *E. coli* and *S.* Typhimurium [6]. *Campylobacter jejuni*, a member of the subphylum Epsilonproteobacteria and close relative of *H. pylori*, shares some, but not all, of these motor embellishments [11-13]. Cryo-ET imaging of the flagellar motors of *C. jejuni* mutants identified genes that encode components of the motor embellishments, as well as revealed a hierarchical assembly pathway for these components [11]. Although a specific structure associated with FlgQ was not identified, deleting *flgQ* in *C. jejuni* arrests flagellum biogenesis following assembly of the L- and P-rings. The basal disk (encoded by *flgP*) and a second, smaller disk just below the basal disk are the next structures assembled, followed by assembly of the periplasmic medial disk and the inner membrane associated proximal disk, which are formed from subunits of PflA and PflB, respectively. Following assembly of the medial and proximal disks, the stator units are recruited to the motor [11]. *H. pylori* has homologs of *flgQ*, *flgP*, *pflA*, and *pflB*, although the structural features associated with these genes differ somewhat from those of *C. jejuni* [6, 12]. Genes

encoding proteins that constitute *H. pylori* motor embellishments not found in the *C. jejuni* motor have yet to be identified.

The stator is a hetero-hexameric complex consisting of four subunits of MotA and two subunits of MotB [14]. MotB, which has a single N-terminal transmembrane region and a large C-terminal periplasmic region, anchors the stator to the peptidoglycan layer through interactions with the P-ring protein FlgI, as well as a predicted association with peptidoglycan through its peptidoglycan-binding motif [15, 16]. MotA has four transmembrane domains and is embedded in the inner membrane. The MotA/MotB stator forms a proton channel in the inner membrane [17, 18], which converts proton flow across the inner membrane into rotation of the flagellar motor. This energy conversion is thought to occur through electrostatic interactions between MotA and the rotor protein FliG [19]. Protons passing through the channel formed by the stator are thought to be bound by a conserved aspartic acid residue in the transmembrane segment of MotB, which results in conformational changes in MotA that are coupled to rotation of the motor [20].

Although stators function as the stationary component of the flagellar rotary motor, stator composition within the motor can be highly dynamic. In *E. coli*, the number of stators in the motor changes depending on external load, with increasing load leading to the incorporation of more stator units [21, 22]. Turnover of stators in the *E. coli* motor is rapid as experiments showed green fluorescent protein-labeled MotB proteins remain in the motor for an average of only 30 seconds and exchange with a pool of stators in reserve in the inner membrane [23]. In contrast, stators appear to associate more stably with the flagellar motors of Epsilonproteobacteria and other bacteria [12].

Cryo-ET revealed high-resolution images of the *H. pylori* flagellar motor [6], although the position of the MotA/MotB stator complex relative to other motor structures was unclear from the study. A unique feature of the *H. pylori* flagellar motor is the periplasmic cage that is proposed to provide a stable platform for the recruitment and stabilization of stators needed to facilitate the high torque generation required by *H. pylori* to swim robustly in viscous environments [6]. We report here on the visualization of the flagellar motor of a *motAB* deletion mutant in *H. pylori* B128 by cryo-ET, which confirmed the location of the MotA/MotB stator complex in the *H. pylori* flagellar motor and its juxtaposition to the periplasmic cage and the C-ring. These findings support the proposed role for the cage in recruitment and/or stabilization of the stator within the *H. pylori* flagellar motor.

RESULTS AND DISCUSSION

***H. pylori motAB* mutant is flagellated but non-motile.** As expected, deletion of *motAB* in *H. pylori* B128 resulted in loss of motility in soft agar medium (Fig. 5.1A). In contrast to the wild-type strain, growth of the Δ*motAB* mutant in the soft agar medium was uniform and dense, and lacked the lighter periphery characteristic of the swim halo, indicating the Δ*motAB* was unable to swim from the point of inoculation. Observation of the *H. pylori* Δ*motAB* mutant cells by transmission electron microscopy (TEM) revealed that although the cells were non-motile they were flagellated. Flagellar counts revealed the Δ*motAB* mutant cells possessed slightly more flagella per cell than wild type (Fig. 5.1B). Both the Δ*motAB* mutant and wild type displayed a Gaussian or normal distribution for number of flagella per cell, with three and four flagella per cell being the most common number for

the wild type and Δ*motAB* mutant, respectively (Fig. 5.1B). The reason for the increased number of flagella per cell for the Δ*motAB* mutant is unclear. Qin and co-workers tentatively identified the stator as being associated with flagellum assembly intermediates that were produced prior to hook and filament assembly [6], suggesting the *H. pylori* motor is functional while the hook and filament are assembled. If this is the case, it is possible that assembly of the hook and/or filament proceeds more efficiently in the absence of motor rotation. Alternatively, movement of the flagella accomplished by the wild type could result in shearing of the flagella due to the mechanical stress of rotation, which may account for the fewer number of flagella observed in the wild type.

Comparison of the motors of *H. pylori* B128 wild type and Δ*motAB* mutant. Visualization of the *H. pylori* flagellar motor by cryo-ET was unable to identify unambiguously some of the specific structural features associated specifically with the stator [6]. To address this issue, as well as clarify the spatial relationship of the stator to other structures in the *H. pylori* flagellar motor, we visualized the flagellar motor of the *H. pylori* Δ*motAB* mutant. The motor of the Δ*motAB* mutant lacked electron densities that were evident in the wild-type flagellar motor (Fig. 5.2). Specifically, in the central slice of averaged structure for the wild-type motor has an electron density in the periplasmic space (Fig. 5.2A; indicated by red arrow) that is absent in the averaged structure for the Δ*motAB* motor (Fig. 5.2C). This structure presumably corresponds to MotB, which has a large periplasmic domain.

The central slice of the averaged structure for the wild-type motor also has electron densities within the inner membrane and on the cytoplasmic side of the inner membrane (Fig. 5.2A; indicated by black arrow) that are absent in the averaged structure for the

Δ*motAB* motor (Fig. 5.2C). The electron density in the inner membrane likely corresponds to the transmembrane regions of MotA and MotB, while the electron density on the cytoplasmic side of the membrane presumably corresponds to MotA. The structure on the cytoplasmic side of the membrane is closely associated with the C-ring, which provides further supporting evidence for MotA corresponding to this structure since MotA is thought to interact with the C-ring protein FliG [19].

The cross section of the wild-type flagellar motor in the periplasmic space shows a circular structure with 18-fold symmetry that is absent in the motor of the Δ*motAB* mutant (Figs 5.2B and 5.2D). The circular structure appears to consist of two half circles, which may correspond to the periplasmic domains of the two MotB subunits in the stator. In both the wild-type and Δ*motAB* motors, two structures with 18-fold symmetry that are slightly offset from each other can be seen, one or both of which correspond to the periplasmic cage (Figs. 5.2B and 5.2D). The results of the cryo-ET imaging indicate that the only stable component of the flagellar motor that is absent in the motor of the Δ*motAB* mutant is the stator, which suggests that the stator is not required for recruitment of other motor components. We can rule out the possibility, however, that the stator may play a role in recruiting components that are transiently associated with the flagellar motor.

CONCLUSIONS

In this report, we unambiguously identify the MotA/MotB stator in the *H. pylori* flagellar motor and demonstrate its position relative to other components of the *H. pylori* motor. The stator does not appear to be required for assembly of other components of the *H. pylori* flagellar motor. Moreover, the stator is not required for flagellar biosynthesis,

and in fact, flagellum assembly is somewhat enhanced in the absence of MotA and MotB. While the *H. pylori* flagellar motor shares core features with the archetype motors of *E. coli* and *S.* Typhimurium, the *H. pylori* motor has a number of embellishments. Little is known about the functions of these motor embellishments, and for some of them, the proteins that constitute these structures are unknown. The data presented here represent an important step towards understanding the structure/function relationships within the *H. pylori* flagellar motor.

MATERIALS AND METHODS

Bacterial strains and growth conditions. *E. coli* DH5α was used for plasmid construction and storage. *E. coli* was grown in Luria-Bertani broth or agar plates supplemented with ampicillin (100 µg/mL) or kanamycin (30 µg/mL) when appropriate. *H. pylori* was routinely grown on tryptic soy agar (TSA) plates supplemented with 5% heat-inactivated horse serum under an atmosphere of 10% CO_2, 4% O_2, and 86% N_2 at 37°C. For growth in liquid culture, *H. pylori* was grown in Brain Heart Infusion (BHI) medium supplemented with 5% horse serum under an atmosphere of 5% CO_2, 10% H_2, 10% O_2, and 75% N_2 at 37°C with shaking.

Strain construction. Primers 91 and 92 were used to amplify a 695 base pair region corresponding to the sequence directly upstream of *motA*, containing 410 bp of the upstream gene, 239 bp of intergenic sequence, and the first 46 bp of *motA*. Primers 93 and 94 were used to amplify a 656 base pair region corresponding to the sequence directly downstream of *motB*, containing the last 34 bp of *motB*, 36 bp of intergenic region, 438 bp of the downstream gene. Primer 92 added an XhoI restriction site along with a 13 base pair

overhang. Primer 93 added a NheI restriction site along with a complementary 13 base pair overhang. The resulting amplicons were joined by PCR SOEing. The resulting amplicon was incubated with *Taq* polymerase (Promega) at 72º C for 1 h to add 3'-A overhangs, which facilitated cloning of the amplicon into the pGEM-T Easy vector (Promega) to generate plasmid pKHG37. Plasmid pJC038 carries a cassette bearing a kanamycin-resistance gene (kan^R) and *Bacillus subtilis sacB* under control of the *H. pylori ureA* promoter [24]. The kan^R-*sacB* cassette from pJC038 was introduced into unique NheI and XhoI sites in plasmid pKHG37 to generate suicide plasmid pKHG39. The suicide plasmid was introduced by natural transformation into *H. pylori* B128 to replace *motAB* with the kan^R-*sacB* cassette through homologous recombination. Recombinants that gained the kan^R-*sacB* cassette were identified by screening for kanamycin resistance. The kan^R-*sacB* cassette was removed by transforming plasmid pKHG37 into a kanamycin-resistant isolate to replace the kan^R-*sacB* cassette with the unmarked *motAB* deletion through homologous recombination using a sucrose-based counter-selection to select for the desired recombinant [25]. The genotype of the resulting *H. pylori* B128 Δ*motAB* mutant (KG54) was confirmed by PCR.

Motility assay. Motility was assessed using a semisolid medium containing Mueller-Hinton broth, 10% heat-inactivated horse serum, 20 mM MES (2-(4-morpholino)-ethane sulfonic acid) (pH 6.0), 5 μM $FeSO_4$ and 0.4 % Noble agar. At least six technical replicates were used to assess the motility of each strain. *H. pylori* strains grown for 4 d on the supplemented TSA medium were stab inoculated into the motility agar and incubated under an atmosphere of 10% CO_2, 4% O_2, and 86% N_2 at 37°C for 7 d, after which the diameters

of the resulting swim halos were measured. A two-sample *t* test was used to determine statistical significance for the results of the motility assay.

Transmission electron microscopy. *H. pylori* strains were grown to late log phase (OD_{600} ~ 0.8) in the supplemented BHI medium. Cells from 1 mL of culture were collected by centrifugation (550 x g) and resuspended in 125 µl of 0.1 M phosphate buffered saline (PBS). Cells were fixed by treating with formaldehyde (4% final) and glutaraldehyde (1% final) for 5 min at room temperature. 10 µl of cell suspension was added to formvar coated 300 mesh copper grids and allowed to adhere to the surface for 5 min at room temperature. Excess cell suspension was removed from the grids with filter paper, followed by 3 washes with 10 µl distilled water. Cells were negatively stained with 1% uranyl acetate for 30 sec at room temperature, followed by a final wash with 10 µl dH_2O. Excess water was removed with filter paper and the grids were air dried. Grids were viewed using a JEOL JEM 1011 electron microscope operated at 100 kV. The number of flagella per cell (n=100) were determined for each strain. A Mann-Whitney U test was used to identify statistically significant differences in number of flagella per cell for the *H. pylori* strains.

Sample preparation for cryo-EM observation. *H. pylori* strains were cultured on plates for 4 d. The cells on the agar surface were collected then washed with PBS buffer. Colloidal gold solution (10 nm diameter) was added to the diluted *H. pylori* samples to yield a 10-fold dilution and then deposited on a freshly glow-discharged, holey carbon grid for 30 seconds. The grid was blotted with filter paper and rapidly plunge-frozen in liquid ethane in a homemade plunger apparatus as described [26].

Cryo-ET data collection and image processing. The frozen-hydrated specimens of *H. pylori* B128 wild-type and Δ*motAB* mutant were transferred to Titan Krios electron

microscope (FEI) equipped with a 300-kV field emission gun and a Direct Electron Detector (Gatan K2 Summit). The images were collected at a defocus near to 0 µm using Volta Phase Plate and the energy filter with 20 eV slit. The data was acquired automatically with SerialEM software [27]. During the data collection, the phase shift is monitored at the range of pi/3~pi2/3; when the phase shift is out of above range, the next spot of phase plate will be switched to be charged for the use. A total dose of 50 e−/Å2 is distributed among 35 tilt images covering angles from −51° to +51° at tilt steps of 3°. The starting tilting angle is +36˚ instead of 0˚. For every single tilt series collection, the dose-fractionated mode was used to generate 8–10 frames per projection image. Collected dose-fractionated data were first subjected to the motion correction program to generate drift-corrected stack files [28-30]. The stack files were aligned using gold fiducial markers and volumes reconstructed by the weighted back-projection method using IMOD and Tomo3d software to generate tomograms [31, 32].

Sub-tomogram analysis with i3 packages. Bacterial flagellar motors were detected manually using the i3 program [33, 34]. The orientation and geographic coordinates of selected particles were then estimated. The i3 tomographic package was used on the basis of the "alignment by classification" method with missing wedge compensation for generating the averaged structure of the motor as described [26].

AUTHOR CONTRIBUTIONS

TRH, JL designed experiments; KHG constructed and characterized the Δ*motAB* mutant, and assisted with the analysis and interpretation of the cryo-ET data; and SZ acquired, analyzed and interpreted the cryo-ET data. TRH, JL, and KGH contributed to writing the manuscript.

ACKNOWLEDGEMENTS

This work was supported by NIH grant AI140444 to T.R.H. and NIH grants GM107629 and AI087946 to J.L.

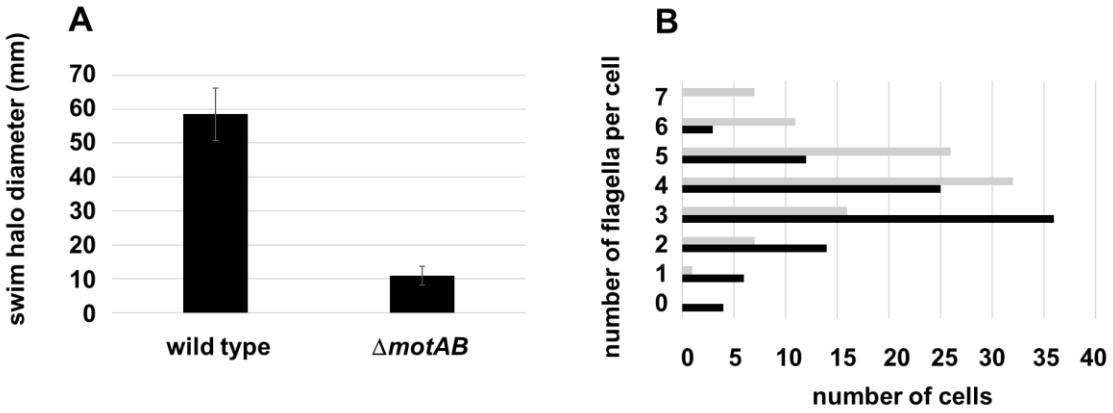

Figure 5.1. Motility and flagellation pattern of wild type and Δ*motAB* mutant. (**A**) Motility of Δ*motAB* mutant and wild type *H. pylori* B128 was assessed by inoculating strains into soft agar medium and allowing the cells to migrate from the point of inoculation. Bars indicate the mean of swim halo diameters measured 7 d post-inoculation (n= 6 for wild type and n = 8 for Δ*motAB* mutant). Error bars correspond to 95% confidence interval. Motility of the Δ*motAB* mutant was significantly reduced compared to that of wild type as determined from a two-sample *t* test (*p*-value < 0.0001). (**B**) *H. pylori* cells were visualized by TEM and flagella were counted for 100 cells. Values on the x-axis indicate the number of cells with a given number of flagella per cell, which is indicated on the y-axis. Black bars indicate flagella counts for wild type and gray bars indicate flagella counts for the Δ*motAB* mutant. Cells of the Δ*motAB* mutant had a significantly higher number of flagella per cell compared to wild type (*p*-value <0.00001). Statistical significance was determined using a Mann-Whitney U test.

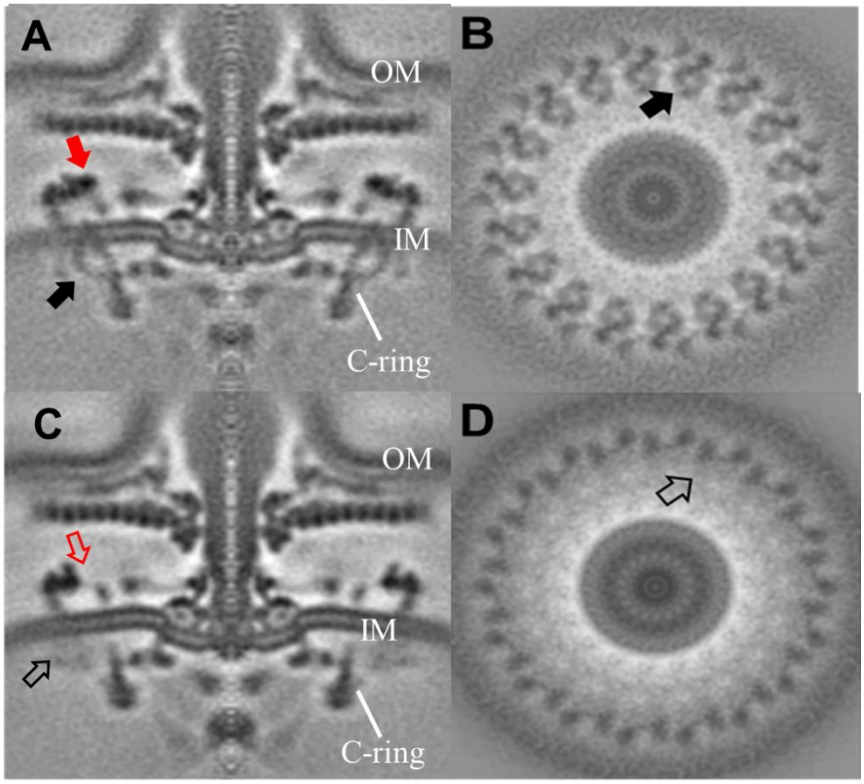

Figure 5.2. Structure of the flagellar motors of *H. pylori* B128 wild type and Δ*motAB* mutant as revealed by cryo-ET and subtomogram averaging. (A) A central slice of the averaged structure of wild-type flagellar motor. (B) Cross section of the wild-type flagellar motor in the periplasmic space showing feature with 18-fold symmetry that corresponds to the MotA/MotB stators. (C) A central slice of the averaged structure of the Δ*motAB* flagellar motor. (D) Cross section of Δ*motAB* flagellar motor in the periplasmic space. Black and red arrows in panels A and B indicate electron densities that are absent in the corresponding images of the Δ*motAB* flagellar motor. Empty arrows show the locations of the missing electron densities in the Δ*motAB* flagellar motor. Outer membrane, OM; inner membrane, IM.

Table 5.1. Primers used in this study.

Primer number	Primer name	Sequence
91	motAB US F	5' TGA TGT ATT TGT GCG CCG
92	motAB US R + XhoI	5' GAA TCC GAT TAT CCT CGA GTA GAA GCG ACC GCC AAT A
93	motAB DS F + NheI	5' GAT AAT CGA ATT CGC TAG CAC GAT TTG AGC AAG ATC CAT T
94	motAB DS R	5' TGC GTA ATT ACA TCT ACA GAA TGG

Table 5.2. Plasmids used in this study.

Name	Description	First used
pKHG37	pGEM-T easy with *motAB* flanking sequences	This study
pKHG39	pGEM-T easy with *motAB::kan-sacB*	This study
pJC038	pGEM-T easy containing *kan-sacB* cassette	24

Table 5.3. *H. pylori* strains used in this study

Strain name	**Genotype**
B128	Wild type
KG51	B128 *motAB::kan-sacB*
KG54	B128 Δ*motAB*

REFERENCES

1. Atherton, J.C. and M.J. Blaser, *Coadaptation of Helicobacter pylori and humans: ancient history, modern implications.* J Clin Invest, 2009. **119**(9): p. 2475-87.

2. Eaton, K.A., D.R. Morgan, and S. Krakowka, *Motility as a factor in the colonisation of gnotobiotic piglets by Helicobacter pylori.* J. Med. Microbiol., 1992. **37**: p. 123-127.

3. Ottemann, K.M. and A.C. Lowenthal, *Helicobacter pylori uses motility for initial colonization and to attain robust infection.* Infect Immun, 2002. **70**(4): p. 1984-90.

4. Celli, J.P., et al., *Helicobacter pylori moves through mucus by reducing mucin viscoelasticity.* Proc Natl Acad Sci U S A, 2009. **106**(34): p. 14321-6.

5. Martinez, L.E., et al., *Helicobacter pylori strains vary cell shape and flagellum number to maintain robust motility in viscous environments.* Mol Microbiol, 2016. **99**(1): p. 88-110.

6. Qin, Z., et al., *Imaging the motility and chemotaxis machineries in Helicobacter pylori by cryo-electron tomography.* J Bacteriol, 2017. **199**(3): p. e00695-16.

7. Berg, H.C., *The rotary motor of bacterial flagella.* Annu Rev Biochem, 2003. **72**: p. 19-54.

8. Chevance, F.F. and K.T. Hughes, *Coordinating assembly of a bacterial macromolecular machine.* Nat Rev Microbiol, 2008. **6**(6): p. 455-65.

9. Macnab, R.M., *How bacteria assemble flagella.* Annu Rev Microbiol, 2003. **57**: p. 77-100.

10. Manson, M.D., et al., *A protonmotive force drives bacterial flagella.* Proc Natl Acad Sci U S A, 1977. **74**(7): p. 3060-4.

11. Beeby, M., et al., *Diverse high-torque bacterial flagellar motors assemble wider stator rings using a conserved protein scaffold.* Proc Natl Acad Sci U S A, 2016. **113**(13): p. E1917-26.

12. Chaban, B., I. Coleman, and M. Beeby, *Evolution of higher torque in Campylobacter-type bacterial flagellar motors.* Sci Rep, 2018. **8**(1): p. 97.

13. Chen, S., et al., *Structural diversity of bacterial flagellar motors.* EMBO J, 2011. **30**(14): p. 2972-81.

14. Kojima, S. and D.F. Blair, *Solubilization and purification of the MotA/MotB complex of Escherichia coli.* Biochemistry, 2004. **43**(1): p. 26-34.

15. Hizukuri, Y., S. Kojima, and M. Homma, *Disulphide cross-linking between the stator and the bearing components in the bacterial flagellar motor.* J Biochem, 2010. **148**(3): p. 309-18.

16. Hizukuri, Y., et al., *The peptidoglycan-binding (PGB) domain of the Escherichia coli pal protein can also function as the PGB domain in E. coli flagellar motor protein MotB.* J Biochem, 2009. **146**(2): p. 219-29.

17. Blair, D.F. and H.C. Berg, *The MotA protein of E. coli is a proton-conducting component of the flagellar motor.* Cell, 1990. **60**(3): p. 439-49.

18. Stolz, B. and H.C. Berg, *Evidence for interactions between MotA and MotB, torque-generating elements of the flagellar motor of Escherichia coli.* J Bacteriol, 1991. **173**(21): p. 7033-7.

19. Zhou, J., S.A. Lloyd, and D.F. Blair, *Electrostatic interactions between rotor and stator in the bacterial flagellar motor.* Proc Natl Acad Sci U S A, 1998. **95**(11): p. 6436-41.

20. Kojima, S. and D.F. Blair, *Conformational change in the stator of the bacterial flagellar motor.* Biochemistry, 2001. **40**(43): p. 13041-50.

21. Lele, P.P., B.G. Hosu, and H.C. Berg, *Dynamics of mechanosensing in the bacterial flagellar motor.* Proc Natl Acad Sci U S A, 2013. **110**(29): p. 11839-44.

22. Tipping, M.J., et al., *Load-dependent assembly of the bacterial flagellar motor.* mBio, 2013. **4**(4): p. e00551-13.

23. Leake, M.C., et al., *Stoichiometry and turnover in single, functioning membrane protein complexes.* Nature, 2006. **443**(7109): p. 355-8.

24. Chu, J.K., et al., *Loss of a cardiolipin synthase in Helicobacter pylori G27 blocks flagellum assembly.* J Bacteriol, 2019. **201**(21).

25. Copass, M., G. Grandi, and R. Rappuoli, *Introduction of unmarked mutations in the Helicobacter pylori vacA gene with a sucrose sensitivity marker.* Infect Immun, 1997. **65**(5): p. 1949-52.

26. Zhu, S., et al., *In situ structural analysis of the spirochetal flagellar motor by cryo-electron tomography.* Methods Mol Biol, 2017. **1593**: p. 229-242.

27. Mastronarde, D.N., *Automated electron microscope tomography using robust prediction of specimen movements.* J Struct Biol, 2005. **152**(1): p. 36-51.

28. Li, X., et al., *Electron counting and beam-induced motion correction enable near-atomic-resolution single-particle cryo-EM.* Nat Methods, 2013. **10**(6): p. 584-90.

29. Morado, D.R., B. Hu, and J. Liu, *Using Tomoauto: a protocol for high-throughput automated cryo-electron tomography.* J Vis Exp, 2016(107): p. e53608.

30. Zheng, S.Q., et al., *MotionCor2: anisotropic correction of beam-induced motion for improved cryo-electron microscopy.* Nat Methods, 2017. **14**(4): p. 331-332.

31. Agulleiro, J.I. and J.J. Fernandez, *Tomo3D 2.0--exploitation of advanced vector extensions (AVX) for 3D reconstruction.* J Struct Biol, 2015. **189**(2): p. 147-52.

32. Kremer, J.R., D.N. Mastronarde, and J.R. McIntosh, *Computer visualization of three-dimensional image data using IMOD.* J Struct Biol, 1996. **116**(1): p. 71-6.

33. Winkler, H., *3D reconstruction and processing of volumetric data in cryo-electron tomography.* J Struct Biol, 2007. **157**(1): p. 126-37.

34. Winkler, H., et al., *Tomographic subvolume alignment and subvolume classification applied to myosin V and SIV envelope spikes.* J Struct Biol, 2009. **165**(2): p. 64-77.

CHAPTER 6

CONCLUSIONS AND FUTURE DIRECTIONS

The roles of *flhFGH* in *H. pylori*

Through my work, I characterized the phenotypes of *flhF* and *flhG* mutants in *H. pylori*, which represented the first detailed study of these genes in a bacterium with a lophotrichous arrangement of flagella. Similar to reports in other bacterial species [1-3], deletion of *flhF* in *H. pylori* resulted in a marked decrease in motility. The motility defect was caused by a large majority of the cells either not producing flagella, or producing them at non-polar locations. I further generated variants of the *flhF* deletion strain that were more motile by repeated passage through soft agar medium, culminating in the isolation of three motile variants (MV1, MV2, and MV3). The motile variants were analyzed by whole genome sequencing (WGS) to identify mutations that resulted in the more motile phenotype. Single nucleotide polymorphisms (SNPs) were identified in *faaA* (a type V autotransporter), *fliF* (MS-ring protein), and HPG27_170 (hypothetical protein). MV3 has a missense mutation in *fliF* that presumably allows this strain to assemble more flagella per cell compared to the *flhF* parent strain. MV1 and MV2 do not assemble any more flagella than the parent strain, but instead allow for more flagella to be properly localized to the cell pole. The specific SNPs that rescue the motility of the *flhF* deletion mutant have yet to be verified, but I am currently reconstructing these mutations in a naïve Δ*flhF* background.

Further characterization of FaaA will provide additional understanding into its role in flagellar biosynthesis. FaaA is an autotransporter that has a β-barrel domain at its C-terminus that inserts into the outer membrane and most of the remaining portion of the protein constitutes a large passenger domain. Radin and co-workers showed that FaaA localizes to the flagellar sheath in *H. pylori* and the passenger domain is surface exposed [4]. It will be of interest to see if FaaA localizes to the cell pole in an aflagellated mutant. Since the flagellar sheath appears to be continuous with the outer membrane, identifying factors involved in localizing FaaA to the flagellar sheath would provide valuable insight into how *H. pylori* partitions FaaA, as well as other proteins, to the sheath. My findings suggest that in the absence of FlhF, FaaA inhibits formation of flagella at the cell pole. This finding indicates that FaaA may function to link flagellum assembly with sheath biosynthesis.

The mechanism by which FaaA interferes with localization of flagella to the cell pole is not known. Moreover, it is not clear if FaaA mediates its inhibitory effect on polar localization of flagella in the Δ*flhF* mutant from the outer membrane, inner membrane or periplasm. A deletion analysis of *faaA* would provide valuable clues on whether the β-barrel domain and/or passenger domain are required for inhibiting localization of flagella to the cell pole. If it turns out the β-barrel domain is sufficient for the inhibition, this would suggest FaaA inhibits flagellum localization at the cell pole by interfering with assembly of flagellar components associated with the outer membrane. Such a model implies assembly of flagellar components associated with the inner and outer membranes occur independently of each other, which is contrary to the present understanding of flagellar assembly based on studies with *E. coli* and *S.* Typhimurium that suggest an inside-to-

outside sequential assembly process that starts with components associated with the inner membrane and culminates in formation of the filament [5-10]. A recent cryo-electron tomography (cryo-ET) study by Kaplan and co-workers with *Legionella pneumophila, Pseudomonas aeruginosa,* and *Shewanella oneidensis* supported the inside-to-outside flagellum assembly process in these bacteria [11]. While Kaplan and co-workers [11], observed outer membrane complexes similar to the periplasmic P- and L-rings that were not associated with the inner membrane flagellar components in all three species, the authors attributed these structures to flagellum disassembly products. Cryo-ET may provide support for the validity of the inhibition from the outer membrane model in *H. pylori,* as disrupting genes encoding flagella components that join the inner and outer membrane components of the flagellum (e.g., *flgBC,* encode the inner rod proteins) may allow us to observe distinct flagellar structures in the two membranes. Cryo-ET will allow us to assess and separate these distinct assembly processes through an up-close 3D reconstruction of the *H. pylori* flagellar motor.

If the passenger domain of FaaA is responsible for inhibiting polar localization of flagella in the Δ*flhF* mutant, it may do so by interfering with flagellum assembly. For example, FaaA may compete with flagellar proteins for a landmark protein at the cell pole, or may inhibit flagellum assembly at the cell pole. Immunoprecipitation can be used to identify potential interaction partners for FaaA, such as a landmark protein or a specific flagellar protein.

In contrast to FlhF proteins from other bacteria [12], I was unable to discern distinct fluorescent foci of a cyan-fluorescent protein-tagged FlhF (FlhF-CFP), suggesting inherent differences in FlhF proteins from *H. pylori* and other species. In *Vibrio alginolyticus,* polar

localization of FlhF appears to be inherent to the protein, while FlhG in *V. alginolyticus* is localized to the cell pole through interactions with a landmark protein, HubP [13]. If polar localization is an inherent property of *V. alginolyticus* FlhF, it would be interesting to switch domains of the *H. pylori* FlhF protein (eg. N or G domains) with those from *V. alginolyticus* FlhF and determine if the chimeric protein localizes to the cell pole in *H. pylori.*

In contrast to the Δ*flhF* mutant, deletion of *flhG* in *H. pylori* did not result in a decrease in motility, although flagellar numbers were impacted. This is in contrast to the impaired motility observed in Δ*flhG* mutants from other bacteria [1, 2, 14]. The number of flagella per cell was impacted in the *flhG* mutant, with a few cells having eight or more flagella and a significantly higher proportion of cells having zero or one flagella. We propose that FlhF activity is hyper-active in the Δ*flhG* mutant and that the increase in the proportion of under-flagellated cells results from the initiation of more MS-rings than can be fully assembled with the number of available FliF subunits. Cryo-ET will allow us to determine how many MS-rings a cell assembles and compare that number directly with the number of mature flagella produced. Alternatively, we could fuse FliF to a fluorescent molecule such as yellow fluorescent protein (YFP) and use high powered fluorescence microscopy such as Stochastic Optical Reconstruction Microscopy (STORM) in order to quantify the number of MS-rings being assembled in the Δ*flhG* mutant.

An interesting question is whether flagellar placement and number are dictated primarily by FlhF and FlhG in *H. pylori*. To address this question, it would be interesting to introduce *flhFG* from *C. jejuni*, a closely related Epsilonproteobacteria, into the genome of *H. pylori* and assess the motility and flagellation phenotypes of the resulting strain.

Expected results include several possibilities, from wild-type *H. pylori* flagellation (2-5 flagella at a single pole), to wild-type *C. jejuni* flagellation (a single flagellum at each pole), to the flagellation pattern of an *H. pylori* Δ*flhF* mutant (mislocalized flagella to lateral positions). If wild-type *H. pylori* flagellation results, this suggests there are no inherent differences between FlhF and FlhG of *H. pylori* and *C. jejuni.* If wild-type *C. jejuni* flagellation pattern is observed, this suggests that flagellar number and placement are inherent to FlhF and FlhG. A Δ*flhF* phenotype would suggest that *C. jejuni* FlhF is not able to substitute for *H. pylori* FlhF.

I further identified a gene directly downstream of *flhFG* that we designated as *flhH*. Deletion of *flhH* resulted in a severe motility defect and an increase in the proportion of aflagellated cells. We initially predicted that due to the position of *flhH* directly downstream of *flhFG* that *flhH* was involved in regulating the activity of either FlhF or FlhG. Deletion of *flhGH* did not result in a motility phenotype that was similar to that of the Δ*flhG* mutant, suggesting a lack of epistasis between FlhG and FlhH. Further, since the Δ*flhF* mutant was more motile than the Δ*flhH* mutant despite being less flagellated, we do not think that FlhH has a role in regulating FlhF activity.

I isolated three motile variants of the *flhH* mutant that produced unusually long flagellar filaments. All three motile variants had SNPs in both *faaA* and *flaG*-2. We predict that the longer flagella were a result of disrupting *flaG*-2 as mutations in *flaG*-2 homologs in *P. fluorescens* and *V. anguillarum* similarly produced very long filaments [15, 16]. Interestingly, a relatively short truncation of 15 amino acids from the C-terminus of FlaG-2 elicited consistently longer flagella than a truncation that resulted in a much shorter protein. These data suggest a domain of FlaG-2 that is close to the C-terminus is required

for the long flagella phenotype, which is a hypothesis that could be tested through a deletion analysis of *flaG*-2. When *flaG*-2 was deleted in a naïve *flhH* background, motility was not rescued to the level of the wild-type, suggesting that either a truncated FlaG-2 protein or mutations in both *flaG*-2 and *faaA* are required to rescue motility. I am currently reconstructing a *faaA* mutation in a naïve Δ*flhH* background and in an Δ*flhH* Δ*flaG*-2 double mutant to determine if the additional mutation in *faaA* is able to rescue the motility. Each motile variant also had an additional unique SNP (MV1: *fliN*, MV2: HPG27_1372, MV3: HPG27_261) that should be explored.

We predict that FlhH may have a role in stabilizing motor stator components or some other motor embellishment. In this model, stators would be unstable in the absence of *flhH* and the greater length of the filament produced by mutations in *flaG*-2 would increase the load on the motor leading to more stably incorporated stator components. Further, as stated above, we postulate that full length FaaA interferes with flagellum biosynthesis and mutations in *faaA* in the absence of *flhH* allow for some motor embellishments to assembly more readily. Cryo-ET will allow us to test this hypothesis. If our model is correct, we expect the stators to associate transiently with the flagellar motor of the Δ*flhH* mutant and not be visible in the tomograms. Moreover, we anticipate that some of the motor embellishments to be absent in the tomograms of the Δ*flhH* mutant since we predict FlhH is required for the assembly or stability of these motor embellishments. However, when either *flaG*-2 and/or *faaA* is disrupted, we expect to see the missing elements in the motor images once again. Our model predicts the Δ*flhH* mutant swims when the load on the flagellar motor is increased, and we can examine this hypothesis by observing the motility of the mutant by phase contrast microcopy under low load and high

load conditions by increasing the viscosity of the medium. Alternatively we could measure the speed of rotation of the flagella under low and high load conditions by tethering cells to latex beads through their flagella [17, 18].

By observing an FlhH-YFP fusion, I was able to see distinct foci at the cell pole in a small percentage of cells. To determine if the cell pole that FlhH localizes to is the flagellated cell pole, we can use FM-464, a fluorescent dye that stains membranes, and thus the flagellar sheath. If this proves unsuccessful, a Myc-tagged FaaA together with a fluorescent-tagged anti-Myc antibody can be used to determine which cell pole is flagellated since FaaA localizes to the flagellar sheath.

Perhaps the most interesting finding from the aforementioned experiments was the apparent role of FaaA in flagellar biosynthesis. Although the exact role of FaaA is still unclear, it could have various roles including flagellar function, stability, or assembly. Identifying mutations in other genes that rescue motility in the Δ*flhH* mutant would provide valuable clues regarding the mechanism by which FaaA affects the function of the flagellum in the *flhH* mutant background. For example, if FaaA exerts its effect by interfering with assembly of a motor embellishment, then we might get mutations in genes encoding proteins that either constitute or engage the embellishment. Given the proclivity for picking up mutations in *faaA* in our suppressor hunt, one approach for identifying novel suppressors would be to introduce into the Δ*flhH* mutant *faaA* on the shuttle vector pHel3 and then enrich for motile variants. With *faaA* in both the chromosome and on a plasmid, we would be less likely to pick up mutations in *faaA* that rescue motility, allowing for the identification of additional genes with roles in flagellum biosynthesis.

Identification of a putative tripartite efflux system in *H. pylori*

We identified a putative efflux system encoded by four genes (*faeABCD*) that are found preferentially in *H. pylori* strains that have a flagellar sheath. Deletion of *faeA* and *faeCD* resulted in decreased motility and fewer flagella per cell. Additional motility data is still needed for a *faeB* mutant. Subtomogram averaging of motors of Δ*faeA* and Δ*faeCD* mutants revealed motors that we classified into three types. The first motor type was only observed in Δ*faeA* motors and included the presence of the hook, filament, and flagellar sheath, while the cage and some motor components were absent. The second class of motors was also only observed in Δ*faeA* motors and lacked the hook and filament, possessed the P-ring motor embellishment, and had a deformity of the outer membrane at the tip of the rod. The final class of motors was observed for both Δ*faeA* and Δ*faeCD* mutants and contained only the P-ring, with a similar outer membrane deformity. These observations suggest that the FaeABCD efflux system forms part of the cage and may be required for the assembly or stability of other motor embellishments. Alternatively, the images of the efflux system mutants, particularly those of class 3 motors, could represent disassembly intermediates. Kaplan *et*. al., recently described motors representing flagellar disassembly steps in *L. pneumophila, P. aeruginosa,* and *S. oneidensis* [11]. The flagellum disassembly products contained decorated P- and L-rings and showed an invagination of the outer membrane in the shape of an upside-down omega [11]. Our study did not show a similar invagination of the outer membrane, instead appearing as if the membrane was being pushed outward.

Observation of additional motors of Δ*faeA* and Δ*faeCD* mutants by cryo-ET will allow for better resolution to be obtained through subtomogram averaging and provide more evidence for the location of the structures formed by the efflux system in the flagellar motor. Further evidence for this hypothesis can be gathered through immunogold labelling of individual efflux system mutants coupled with transmission electron microscopy (TEM) to reveal their localization within *H. pylori* cells.

Thus far, the substrate of the FaeABCD efflux system is unknown. An *H. pylori* 1061 Δ1489 (*faeA*) mutant was found to have increased sensitivity to the dye ethidium bromide, suggesting the Fae efflux system may be responsible for the efflux of this molecule [19]. However, our lab was not able to reproduce this result in a Δ*faeA* mutant in *H. pylori* G27 (J. Chu, unpublished). Additional potential substrates for the Fae efflux system could include proteins, metal ions, antibiotics, or other small molecules. To identify potential protein exports, deletion strains can be grown in a minimal or defined medium and changes to the extracellular proteome assessed. We can also test mutants for increased sensitivity to metal ions. In all, the identification of this efflux system provides an interesting avenue of future study into the flagellar motor of *H. pylori.*

Ultrastructural studies of the *H. pylori* MotAB stator

Previous studies of the flagellar motor of *H. pylori* failed to positively identify the location of the MotA/MotB complex, which comprise the stator components in bacterial flagellar motors [20, 21]. Through cryo-ET of *H. pylori* Δ*motAB* mutant we were able to definitively show the localization of the MotAB stator complexes. In the averaged images, MotA traverses the inner membrane and contacts the C-ring, while MotB extends into the periplasmic space and appears to contact the cage-like structure that surrounds the *H. pylori*

motor. We plan to explore further the *H. pylori* motor by deleting chemotaxis genes *cheY1* and *cheAY2* and examining the ultrastructure of the motors of the resulting mutants. Deletion of *cheY1* in *H. pylori* N6 was found to lock flagellar rotation in the clockwise direction, as these cells exhibited almost constant tumbling motion with no smooth swimming [22]. Conversely, deletion of *cheAY2* in *H. pylori* N6 appeared to be locked into counterclockwise rotation, swimming almost exclusively in smooth trajectories [22]. It is our hope that these mutations will allow us to 'freeze' the motor in one rotational direction to observe how the motor components may change during clockwise versus counterclockwise rotation.

Since MotB appears to contact the cage in the *H. pylori* motor, immunoprecipitation of MotB may allow us to identify proteins in the cage that are potential binding partners of MotB. Such new information may lead to identification of unknown cage proteins, as well as potentially provide evidence for the Fae efflux system as forming part of the cage.

Summary

This dissertation has focused on furthering our understanding of the structure and function of the *H. pylori* flagellar motor. My work has produced some interesting findings that are unique to the *H. pylori* flagellar system while providing avenues for additional studies. My work highlights the structural and functional differences among flagellar motors from different bacterial species and shows the need to move beyond the *E. coli/ Salmonella* paradigm when studying flagellum function, localization, assembly and disassembly.

References

1. Kusumoto, A., et al., *Collaboration of FlhF and FlhG to regulate polar-flagella number and localization in Vibrio alginolyticus.* Microbiology, 2008. **154**(Pt 5): p. 1390-1399.

2. Correa, N.E., F. Peng, and K.E. Klose, *Roles of the regulatory proteins FlhF and FlhG in the Vibrio cholerae flagellar transcription hierarchy.* J Bacteriol, 2005. **187**(18): p. 6324-32.

3. Balaban, M., S.N. Joslin, and D.R. Hendrixson, *FlhF and its GTPase activity are required for distinct processes in flagellar gene regulation and biosynthesis in Campylobacter jejuni.* J Bacteriol, 2009. **191**(21): p. 6602-11.

4. Radin, J.N., et al., *Flagellar localization of a Helicobacter pylori autotransporter protein.* mBio, 2013. **4**(2): p. e00613-12.

5. Jones, C.J. and R.M. Macnab, *Flagellar assembly in Salmonella typhimurium: analysis with temperature-sensitive mutants.* J Bacteriol, 1990. **172**(3): p. 132739.

6. Kubori, T., et al., *Morphological pathway of flagellar assembly in Salmonella typhimurium.* J Mol Biol, 1992. **226**(2): p. 433-46.

7. Macnab, R.M., *How bacteria assemble flagella.* Annu Rev Microbiol, 2003. **57**: p. 77-100.

8. Li, H. and V. Sourjik, *Assembly and stability of flagellar motor in Escherichia coli.* Mol Microbiol, 2011. **80**(4): p. 886-99.

9. Fabiani, F.D., et al., *A flagellum-specific chaperone facilitates assembly of the core type III export apparatus of the bacterial flagellum.* PLoS Biol, 2017. **15**(8): p. e2002267.

10. Fukumura, T., et al., *Assembly and stoichiometry of the core structure of the bacterial flagellar type III export gate complex.* PLoS Biol, 2017. **15**(8): p. e2002281.

11. Kaplan, M., et al., *In situ imaging of the bacterial flagellar motor disassembly and assembly processes.* EMBO J, 2019. **38**(14): p. e100957.

12. Green, J.C., et al., *Recruitment of the earliest component of the bacterial flagellum to the old cell division pole by a membrane-associated signal recognition particle family GTP-binding protein.* J Mol Biol, 2009. **391**(4): p. 679-90.

13. Takekawa, N., et al., *HubP, a Polar Landmark Protein, Regulates Flagellar Number by Assisting in the Proper Polar Localization of FlhG in Vibrio alginolyticus.* J Bacteriol, 2016. **198**(22): p. 3091-3098.

14. Balaban, M. and D.R. Hendrixson, *Polar flagellar biosynthesis and a regulator of flagellar number influence spatial parameters of cell division in Campylobacter jejuni.* PLoS Pathog, 2011. **7**(12): p. e1002420.

15. Capdevila, S., et al., *Analysis of Pseudomonas fluorescens F113 genes implicated in flagellar filament synthesis and their role in competitive root colonization.* Microbiology, 2004. **150**(Pt 11): p. 3889-3897.

16. McGee, K., P. Horstedt, and D.L. Milton, *Identification and characterization of additional flagellin genes from Vibrio anguillarum.* J Bacteriol, 1996. **178**(17): p. 5188-98.

17. Tipping, M.J., et al., *Load-dependent assembly of the bacterial flagellar motor.* mBio, 2013. **4**(4).

18. Lele, P.P., B.G. Hosu, and H.C. Berg, *Dynamics of mechanosensing in the bacterial flagellar motor.* Proc Natl Acad Sci U S A, 2013. **110**(29): p. 11839-44.

19. van Amsterdam, K., A. Bart, and A. van der Ende, *A Helicobacter pylori TolC efflux pump confers resistance to metronidazole.* Antimicrob Agents Chemother, 2005. **49**(4): p. 1477-82.

20. Kojima, S. and D.F. Blair, *Solubilization and purification of the MotA/MotB complex of Escherichia coli.* Biochemistry, 2004. **43**(1): p. 26-34.

21. Qin, Z., et al., *Imaging the motility and chemotaxis machineries in Helicobacter pylori by cryo-electron tomography.* J Bacteriol, 2017. **199**(3): p. e00695-16.

22. Foynes, S., et al., *Helicobacter pylori possesses two CheY response regulators and a histidine kinase sensor, CheA, which are essential for chemotaxis and colonization of the gastric mucosa.* Infect Immun, 2000. **68**(4): p. 2016-23.